The Dissertation Committee for Vaidyanathan Krishnamurthy Certifies that this is the approved version of the following dissertation:

Microgrid Availability during Natural Disasters

Committee:

Alexis Kwasinski, Supervisor

Ross Baldick

Aristotle Arapostathis

Gustavo de Veciana

Robert Hebner

Microgrid Availability during Natural Disasters

by

Vaidyanathan Krishnamurthy, B.E., M.S.E.

Dissertation

Presented to the Faculty of the Graduate School of

The University of Texas at Austin

in Partial Fulfillment

of the Requirements

for the Degree of

Doctor of Philosophy

The University of Texas at Austin

August 2014

FOR MIDGARD!!!

Acknowledgements

First and foremost, I have to thank Professor Alexis Kwasinski who has been my advisor and mentor since Spring 2009. Taking his distributed generation class along with other classes I was taking in operations research opened a new world to me. He has been incredibly patient, understanding and has given me various opportunities to learn and explore. I would also like to thank him for helping me get outage data and various information and photographs from his field damage assessments in order to support and validate the models in my research.

I would like to thank the National Science Foundation who provided the grant through which my masters and PhD studies were supported.

I would like to thank the members of my dissertation committee and other professors at UT who have directly or indirectly helped in this dissertation.

Professor Ross Baldick from who I have learned a lot, his optimization class really helped in learning how to formulate problems and for being there for discussions in these past 6 years during grad school. Professor Robert Hebner, for his great ideas and for bringing my attention to a lot of research in microgrids and also his detailed inputs toward my dissertation. Professor Aristotle Arapostathis, his stochastic control class has truly changed my life and also for his incredible input while discussing energy storage modeling. Professor Gustavo de Veciana, for all his inputs and also for taking his time and his patience in helping me out with all my questions and helping me become better at modeling. I would also like thank to Professor John Hasenbein for his awesome courses in stochastic processes, queuing and markov decision processes and Professor Clint

Dawson for guiding me to various hurricane related information that has been of immense value in understanding the data.

I would like to thank my lab-mates at the Power Electronics Research Group, Myungchin Kim, Rossen Tsartzev, Mahesh Srinivasan, Junseok Song, Amir Toliyat, Harsha Kumar, Youngsung Kwon, Joon Hyun Kim, Juyoung Jung, Hunter Blake Estes, Ruichen Zhao, Shengyang Yu, Chimaobi Onwuchekwa and others who have been totally awesome, entertaining and helpful. I will miss the fun times. I would especially like to thank Myungchin for all his help, critical feedback in research and reading this dissertation. I would also like to thank Mahesh for reviewing and providing help in the writing process. I would also like to thank Deepjyoti Deka and Yezhoa Wang for all the discussions and giving me a lot of information.

The staff at ECE, especially Melanie Gulick and Melodie Singleton, have made my life in ECE a smooth experience. They have been immense help to me as they have been to so many other graduate students and I will forever be grateful.

Also have to thank my friends at UT and in Austin. There are too many to mention here but you know who you are and I know who you are but I will mention a few nonetheless. Sunil Kowlgi, Vivek Subramanian, Tanuj Trivedi, Raghunandan Kolar, Praveen Pasupathy, Shayak Banerjee, Kumar Appaiah and also Sangamitra Narasimhan for proofreading my dissertation.

I have to thank my aunt Brinda and uncles Narayan, Kasinathan, Radhakrishnan, Ganeshan who have been very caring supportive and inspiring that I have done. I would also like to thank my grandmom for being awesome and cool.

Finally, I thank the two most important people in my life, my mom Chitra and dad Krishnamurthy for their infinite patience and letting me do whatever I want and for giving me life and their love. Both of you are awesome!

Microgrid Availability during Natural Disasters

Vaidyanathan Krishnamurthy, PhD

The University of Texas at Austin, 2014

Supervisor: Alexis Kwasinski

A common issue with the power grid during natural disasters is low availability. Many critical applications that are required during and after natural disasters, for rescue and logistical operations require highly available power supplies. Microgrids with distributed generation resources along with the grid provide promising solutions in order to improve the availability of power supply during natural disasters. However, distributed generators (DGs) such as diesel gensets depend on lifelines such as transportation networks whose behavior during disasters affects the genset fuel delivery systems and as a result affect the availability. Renewable sources depend on natural phenomena that have both deterministic as well as stochastic aspects to their behavior, which usually results in high variability in the output. Therefore DGs require energy storage in order to make them dispatchable sources. The microgrids availability depends on the availability characteristics of its distributed generators and energy storage and their dependent infrastructure, the distribution architecture and the power electronic interfaces. This dissertation presents models to evaluate the availability of power supply from the various distributed energy resources of a microgrid during natural disasters. The stochastic behavior of the distributed generators, storage and interfaces are modeled using Markov processes and the effect of the distribution network on availability is also considered. The presented models supported by empirical data can be hence used for microgrid planning.

Table of Contents

List of Tables

List of Figures

Chapter 1: Introduction

MOTIVATION:

Low reliability of the power system during and after natural disasters is of great concern as many critical applications such as hospitals and communication systems require a highly reliable power supply especially in the wake of a natural disaster. Also recent natural disasters like Super storm Sandy in 2012 and the Japanese earthquake of 2011, have raised doubts about the capability of conventional power grids to sustain operation of important services such as communications, rescue, oil refining and make sure they are not interrupted during disasters and in their aftermath. The common experience during disasters like tropical cyclones is that conventional power grids are fragile systems in which damage to less than 1% of their components can lead to extensive high-incidence outages [Fahimi et al. 2011] and it is likely that the grid is unavailable at the critical load mains tie and its neighboring area for several weeks. This fragility can be attributed to the bulk power grid's large geographical layout, combined with their centralized generation and control architectures. Examples for such cases are observed during hurricanes Katrina [Kwasinski et al. 2009] and Ike, the 2008 Sichuan earthquake in China [Tang 2008] and the 2011 earthquake and tsunami in Japan. Fig. 1.1 shows a telecommunication base station in Gilchrist, TX after Hurricane Ike in 2008. The main power at this site was out for about 2 weeks. The site had a diesel genset which had a capacity of 48 hours and a battery backup of 8 hours. The only road providing access to the site was unusable for about a week.

Fig. 1.1 Telecommunication base station after Hurricane Ike 2008.

Low reliability of the grid can be attributed to a number of reasons. Major factors that contribute to the low availability of the grid are its centralized control, inefficiencies introduced due to operation coordination over extensive area, aging components, insufficient or inhomogeneous infrastructure distribution which leads to insufficient generation and/or congestion, lack of active elements in transmission and distribution systems, lack of diverse power alternatives, lack of redundant paths in sub-transmission and distribution systems. Additionally, due to higher penetration of advanced loads, such as PHEVs availability issues are increased. Interdependencies between various lifelines can also introduce some availability issues and these issues become more prominent during extreme events like natural disasters. Such observations can be made in two prominent natural disasters of recent times such as the Chilean earthquake of 2010 and the Japanese earthquake of 2011[TCLEE 2012, Dueñas-Osorio and Kwasinski 2010].

Improving Power supply availability

Multiple solutions are possible in order to improve the power supply availability. They can be broadly classified into two major types:

1) Utility side solutions, which involve grid hardening techniques.

2) User side solutions, which include back-up or standby generators, energy storage, such as batteries, or in general, local generation in the form of microgrids, which is the primary focus of this dissertation.

MICROGRIDS

Overview

Microgrids have been prescribed as a way to improve power supply availability during natural disasters [Kwasinski et al. 2012]. Microgrids can be defined as follows:

Micro-grids are locally confined and independently controlled electric power grids in which a distribution network with a given architecture integrates distributed energy resources (DERs) with the loads.

That is integration of local distributed generators and energy storage devices and loads. A key fundamental difference with respect to conventional grids is that micro-grids add active network components at the distribution level of a power grid that provide more operational flexibility and reduce conventional power grids vulnerabilities caused by centralized generation and control architectures and long distances between power sources and loads.

Though a large spread of power outages are observed after many natural disasters, such as hurricanes, earthquakes and tsunamis, damage assessments indicate that areas with intense infrastructure and dwellings damage are generally a much smaller area than that observed with high-incidence power grid outages. Moreover, the damage distribution

is very inhomogeneous and with abrupt variations in the damage severity i.e. it is very common to find a zone with extreme damage surrounded just a few meters away by areas with little damage. These are two important observations that support the use of micro-grids to power electric loads during disasters from a user perspective because the fundamental problem for electricity consumers is the lack of powering alternatives—i.e. lack of diversity—to continuously power their loads other than conventional grids or stand-by power systems—commonly, diesel gensets. These stand-by systems also have reliability issues, such as a relatively high failure to start probability for gensets that limits stand-by power plants availability to about 0.9999 or 4-nines [Kwasinski 2011a] and the possibility that the microgrid components can themselves be damaged. These damages can be prevented by locating the sources strategically so that the chances of damage are very low and has been demonstrated in some cases. For example, during the earthquake and tsunami of March 2011 in Japan, a micro-grid in Sendai [Hirose et al. 2006] was able to maintain operation by powering its local loads shown in Fig. 1.2. Another notable example is the Verizon central office in Garden City, New York shown in Fig. 1.3

Fig. 1.2 Sendai NTT microgrid

Fig. 1.3. Microgrid in Garden City

Availability issues with Microgrids.

There are some other potential sources of problems that have been little explored in the past. Many microgrids generation technologies, such as engine generators or microturbines, depend on infrastructures called lifelines, such as roads or natural gas distribution networks. These lifelines may be affected by the disasters just like conventional grids. Energy storage may be used to reduce the lifeline dependencies as demonstrated in [Kwasinski 2011a] and another option is to rely on renewable energy sources, such as photovoltaic modules or wind turbines that do not depend on a lifeline. But there are limitations regarding the use of renewables because of their large footprints and sites may have limited space or relatively high power demand and the variable output of the renewables limits the application of renewable energy sources. Energy storage can again be used to address this variability issue as in the case of the lifelines but this added energy storage cost can significantly increase the micro-grid capital cost with respect to the micro-grid design intended for operation during normal conditions because well designed micro-grids may not have significant requirements in terms of energy storage in order to reach high availabilities [Kwasinski et al. 2012]. In order to make microgrids work as a reliable power supply alternative, the behavior of all the DERs, storage and lifelines put together must be understood. This research is intended toward the development of models, supported by data of recent natural disasters to understand the performance of microgrids under extreme events. The analysis here will focus on problems motivated by critical loads, which could be military bases, data centers, or hospitals, which require very high power availability because their downtime costs tend to be high. A better understanding of microgrid performance during natural disasters considering its various interdependencies and storage can function as a valuable tool for planners and operators of power supplies for critical loads.

Problem Statement:

The primary problem addressed in this dissertation is to develop models to calculate the availability of a microgrid during natural disasters i.e. find the probability that the loads served by a microgrid can be supported by the various resources available to the microgrid during a natural disaster.

Approach:

Figure 1.4 shows a simplified schematic of a typical microgrid considered for the analysis, which could have an ac, dc, or hybrid distribution system. It can be seen that all the loads and DERs are on the micro-grid side of the power electronic interface separating the grid from the micro-grid.

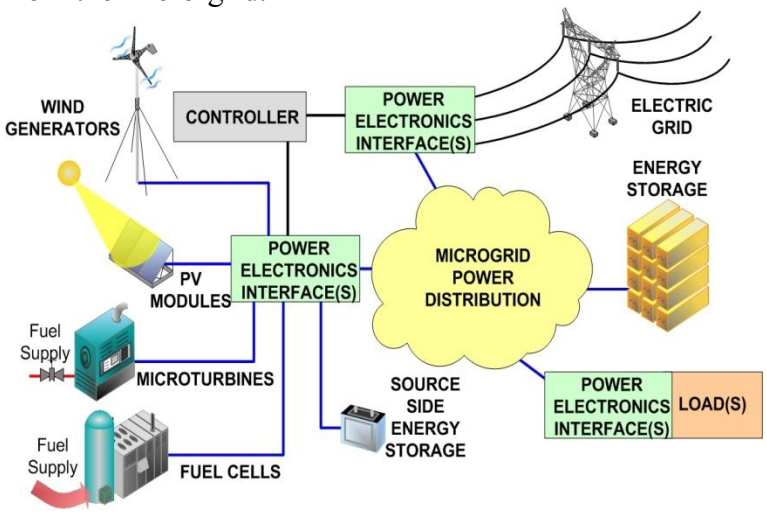

Fig. 1.4. General representation of a microgrid.

This interface acts as a boundary that provides electrical confinement to the microgrid and enables the analysis of the components in relative isolation. It also allows such a microgrid to meet interconnection standards [ieee1547] and operate in an island mode enhancing local power supply availability during natural disasters when grid outages are expected to happen [Kennedy 2009].

During natural disasters, microgrids are expected to operate in island mode and therefore, the power supply availability is predominately influenced by the microgrid's DERs performance [Tanrioven 2005]. The analysis will focus on the DERs and their availability dependency on the local energy storage and lifelines. As part of the analysis, evaluation of lifeline performance during natural disasters and their impact on micro-grids availability is also proposed. In order to construct the availability model, discrete time Markov chains are used to describe the evolution between the various failed and working states of the microgrid components as well as describing the evolution of the amount of energy in each storage unit of the microgrid.

CONTRIBUTIONS:

A key contribution of this research is representing the effect of two critical aspects affecting micro-grid availability during natural disasters and in their aftermath: lifelines performance and local energy storage contribution. The impact of energy storage on the DERs availability can be used as a measure of analyzing the dependency and energy storage can be used in reducing the dependency of the DERs performance on the lifelines performance in natural disasters. In chapter 5, this dissertation presents the modeling of the behavior of diesel gensets under deterministic and stochastic loads with fuel arrival facing delays with finite fuel storage capacity.

Another contribution of this research is the characterization of hurricane-caused power systems outages through the developed localized tropical cyclone intensity indices that enables power grid planners and operators to perform risk assessments in order to evaluate different infrastructure deployment alternatives or anticipate logistical needs during the recovery period after a tropical cyclone affects a given area.

Using the developed intensity indices, this dissertation derives a Markov chain model to calculate the main grid availability under various tropical cyclones conditions, which can help users plan and schedule various resources required for the operations during and in the aftermath of the natural disaster.

Finally, a major contribution of the dissertation is that it develops a framework for calculating the availability of a microgrid given its distribution architecture in the presence of various interfaces that forms part of the power management system or in the case of smart grids, also performs the role of power routing systems.

ORGANIZATION OF THE DISSERTATION

The rest of the dissertation is organized as follows. Chapters 2 and 3 discuss the behavior of the main power grid during natural disasters. Chapter 2 discusses the characterization of power system outage caused by tropical cyclones and Chapter 3 discusses the grid availability modeling at the main ties for a microgrid.

Chapter 4 provides a broad overview of the various distributed energy resources of a microgrid for their use in disaster conditions and develops the availability model for renewable energy power supply systems and the effects of storage on the availability is discussed.

In Chapter 5, the modeling of the diesel genset availability with storage and transportation delays is discussed.

In Chapter 6, the models developed for the DERs in the preceding chapters are used and the microgrid availability model is developed considering the distribution architecture of the microgrid and the various interfaces present in the microgrid distribution and results are discussed.

Using the availability models developed in the previous chapters, Chapter 7 presents cases studies for information and communication technology facilities during hurricanes. The availability models are validated using the empirical observations from hurricanes Katrina, Ike and Sandy considering the diesel fuel, and grid outages during these storms for central offices, cell sites and digital loop carriers.

Finally, Chapter 8 summarizes the dissertation with important conclusions that can be drawn from the models that were developed in Chapters 2 to 7 and discusses the scope for future work.

Chapter 2: Characterization of Outages Caused by Tropical Cyclones

This chapter discusses characterization of hurricane-caused outages in power systems through simple to calculate indices that represent hurricane intensity. With the proposed indices, power grid planners can perform risk assessments in order to evaluate different infrastructure deployment alternatives [Kwasinski et al. 2009] or system operators may anticipate logistical needs during the recovery period after a hurricane affects a given area. There are various methods to calculate hurricane intensity, such as the Saffir-Simpson (SS) scale [Saffir-Simpson], the National Oceanographic and Atmospheric Administration's (NOAA) experimental Saffir-Simpson scale [Saffir-Simpson], Hurricane Hazard Index (HHI) [Kantha 2006], Hurricane Surge Index (HSI) [Kantha 2006], generalized linear models [Liu et al .2007], generalized additive models [Han et al .2009], accelerated failure time models [Liu et al .2009a] and models using the Integrated Kinetic Energy [Hebert 2009] and various topological and statistical analysis in [Winkler et al. 2010-Galvan et al. 2009]. Due to its simplicity based on a five-level—or categories of which Category 1 [Kantha 2006] is the lowest, the SS scale has been the most popular method to measure hurricane intensity. Although the SS scale has been used many times to anticipate potential damage from a hurricane [Kantha 2006], it presents, however, inconsistencies when trying to use it as a way to assess the damaging potential of a hurricane on networked infrastructure, such as the power grid and telecommunications networks. Issues with this scale were discussed in [Kantha 2006] such as quantization errors that lead to incorrect classifications of vastly different hurricanes into the same category. The most devastating hurricane effects are caused by the storm surge [NOAA Surge], which is a body of water forced inland by the hurricane. The SS scale estimates expected surge levels for a hurricane of a given category but this

estimation is not very reliable as the scale fails to take into account many other factors that affect the storm surge, such as topographic characteristics [Kantha 2006] and hurricane atmospheric pressure and size [Kantha 2006]. Two notable examples are Ike (2008) which made landfall as a Category-2 hurricane [Saffir-Simpson] and Katrina (2005) [Kwasinski et al. 2009] which made landfall as a Category 3 hurricane and affected New Orleans with winds of a Category 1 storm, but their storm surge levels were in the range of a category 4 or 5 hurricane.

Of the other indices different from the SS, the HHI and HSI are only applicable over a large area spanning the entire storm diameter. The HHI is based on the total energy dissipated by the storm and the HSI calculates storm surge intensity based on the central pressure drop and multiplies it by the storm radius, which does not give any indication of the surge intensity in a specific area. In order to provide information on smaller geographical resolutions required for analyzing power system outages there is a need to develop indices that can be applied to scales smaller than the storm radius. The HHI considers the damaging potential of a hurricane to be proportional to the size of the hurricane, but Andrew (1992) which was a very intense hurricane in terms of localized infrastructure damage, was a small hurricane [NOAA 1999]. Reference [Zhu et al. 2007] discusses prediction of outages via storm surge modeling and [Powell et al.] explores wind destructive potential and surge destructive potential. Both models consider the total energy contained in the wind field but *a priori* there is no direct relation that indicates how the restoration process and average outage duration would be affected. Also, resiliency models developed in [Reed et al. 2009] using quality curves defined in [Bruneau] are limited to wind speeds. The effect of hurricanes on transmission lines have been studied in [Zhou 2006], [Liu and Singh 2009] and time varying failure rates have been generally studied [Moon et al. 2006], [Retterath et al. 2004] in order to analyze

distribution systems reliability. However, these studies do not provide a simple approach to estimate potential effects of hurricanes that could be used in a practical setting to plan network deployments or logistics.

This chapter presents indices that allow characterizing hurricane intensity with respect to the outages they cause on power grids. The goal is to develop indices that consider all relevant hurricane-damaging actions that are also simple to calculate. Initially, this chapter follows the approach in [Kantha 2006] and presents a General Localized Tropical Cyclone Intensity Index (GLTCII) that considers hurricane energy content and the time a given site is at least under tropical storm winds—maximum 1–minute average sustained winds at 10 meters above the surface between 39 and 73 mph. The study follows a classical empirical approach based on statistics from relevant hurricanes from the 2004, 2005 and 2008 Atlantic seasons: Charley, Dolly, Dennis, Frances, Jeanne, Gustav, Ike, Ivan, Katrina, Rita and Wilma. Power systems outage data are from the states of Texas, Louisiana and Florida. Pseudo confidence bands for each of the indices are provided. Results are interpreted within the context of the 2008 hurricanes Dolly, Gustav and Ike.

OUTAGE METRICS AND DATA VALIDATION

Outage Metrics:

One of the limitations found with the study of power systems outages during tropical storms or hurricanes is that commonly used outage metrics, such as those specified in IEEE 1366 [IEEE 1366], may be difficult to apply because those metrics refer only to distribution portions of the grid and because outages caused by tropical cyclones are considered to occur during a major event day, and, thus, they are excluded from all statistics. That is, metrics in IEEE 1366 may not represent well outage

characteristics during hurricanes. Hence, this work first introduces relevant outage metrics that are used in the analysis generated by tropical storm or hurricane conditions. In reality, the introduced outage metrics fit into those indicated in IEEE 859 [IEEE 859]. In order to provide consistency with the obtained outage data, outage metrics are considered for each county (or parish in the case of Louisiana). The outage metrics considered in this work are the maximum outage incidence percentage $O\%_{max,j}$: the restoration time $T_{r,\tau\,\%;j}$: and the average outage duration M_j: A more detailed description of these metrics is provided next.

Fig. 2.1. Area where all the power infrastructure was destroyed (Gilchrist, TX).

Maximum Outage Incidence:

This metric indicates the maximum number or percentage of electricity customers that lost power in county j. Consider that a county j is affected by hurricane h that causes outages. Outage data are first available at time $t_{start,h,j}$ and last available at time $t_{end,h,j}$. During the time interval $T_{|h,s} = [t_{start,h,j}, t_{end,h,j}]$, the number of customers without power in county j increases during a few hours until reaching a peak and then they decrease over several days. This varying number of outages in the sampled time t is $O_j(t)$. Thus, the maximum number of outages in county j during hurricane h and its aftermath is given by

$$O_{\max,j} = \max\{O_j(t) : t \in T_{|h,s}\} \tag{2.1}$$

Thus, if B_j represents the total number of customers in county j, then the maximum outage incidence percentage $O\%_{max,j}$ is

$$O\%_{\max,\,j} = 100\frac{O_{\max,\,j}}{B_j} \tag{2.2}$$

Restoration times:

They are the times needed to restore $\tau\%$ of the maximum number of outages in county j since those outages first peak. The absolute restoration time, $t_{rest,\tau\%,j}$, for an $\tau\%$ restoration and computed from the initial time $t_{start,h,j}$ is defined as

$$t_{rest,\tau\%,j} = \min\{t : O_j(t) \le (1-0.01\tau)O_{\max,j})\} \tag{2.3}$$

The relative restoration time $T_{r,\tau\%}$ with respect to the time $t_{max,j}$ when $O_{max,j}$ occurs is

$$T_{r,\tau\%} = t_{rest,\tau\%,j} - t_{max,j} \tag{2.4}$$

Observations during damage assessments after hurricanes Katrina, Dolly, Gustav, and Ike helped to properly consider some practical complexities in restoration time data and to provide additional empirical context to the analysis. One of these complexities is found in areas such as Gilchrist in Texas under the influence of Hurricane Ike in 2008, where all or almost all of the customers were lost from the hurricane (Fig. 2.1). These are, typically, relatively small areas affected by the hurricane storm surge. In these cases, the damage assessments indicate that power grid infrastructure can be completely rebuilt within 45 days after the hurricane. This restoration time limit was even observed in areas flooded by Hurricane Katrina, where loads could have been restored in about 3 weeks after the flood waters were drained within 3 to 4 weeks after the storm. Since overhead distribution lines were not excessively damaged in the flooded areas,, most of the long

restoration times were caused by damage caused in substations that were submerged in flood waters. The other of these complexities were caused by a second or, as it happened in Florida in 2004, a third hurricane affecting the same area before enough outages were restored, or before the infrastructure was restored to the same condition it had before the first hurricane struck the area—i.e., that only temporary repairs were made before a subsequent hurricane affected the area. The result of temporary repairs made immediately after a first—or primary—hurricane affected an area is that both outage incidence and restoration times of the hurricanes that followed—secondary or tertiary hurricanes—are not reliable data because the power grid infrastructure is in a more vulnerable condition than when the first hurricane struck. Hence, in these cases, data for the primary hurricanes and secondary or tertiary hurricanes are separated and only data from the primary hurricanes are considered in the analysis.

Average outage duration:

This metric indicates the average duration of an outage in county *j*. The average outage duration M_j for a county *j* is defined as

$$M_j = \frac{\int_{t_{start,j}}^{t_{end,h,j}} t f_j(t)dt}{\int_{t_{start,j}}^{t_{end,h,j}} f_j(t)dt}, j \in C \tag{2.5}$$

where $f_j(t)$ is a continuous non-negative function that approximates the evolution of the outage profile for each county. Two possible curve interpolation approaches were used for each available county outage data based on the best R^2 value: cubic splines or exponential curves.

Data Validation

Total number of customers:

Ideally, the total number of customers reported in each county or parish is expected to remain constant in all reports filed by the utilities for a same hurricane. However, data show differences in the total number of customers in different reporting periods. There are several possible explanations for this discrepancy in the total number of customers. The most common ones are miscommunications due to the difficult conditions in which utilities operate during and after a hurricane, errors in records, different reporting practices—e.g. reporting the total number of customers in affected feeders instead of total number of customers in all feeders in an affected county—and other operational and logistical priorities preceding outage reporting. Thus, outage data was evaluated for consistency in order to keep only those data points that could be considered valid based on a simple-to-test objective criteria. First, a total number of customers for each county needs to be considered. Hence, the total number of customers in each county was calculated as

$$B_j = \sum_{k \in \mathbf{K}_j} \max(B_{j,k}(t)) \tag{2.6}$$

where $B_{j,k}(t)$ is the number of reported customers in county j for utility k at time t and $\mathbf{K_j}$ the set of all utilities in county j.

Ratio test:

This simple test implemented in order to validate outage data, required that in each county the total number of electricity customers must be at least greater than the total number of housing units Γ_j indicated in [US Census 2008]. Data points not meeting this condition were discarded. Thus, the equation that represents the test performed to check each data point validity is:

$$B_j \geq \gamma \Gamma_j \tag{2.7}$$

where $\gamma = 1$. This selection for γ was considered to be a reasonably good compromise choice between having some data points with relatively small errors in the value for B_j and reducing the confidence in the statistical significance of the remaining data by eliminating an excessive number of data points that do not pass (2.7). That is, in the limit case when $B_j = \Gamma_j$ the relative error e_r made by considering that the total number of customers is the value B_j contained in the outage data instead of the actual value B_j^* is

$$e_r = \frac{B_j^* - \gamma \Gamma_j}{B_j^*} \tag{2.8}$$

Evidently, as γ is reduced, the relative error increases. Hence, γ could be increased above 1 in order to consider the contribution of industrial customers. However, the ratio of residential to industrial customers may change significantly from county to county so data processing becomes extremely complex and more prone to errors. Another issue with selecting $\gamma > 1$ relates with the fact that part of the problem to be solved here is a non linear least squares regression problem that attempts to find a curve that fits the outage observations. In order to numerically solve this part of the problem a trust-region-reflective algorithm was used. For a more numerically stable solution, it was found that the ratio of the number of data points to the number of parameters that define the fit curve needs to be greater than 10. But, as γ is increased fewer data points pass the test and the regression curves obtained in the analysis are less reliable than those obtained with a larger set of data points, even when some of these points may include some small relative error in B_j. Thus, it was found that a value of γ equal to 1 provides a reasonably good compromise solution between considering an exact number of electricity customers and using enough data points in order to find a suitable curve fit.

HURRICANE ACTIONS INFLUENCING OUTAGES

Four hurricane actions that influence outage incidence and/or duration are considered: storm surge, wind speed, size, and duration under at least tropical storm conditions. These actions may influence outage metrics from the damage they directly cause or from the influence they have in restoration logistic operations.

Storm Surge H:

A storm surge is a large volume of water that the hurricane forces inland. From [Tankut] the force acting on the objects by a surge of water of height H is proportional to H^2. Hence, its energy per unit length can be considered proportional to H^2. Storm surge effects are measured with respect to a reference value H_0 that is considered equal to 4 feet, which is the typical minimal storm surge of a category 1 hurricane. Since any changes in water level within the range 0 to H_0 would yield minor differences in damages to electrical infrastructure, then for all $H_i \leq H_0$ the ratio $H_i/H_0 = 1$, where H_i is the storm surge height at location i. Beyond the reference level, severity of storm surge effects on electrical equipment and supporting structures rapidly increases. Some of the highest recorded surges for the data set used for the analysis were about 16 feet and the outage incidences recorded at these points were 100%.

In the analysis presented here and for the locations under consideration, values for H_i were obtained using storm surge contour maps from NOAA's post storm analysis reports [Wang et al. 2005], [FEMA 2009], except in the case of Hurricane Gustav for which the ADCIRC storm surge simulation [ADCIRC 2009] was used because post storm data was incomplete. Other methods already available or under development can also be used to find the impact of the surge level on the system at the required location. There is a considerable amount of work already being done in storm surge modeling [Dawson et al. 2006] [Graber et al. 2006]. These estimates can be used to sufficiently

evaluate the index in cases where post storm data is not available or in anticipation of a storm. These surge estimation techniques have been shown to be around 20% accurate over a mile from the point of estimation [Glahnl et al.].

Maximum one minute sustained wind speed $V_{max,i}$ at location i

The wind kinetic energy is proportional to the square of the wind speed [Kantha 2006]. Since wind speed at a given point is not constant, unless indicated otherwise the analysis considers the value of the maximum sustained wind speed measured at 10 meters over the earth surface during a one-minute interval. To normalize this parameter, the minimum wind speed of a category 1 hurricane is used as a reference. Thus, $V_{max,0}$ = 74 mph. The maximum wind speed contours [Powell et al. 1998], [H*wind] indicate the maximum wind speeds experienced at each point over the entire storm period. These contours generated by 1-minute "best track" for all hurricanes and 10-minutes "best track" for Jeanne are used to find $V_{max,i}$. This 10-minutes value is based on the World Meteorological Organization recommendation and is, typically, a slightly lower value than the 1-minute value used by the U.S. National Hurricane Center.

Time under Storm Conditions $T_{TS,i}$ at location i

It has been known that the damaging potential of a hurricane is dependent on its translation speed [Kantha 2006]. The faster it moves, the shorter the time a given point is under damaging winds. Time duration under at least tropical storm conditions $T_{TS,i}$ is considered because it is about at this wind speed that logistic operations involved in deploying repair crews start to be affected due to safety concerns. The $T_{TS,i}$ is normalized using a reference $T_{TS,0}$ =12 hours. The wind fields are obtained from H*Wind analysis [Powell et al. 1998], [H*wind]. This wind field snapshots are used to find the first instant $t_{fp,h,i}$ that a location i comes under the influence of the tropical storm winds and the last

instant $t_{lp,h,i}$ that the same location i is under the influence of the tropical storm winds. Then, T_{TS} is given by

$$T_{TS,i} = t_{lp,h,i} - t_{fp,h,i} \tag{2.9}$$

Note: if $V_{max,i} < V_{th}$, $T_{TS,i} = 1$.

A_h, Area swept on land by hurricane h

A_h is the total area of land that experiences maximum wind speeds over V_{th} mph, which, in this case, it was considered equal to the lower bound of tropical storm wind speeds of 39 mph. The area A_h is considered here because the bigger a hurricane swept area is, the more complex survey and repair logistic operations are. Hence, it is reasonable to expect that larger hurricanes lead to longer repair times. The maximum wind speed contours [Powell et al. 1998], [H*wind] were used to find the area swept by a hurricane. A_h is normalized to a reference area A_0 which is defined as the area swept by at least tropical storm winds of a typical category 1 hurricane with a fixed radius of 150 miles moving at an average speed of 12.5 mph in 12 hrs therefore A_0 = 35,342 mi^2.

Hurricane action parameters evaluation

As mentioned earlier, outage data was available for each county or parish, depending on the state. However, in some cases, such as large counties, the value of each of the four relevant hurricane actions may change somewhat within each county or parish. Hence, the value considered for each hurricane action in each county is their weighted average with respect to the portion of the area occupied in each county or parish. That is, if $\boldsymbol{I_j}$ is the set of all locations in county j and the weight factor is α, then

$$H_j = \sum_{i \in I_j} \alpha_i H_i \tag{2.10}$$

$$V_{\max,j} = \sum_{i \in I_j} \alpha_i V_{\max,i} \tag{2.11}$$

$$\text{and } T_{TS,j} = \sum_{i \in I_j} \alpha_i T_{TS,i} \tag{2.12}$$

DATA ANALYSIS

General Local Tropical Cyclone Intensity Index(GLTCII)

On a first simple approach and based on the energy content of each hurricane damaging action, the *GLTCII* at a location *i* is intuitively formulated similar to that in [Kantha 2006] as:

$$GLTCII_i = \left[\frac{H_i}{H_0}\right]^2 \left[\frac{V_{\max i}}{V_{\max 0}}\right]^2 \left[\frac{T_{TS\,i}}{T_{TS0}}\right] \left[\frac{A_h}{A_0}\right] \tag{2.13}$$

The following R^2 values are obtained for various outage metrics when the outage data was compared with the *GLTCII*. For $O\%_{max}$, $R^2 = 0.78$; for $T_{r,95\%}$, $R^2 = 0.5$; for $T_{r,98\%}$, $R^2 = 0.45$; for *M,* $R^2 = 0.37$.

Regression Analysis: LTCII versus $O\%_{max}$,T_r and M:

Although some of the R^2 values yielded by (2.13) are reasonably good, regression analysis was used to find forms for the *LTCII* that yield better correlation with the curves that approximates the distribution of the data points. For simplicity of notation let $H = x_1 = H_i/H_0$, $V = x_2 = V_{\max,i}/V_{\max,0}$, $T = x_3 = T_{TS,i}/T_{TS0}$, $A = x_4 = A_h/A_0$ be the normalized values with respect to $\{H_0, V_{th}, T_{TS0}, A_0\} = \{4, 38, 12, 35342\}$. The basis function for the regression analysis is built as the following response surface model.

$$\begin{aligned} LTCII = {} & p_1 x_1 + p_2 x_2 + p_3 x_3 + p_4 x_4 + p_5 x_1 x_2 + \ldots \\ & + p_{20} x_1^2 x_2^2 x_3^2 x_4^2 + p_{21} x_1 x_2^2 x_3 x_4 + p_{22} x_1 x_2 x_3^2 x_4 \\ & + p_{23} x_1^2 x_2^2 + p_{24} x_1^2 x_2^2 x_3 \end{aligned} \tag{2.14}$$

where p_h are the coefficients that are to be found. When p_{18}=1 and the rest of the coefficients are 0, (2.14) is (2.13). Other forms of (2.14) may provide better results but they are more complex because they involve more terms. Also, as mentioned above the

number of parameters that can be obtained is limited by the number of data points available in the data set.

Procedure to find LTCII for each of the outage metrics:

- Step 1: Formulate the basis:

Let D_i, be the ith observed value of the outage metric D, where **D** is the set of all outage metrics; i.e., $\mathbf{D}= \{O\%_{max}, T_{r,95\%}, T_{r,98\%}, M\}$. For the maximum outage incidence—i.e. $D=\{O\%_{max}\}$—a logistic curve is proposed as a general fit based on the observed distribution of data points

$$Y: y_1(LTCII_i) = \frac{1}{1+e^{-a(L_i-b)}} \tag{2.15}$$

where Y is the fitted curve for $O\%_{max}$, L_i equals $\log(LTCII_i)$ and $a,b \in \Re$ are parameters that need to be determined. The values for Y and $O\%_{max}$ are percentage values so when they are normalized to 1 they lie in the interval [0, 1], thus $k_1 = 1$.

For D equal to $\{T_{r,95\%}\}$, $\{T_{r,98\%}\}$ or $\{M\}$ a third order polynomial form is proposed:

$$Y: y_2(LTCII_i) = a_3 L_i^{\,3} + a_2 L_i^{\,2} + a_1 L_i + a_0 \tag{2.16}$$

where Y now is the fitting curve for $T_{r,95\%}$, $T_{r,98\%}$, or M, $L_i = LTCII_i$ and a_3, a_2, a_1, and a_o are real number parameters that need to be determined. In both (2.15) and (2.16) the general basis for the *LTCII* is given in (2.14).

- Step2: Combine Bases for LTCII and Y:

For $D = O\%_{max}$ let $\mathbf{z}= \{a, b, \mathbf{p}\}, \mathbf{p} \in \Re^{24}$. From (2.14) and (2.15) with $k_1 = 1$:

$$g_1(\mathbf{z}) = \frac{1}{1+e^{-a(\log(p_1x_1+p_2x_2+\ldots+p_{24}x_1^{\,2}x_2^{\,2}x_3)-b)}} \tag{2.17}$$

where **x** is the set of normalized hurricane damaging actions at a particular location i; i.e., $\mathbf{x} = \{x_1, x_2, x_3, x_4\}$.

For D equal to $\{T_{r,95\%}\}$, $\{T_{r,98\%}\}$ or $\{M\}$, let $\mathbf{z} = \{a_3, a_2, a_1, a_o, \mathbf{p}\}$, with $\mathbf{p} \in \Re^{24}$ and using (2.14) and (2.16):

$$g_2(\mathbf{z}) = a_3(p_1x_1 + p_2x_2 + ..)^3 + ...a_0 \qquad (2.18)$$

- *Step 3: Solve for the parameters i.e.* **z**:

The functions LTCII, y_1 and y_2 are found by solving a least squares problem which is described by the objective function $e(\mathbf{z})$ given by

$$e = \sum_i (g_i(z) - D_i)^2 \qquad (2.19)$$

Then the problem involves finding the minimum of $e(\mathbf{z})$. I.e.,

$$e^* = \min_{z \geq 0} \sum_i (g_i(z) - D_i)^2 \qquad (2.20)$$

With **z** known, the optimum fitting curves y_1 and y_2 for specific indices *LTCII* in (2.15) and (2.16) can now be known.

Metrics for goodness of fit:

Two metrics are used to estimate the goodness of fit of the regression curves obtained by the above analysis.

a) R^2, the coefficient of determination.

b) r_s

The proportion of residuals of the regression fit whose magnitude is less than s times the maximum observed value of the outage metric. In the analysis $s = 0.2$ and $s = 0.1$ are used.

Implications of the regression analysis

Since for each outage metric D the regression analysis yields a different set **p** of coefficients p, then for each D there are different forms of *LTCII* within the general

family of *LTCII*s represented by (2.14). Hence, new specific *LTCII* are named for each particular metric *D*. These specific *LTCII* are detailed next.

$LTCII_{MOI}$:

This is the specific *LTCII* for the maximum outage incidence. Points satisfying (2.6) and (2.7) were considered and the $O\%_{max}$ for these points were plotted vs. $L=log\ (LTCII_{MOI})$ in Fig. 2.2. In this plot, $LTCII_{MOI}$ is given by

$$LTCII_{MOI}=111V+120V+107VA+15VHA+359V^2T \qquad (2.21)$$

because this form was the solution for the least squares problem (2.21). That is, (2.21) yields the best R^2 values for *Y* when considering $O\%_{max}$. The resulting logistic curve indicated by (2.15) with a = 2.6 and b = 5.8, and $L = log\ (LTCII_{MOI})$ with $LTCII_{MOI}$ given in (2.21) is also shown in Fig. 2.2. The results of the curve fitting process are summarized in Table 2.1.. The logistic growth function obtained has an R^2 = 0.80 and r_s = 0.83 for s = 0.2. Larger deviations from the fit occur at lower $LTCII_{MOI}$ values where the storm is less intense and damage is expected to be milder. Yet, despite these expectations, wide disperse data are observed.

Sensitivity of the maximum outages to the maximum sustained wind speeds *V* in a given location can be easily observed from the $LTCII_{MOI}$ equation in (2.21) obtained from the regression analysis. The maximum sustained wind speeds are a common factor in the LTCII. Therefore, for a given set of values for the hurricane actions *H*, *T* and *A*, the wind speeds can be scaled to produce various LTCII conditions and therefore get various outage incidence values depending only on the wind speed. That is $LTCII_{MOI} \propto V$. This makes the evaluation of the sensitivity of the LTCII and hence the maximum outage incidence to the hurricane wind speed a simple characterization.

LTCII$_{Trτ}$:

Two specific *LTCII* are found for the 95 % and 98 % completed restoration times. These *LTCII* obtained for the τ% restoration times are collectively called $LTCII_{Tr\tau}$. Thus, for $\tau = 95$ the index is called $LTCII_{Tr95}$ and for $\tau = 98$ the index is called $LTCII_{Tr98}$. Using the basis in (2.14) and (2.16), a polynomial fit was obtained for each of the restoration times with R^2 of *0.65* and $r_{0.2}$=*0.91* for both $T_{r,95\%}$ and $T_{r,98\%}$. The values of **a** for $T_{r,95\%}$ are **a** $=\{a_3,a_2,a_1,a_0\}=\{0,\ 9.0095\ 10^{-3},\ 0.2,\ 0\}$. The values of **a** for $T_{r,98\%}$ are **a** $=\{a_3,a_2,a_1,a_0\}=\{0,\ 9.8314\ 10^{-3},\ 0.2,\ 0.137\}$. Their outcome as a result of solving the least squares problem is

$$LTCII_{Tr95}=14V+2TA+2V^2T \tag{2.22}$$

$$LTCII_{Tr98}=15V+2VT+TA \tag{2.23}$$

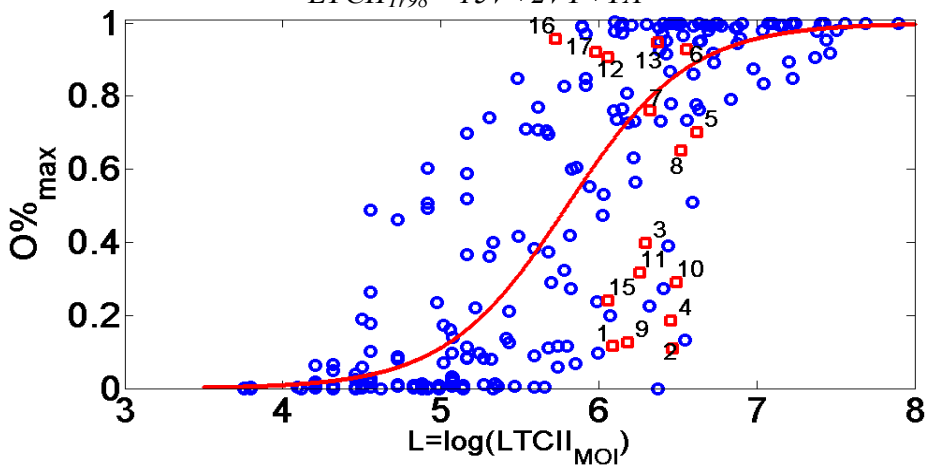

Fig. 2.2 $O\%_{max}$ vs. L

Figure 2.3 shows the observed points for $T_{r,95\%}$ and the curve fit Y given by (2.16) versus $LTCII_{Tr95}$, whereas Fig. 2.4 shows the same respective information but for the 98% restoration time. Restoration times are influenced not only by damage intensity but also by "soft" factors, such as management policies, logistical strategies, and restoration techniques employed by utilities. This may be the fundamental reason why R^2 results for

restoration times are somewhat lower than those for the outage intensity. Still, as anticipated, both $LTCII_{Tr\tau}$ depend on all damaging actions that are expected to influence logistical and restoration operations, such as hurricane size A, except for the storm surge height, which despite being the leading action that causes more severe damage, the damage is almost always limited to relatively small areas (narrow coastal strips).

$LTCII_{AOD}$ versus Average Outage Duration M:

This is the specific *LTCII* for the average outage duration. Following the same aforementioned process, it was found that in (2.18) the fitting curve is a 3rd degree polynomial with $\mathbf{a} = \{a_3, a_2, a_1, a_0\} = \{0, 0, 0.28, 0\}$ and the $LTCII_{AOD}$ equal to

$$LTCII_{AOD}=3V+4VA+4V^2T \tag{2.24}$$

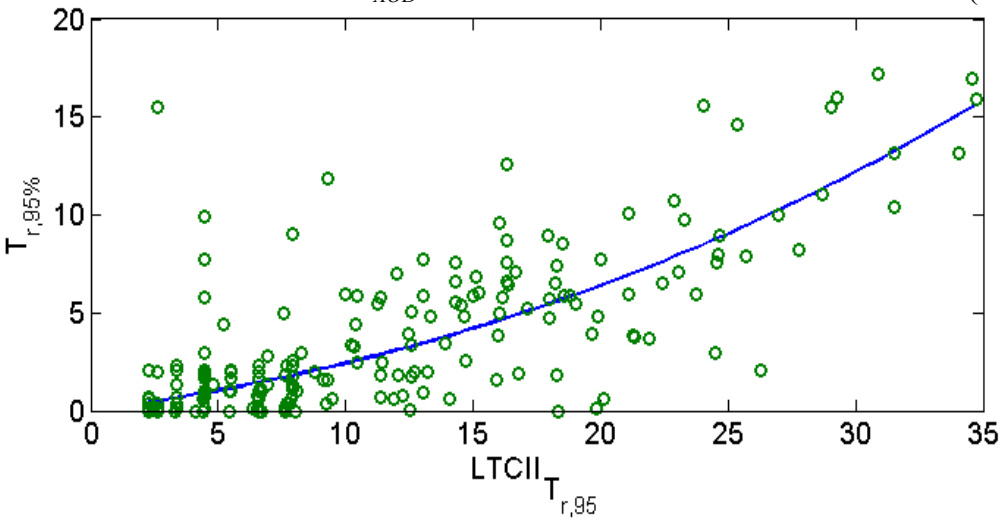

Fig. 2. 3. $T_{r,95\%}$ vs. $LTCII_{Tr95}$

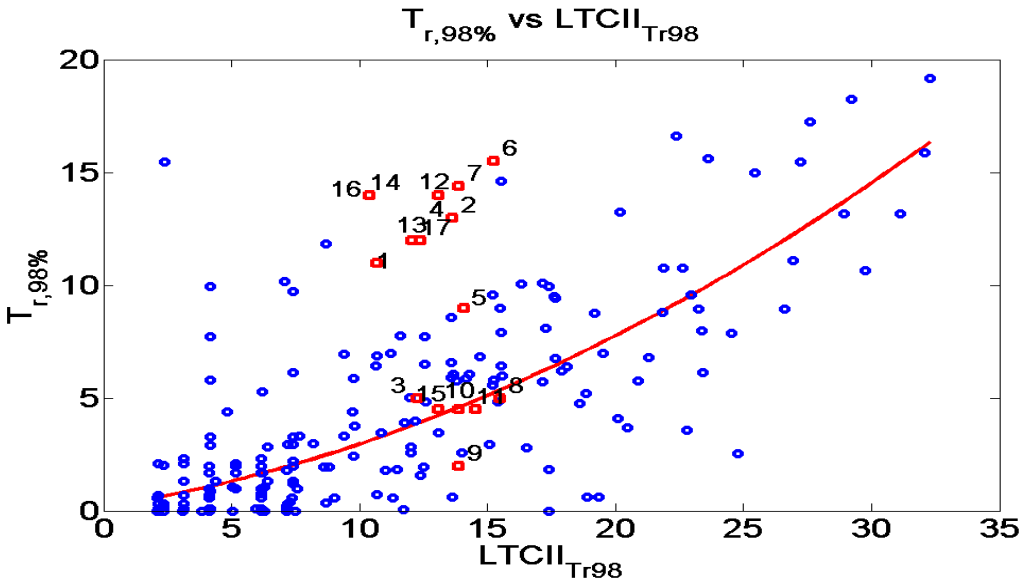

Fig. 2.4. $T_{r,98\%}$ vs. $LTCII_{Tr98}$

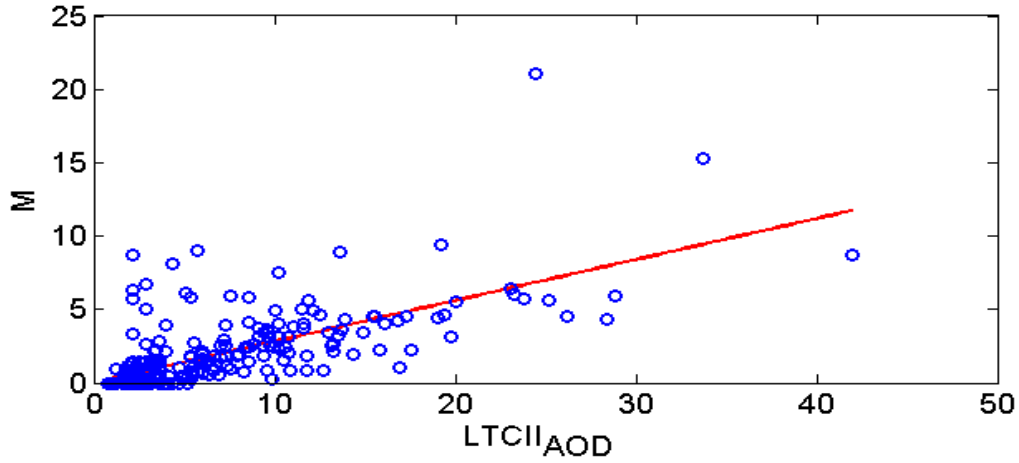

Fig. 2.5. *M* versus $LTCII_{AOD}$

The metrics for goodness of the found fitting curve is $R^2 = 0.51$ and $r_{0.2} = 0.96$. The resulting plot with observed data and fitting curve is shown in Fig. 2.5. Like both $LTCII_{Tr\tau}$ this *LTCII* depends on all damaging actions that are expected to influence logistical and restoration operations and it does not depend on the storm surge height.

CASE STUDIES

Outage metric	Fitting curve equation	Index Equation	R^2	$r_{0.2}$	$r_{0.1}$
$O\%_{max}$	(2.15)$L=log(LTCIII_{MOI})$	(2.21)	0.80	0.83	0.7
$T_{r,95\%}$	(2.16)$L=LTCIII_{Tr95}$	(2.22)	0.65	0.91	0.8
$T_{r,98\%}$	(2.16)$L=LTCIII_{Tr98}$	(2.23)	0.65	0.91	0.78
M	(2.16)$L=LTCIII_{AOD}$	(2.24)	0.51	0.96	0.9

Table 2.1: Curve Fit Results: R^2, $r_{0.2}$ and $r_{0.1}$

A brief account of the outage and their corresponding *LTCII* for the three last hurricanes to directly strike the U.S. coast in 2008—Dolly, Gustav, and Ike—is presented in this section. In general, larger deviations of the data from the regression curves in Figs. 2.2 to 2.5 is observed at lower values of *LTCII*, which occurred in fringe regions where storm intensity diminished and in places at the edge of the hurricane/tropical storm wind-fields. However, the presented statistics show a remarkable high correlation considering the fact that, as it is going to be shown, most of the area affected by a hurricane and with widely varying outage incidence and restoration times show relatively very little damage.

Dolly made landfall in Cameron County, Texas on July 23rd, 2008 as a Category 1 hurricane on the SS scale with wind-speeds of 85 mph. Gustav struck Louisiana on September 1st, 2008 as a Category 2 hurricane on the SS scale with maximum sustained wind-speeds of 110 mph. Finally, Ike's eye made landfall on the northern tip of Galveston Island in Texas on September 13th, 2008. At the time of landfall Ike was as a category 2 hurricane on the SS scale. However, its storm surge was similar to what it is expected in a much stronger hurricane. Dolly's and Ike's peak outage incidence are

shown in Figs. 2.6 (a) and 2.9 (a) and the variation of the $log(LTCII_{MOI})$ are shown in Figs. 2.6 (b) and 2.9 (b) respectively. The average outage duration maps are given in Figs. 2.7 (a) and 2.10 (a) and the $LTCII_{AOD}$ contours are given in Figs. 2.7 (b) and 2.10 (b), respectively. Percentage of damaged power infrastructure obtained from field damage assessments for Dolly and Ike are shown in Figs. 2.8 and 2.11, respectively. Similar maps to those shown here were also produced for Gustav. Comparison of the maps showing the $log(LTCII_{MOI})$ contour and the percentage of damage power infrastructure indicate a moderate relationship between damage to more than 1 % of the power grid components and values for $log(LTCII_{MOI})$ equal or higher than 7. In these areas the maps also show that the maximum outage incidence in almost all counties or parishes is higher than 95 %. However, it is also possible to observe that large variations of outage incidence, ranging from small percentages to total blackout, in areas where the percentage of damage infrastructure components is less than 1 % and where it is possible to observe important variations in $log(LTCII_{MOI})$. This observation leads to two important conclusions. The first conclusion confirms results in [Albert et al. 2004] and demonstrates that the electric power grid is a very fragile system in which less than 1 % of component failures may lead to total blackouts. The second conclusion highlights the merits of the indices presented here because it is possible to observe a high correlation (R^2 = 0.8) between maximum outage incidence and $log(LTCII_{MOI})$ despite the fact that in areas with $log(LTCII_{MOI})$ less than 7 the percentage of electric grid's damaged components is homogeneously small. One aspect that may contribute to this high correlation is based on the fact that from (2.21), $log(LTCII_{MOI})$ depends on all damaging actions influencing the intensity of a hurricane but none of these actions represent in an indirect way other factors that may affect maximum outage incidence, as it occurs with the restoration times, that depends not only on the grid and hurricane characteristics, but

they are also influenced by "soft" factors that depend on human decision processes, such as logistical management of the restoration process.

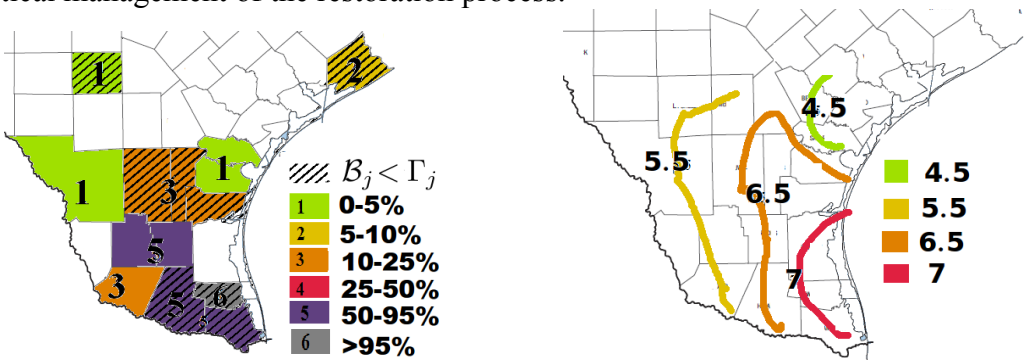

Fig. 2.6. Hurricane Dolly, Texas (a) Maximum Outages (b) *log(LTCII$_{MOI}$)*

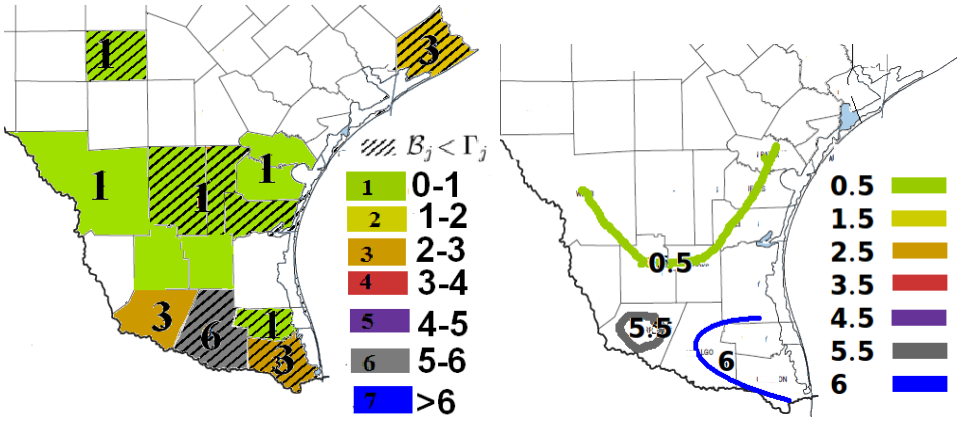

Fig. 2.7. Hurricane Dolly, Texas (a) Average Outage Duration (days) (b) *LTCII$_{AOD}$*

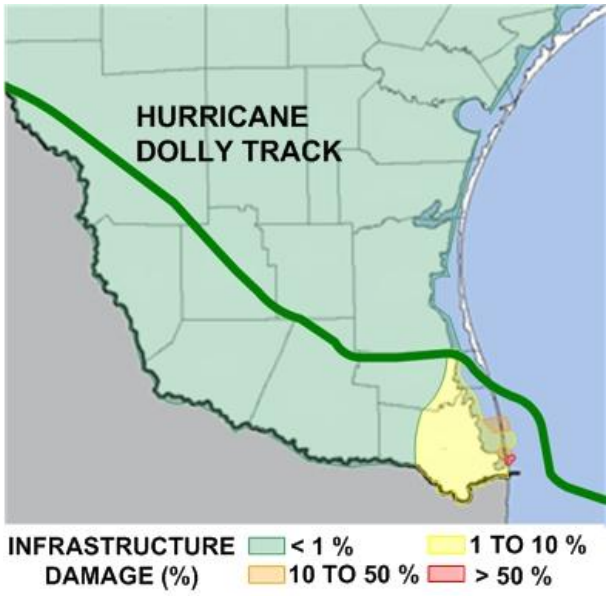

Fig. 2.8. Power infrastructure damage intensity caused by Hurricane Dolly.

Influence of indirect factors external to the hurricane or the grid characteristics may explain why correlation for the $LTCII_{AOD}$ values is not as high as for the $log(LTCII_{MOI})$. In particular, logistical and management based on human decisions may influence restoration times and affect the uniform comparison of different hurricanes. In the case studies presented here, it was observed that for Gustav and Ike, $LTCII_{AOD}$ values of 4.5 or higher relate to more than 1 % of damaged infrastructure components and average outage durations of about 6 days or longer. However, in Dolly it is possible to observe somewhat shorter outage durations for values of $LTCII_{AOD}$ equal to 4.5 or higher. One explanation for this discrepancy can be found in the fact that restoration process with Dolly may have been simpler than in the case of Gustav or Ike because with Dolly there were fewer counties affected by the disaster. Restoration operations and logistics management may also contribute to produce a more dispersed outcome in terms of the $LTCII_{AOD}$ when compared with the $log(LTCII_{MOI})$, particularly in fringe regions where the hurricane is dissipating or in places that are at the edge of the hurricane wind-fields.

Figures 2.2 and 2.4 also display points corresponding to preliminary data of some counties affected by Hurricane Sandy (in red squares). Numbers are used to indicate the following counties and boroughs: New York: Bronx 1, Brooklyn 2, Manhattan 3, Queens 4, Staten Island 5, Nassau 6, Suffolk 7; New Jersey: Atlantic 8, Camden 9, Cape May 10, Cumberland 11, Hunterdon 12, Monmouth 13, Morris 14, Salem 15, Sussex 16 and Warren 17. In Fig. 2.2, it can be seen that points 1 to 4 corresponding to areas in New York City with substantial underground power infrastructure have, as expected, outage incidences much lower than the regression curve. Figure 2.4 shows statistically unusual long restoration times in some areas. Longer restoration times in areas 1, 2 and 4 may be explained by the high percentage of underground power facilities. However, at this point it is unknown the reason for the statistically longer restoration times in other areas, such as Long Island (points 6 and 7) where power infrastructure is mostly overhead.

CONCLUSIONS

This chapter has discussed the characterization of hurricane-caused power systems outages through localized tropical cyclone intensity indices. The analysis uses a empirical statistical approach based on data from the 2004, 2005 and 2008 hurricane seasons. Four outage metrics are defined for each county or parish: maximum outage incidence, 95% restoration time, 98% restoration time, and average outage duration. First, a generalized index *GLTCII* was introduced considering four relevant characteristics of a tropical cyclone: storm surge, maximum sustained wind speeds, size, and time of influence under damaging winds. Then, improved specific indices for each outage metric were derived through a curve fitting process that involves solving a least squares problem in order to find the curve parameters. These new four indices are called $LTCII_{MOI}$, $LTCII_{Tr95}$, $LTCII_{Tr98}$ *and* $LTCII_{AOD}$ for each outage metric $O\%_{max}$, $T_{r,95\%}$, $T_{r,98\%}$ and M

respectively. A high correlation with an R^2 of 0.80 is observed in the maximum outage incidence, which follow a logistic curve with respect to $log(LTCII_{MOI})$. The residual $r_{0.2}$ is evaluated to equal 0.83. These are relatively very well correlated fitting curves considering the fact that damage assessments have observed a relatively uniform damage distribution in power grids with a wide range of power outage incidence occurring with fewer than 1 % of the grid components damaged. The observed restoration times fit a 3rd degree polynomial with respect to $LTCII_{Tr\tau}$ with an R^2 of 0.65. It is considered that these more moderate correlations observed in the regression curves for the restoration times are caused by the effect of external human dependent "soft" factors associated with restoration logistical operation management that are added to intrinsic grid characteristics influencing infrastructure damage intensity. The average outage duration M fits a 3rd degree polynomial with respect to $LTCII_{AOD}$ with an R^2 of 0.51 and $r_{0.2}$ = 0.96. Future work will focus on adjusting the fitting curves considering more data points from new storms.

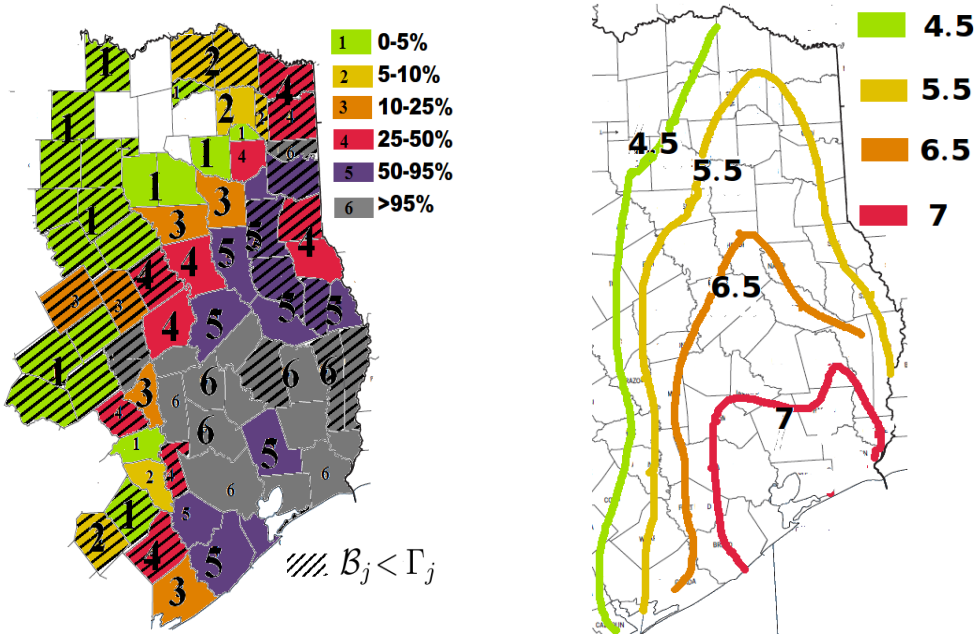

Fig. 2. 9. Hurricane Ike,Texas: (a) Maximum Outages (b) $log(LTCII_{MOI})$

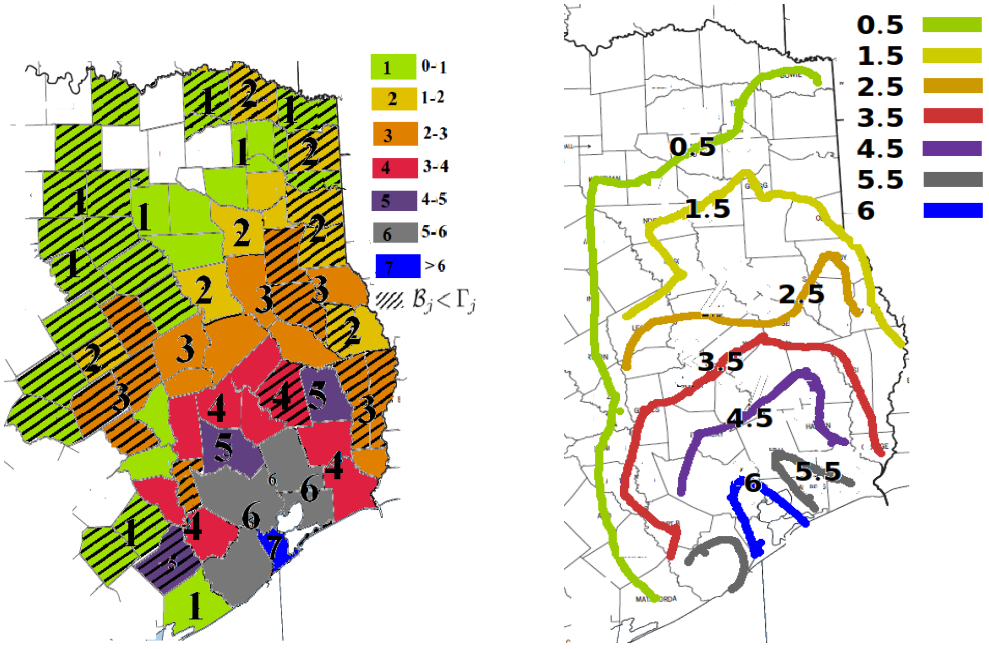

Fig. 2.10. Hurricane Ike, Texas: (a) Average Outage Duration (in days) (b) $LTCII_{AOD}$

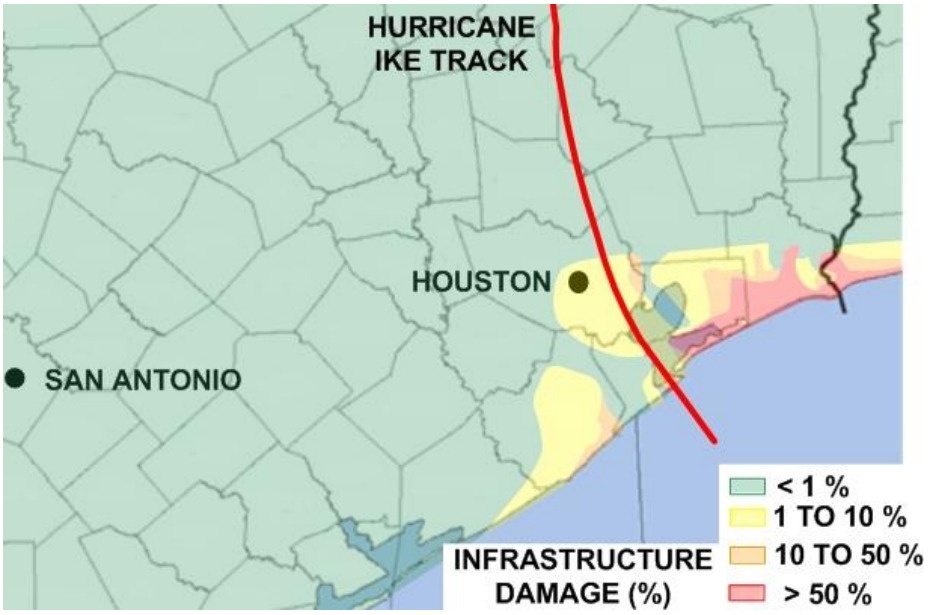

Fig. 2.11. Power infrastructure damage intensity caused by Hurricane Ike.

Chapter 3: Main Grid Availability during Tropical Cyclones

This chapter develops a model for calculating the grid availability during tropical cyclones using a Markov chain. First the grid availability model using Markov chains is described, then the model is evaluated for historical power system outage data observed in hurricanes from 2004-2008 in Texas, Louisiana and Florida.

MARKOV CHAIN MODEL OF THE GRID FOR CALCULATING GRID AVAILABILITY:

A diagram of a power supply system that has the grid is shown in Fig. 3.1. The three components transmission, substation and distribution represent the collective infrastructure used to transport power to the load. The grid is in a working state when all these components are working and the grid fails when one or more of these components are failed. From the perspective of the user, two states: grid on or grid off are all that are required to calculate the grid availability. Traditionally, in normal operating conditions, the two state model is sufficient in order to characterize the grid availability. However during extreme condition such as tropical cyclones this is not sufficient for the following reasons. This 2 state model does not account for the arrival of the next hazard and the failure time given a certain hazard has occurred and the amount of time the hazardous conditions exist. Therefore here, the grid availability model is built of a single hazard event.

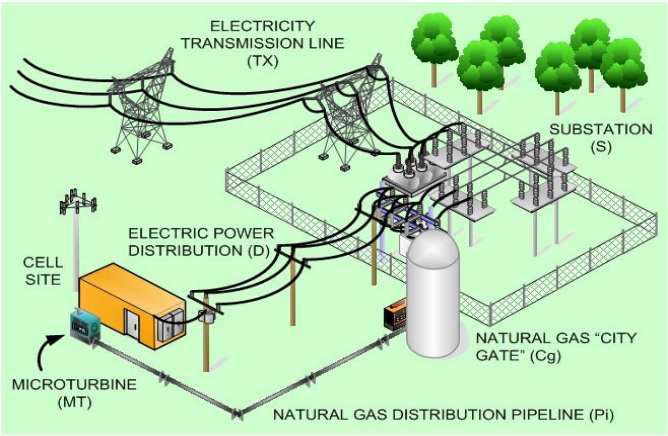

Fig. 3.1 Grid feeding a cell site schematic supported by a micro turbine

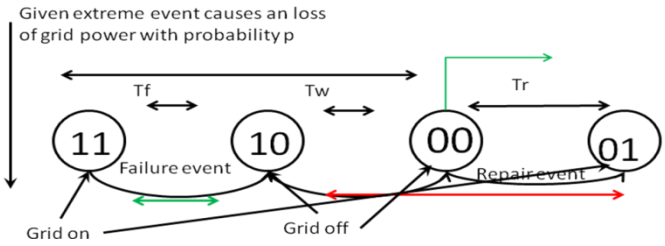

Fig. 3.2 Markov chain state transition diagram for calculating grid availability in a microgrid

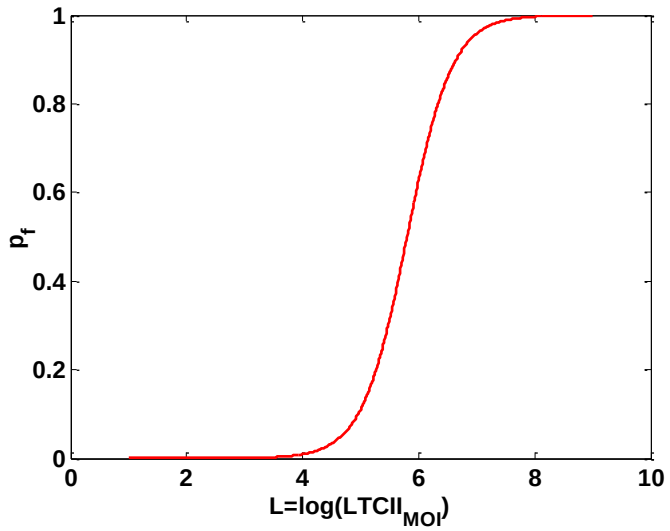

Fig.3.3 Grid outage probability given hazard intensity

The 2-state grid model is modified to include the existence of an extreme event of a given intensity which in turn becomes a 4-state model as shown in Fig. 3.2. The state space with 4 states is represented using a 2 bit binary number where the MSB indicates the presence of a hurricane, and the second bit the state of the grid. Therefore the first state indicated by 11 represents the state where there is a hurricane present and the grid is in the ON state. The second state 10 represents the failed grid and the presence of hurricane conditions. The third state 00 represent the condition when the hurricane conditions have dissipated and the grid is OFF. The final state represents the grid being restored after the hurricane conditions have subsided.

The Markov chain model for the grid behavior using the failure time T_f, wait time T_w and repair time T_r distributions for an extreme event of given intensity can be represented by the stochastic system in Fig. 3.2 with the initial conditions that of the grid being in state grid on. Failure time is the time taken for a gird outage to occur given the grid was working when it came under the influence of a hurricane causing outages and under the condition such that under the condition imposed by that hurricane a grid outage will occur with probability p_f. The probability that a grid outage will occur is calculated as follows.

In chapter 2 [Krishnamurthy and Kwasinski 2013], characterization of power systems outage caused by hurricanes was derived for the maximum outage incidence in a localized geographical area caused by a hurricane given the four damaging actions: maximum wind speed, storm surge, exposure time to at least tropical storm conditions and the area affected by tropical storm winds. The grid outage probability given tropical cyclone intensity can be calculated using [Krishnamurthy and Kwasinski 2013]

$$p_f = \frac{1}{1+e^{-a(L_i-b)}} \tag{3.1}$$

From [Krishnamurthy and Kwasinski 2013] a = 2.6 and b = 5.8 and L_i=log($LTCII_{MOIi}$) where

$$LTCII_{MOi} = 111V + 120VH + 107VA + 15VHA + 359V^2T \tag{3.2}$$

V the maximum wind speed, T is the exposure time under at least tropical storm conditions, H is the storm surge height and A is the total area of land exposed to at least tropical storm winds[Krishnamurthy and Kwasinski 2013]. The plot of L versus the outage probability is given in Fig. 3.3.

In the Markov chain state transition diagram given that an outage will occur for a given hurricane intensity, the transition probabilities are governed by the probability mass functions of the event times T_F, T_W and T_R. The instantaneous probability of an event occurring is calculated as follows in (3.3)

$$p_i = \frac{f_i}{1-F_i} = \frac{f_i}{1-\sum_{j<i} f_j} \tag{3.3}$$

The p_i in (3.3) represents the instantaneous probability in discrete time that the event described by f is going to occur given that it has not occurred. This can be termed as the discrete hazard rate. If failure and repair time distributions are used, then the function p_i is the discrete failure rate, discrete repair rate.

Since the failure, wait and repair times are arbitrary with finite support the resulting Markov chain has additional clock state which keeps track of the time spent in each state. The resulting state transition diagram is shown in Fig. 3.4.

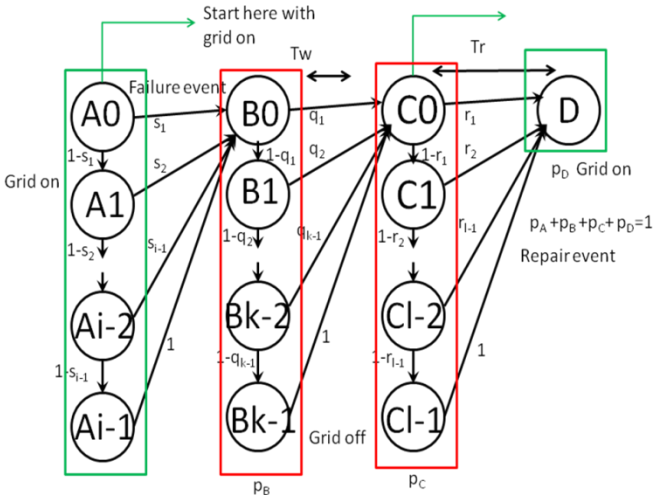

Fig.3.4 . State transition diagram for the evolution of the grid during a tropical cyclone the chain occurs with probability p_f

The states of Fig. 3.2 are relabeled as *A*, *B*, *C*, and *D* in Fig. 3.4 along with a number indicating the time spent in each of the states. The probability of the grid being on given that an outage will occur with probability p_f is $p_A(t)+p_D(t)$. The transient solution to grid availability under given intensity given that an outage will occur is [Kulkarni 2010]

$$\boldsymbol{\pi}_{\mathbf{grid}}(t+1) = \boldsymbol{\pi}_{\mathbf{grid}}(t)\mathbf{P}_{\mathbf{grid}} \tag{3.4}$$

With $\boldsymbol{\pi}_{\mathbf{grid}}(t) = [\pi_{A0} \quad \pi_{A1} \quad \ldots \quad \pi_D]$ and $\boldsymbol{\pi}_{\mathbf{grid}}(t)$ is the probability is distribution over that state space in Fig. 3.4 at time *t* and $\mathbf{P}_{\mathbf{grid}}$ is the one-step transition probability matrix which is given by

$$\mathbf{P}_{\mathbf{grid}} = \begin{bmatrix} 0 & 1-s_1 & 0 & \cdots & s_1 & 0 & \cdots & & \cdots & & & 0 \\ 0 & 0 & 1-s_2 & \cdots & s_2 & 0 & & & & & & \\ & & \ddots & \cdots & \vdots & 0 & \cdots & & \ddots & & & \vdots \\ & & & \ddots & 1 & 0 & \cdots & & \cdots & & & \\ & & & & \ddots & 1-q_1 & 0 & \cdots & q_1 & 0 & 0 & 0 \\ \vdots & \vdots & \vdots & \vdots & & \ddots & 1-q_2 & \cdots & q_2 & 0 & 0 & 0 \\ & & & & & & \ddots & \cdots & \vdots & \vdots & \vdots & \vdots \\ & & & & & & & \ddots & 1 & 0 & 0 & 0 \\ & & & & & & & & \ddots & 1-r_1 & \cdots & r_1 \\ & & & & & & & & & \ddots & \cdots & \vdots \\ & & & & & & & & & & \ddots & 1 \\ 0 & & \cdots & & \cdots & & & \cdots & & & & 1 \end{bmatrix} \quad (3.5)$$

The grid availability function versus time is found with the initial conditions that the grid was in a working condition. The initial conditions are given by

$$\boldsymbol{\pi}_{\mathbf{grid}}(0) = \begin{bmatrix} 1 & 0 & \dots & 0 \end{bmatrix} \quad (3.6)$$

The probabilities in the states of Fig. 3.2 are calculated as $p_A(t) = \sum_{j=0,\dots,i-1} \pi_{Ai}(t)$, $p_B(t) = \sum_{j=0,\dots,k-1} \pi_{Bj}(t)$ and $p_C(t) = \sum_{j=0,\dots,l-1} \pi_{Cj}(t)$

The total grid availability is therefore

$$A_{grid}(t) = p_f\,(p_A(t) + p_D(t)) + 1 - p_f \quad (3.7)$$

The numerical results are given next.

NUMERICAL STUDIES FOR DATA HURRICANES FROM 2004-2008

Estimation of the Failure, Wait and Repair time distributions and rates:

The failure, wait and repair times are obtained using the power system outage time series from the hurricane in the years 2004 to 2008. Due to limited data, the LTCII range is discretized and the data is grouped into clusters based on their LTCII values. The

discretized clusters are labeled as C1 through C6. The values and the corresponding outage probabilities are given in Table 3.1.

The symmetric triangular distribution is used to fit the failure, wait and repair time distribution. The equation for the triangular distribution used here is

$$g(t)=\begin{cases}\dfrac{2t}{bc} & 0\le t\le c\\ \dfrac{2(b-t)}{b(b-c)} & c<t\le b\\ 0 & t>b\end{cases} \tag{3.8}$$

Since the distribution is taken to be symmetric the $b=2c$ and c is the mean of the distribution. This triangular distribution is discretized and used in the Markov chain model.

The discretization formula is

$$f_i=\int_i^{i+1} g(t)dt, i=0,1,2...b-1 \tag{3.9}$$

A histogram of the data for each cluster is given in figures 3.5, 3.6 and 3.7. The resulting parameters computed from the data for each of the clusters C1 through C6 are given in Tables 3.2, 3.3 and 3.4. The resulting distributions are plotted in figures 3.8, 3.9 and 3.10. Using these distributions as input the availability function of the grid is calculated for each value of $LTCII_{MOI.}$

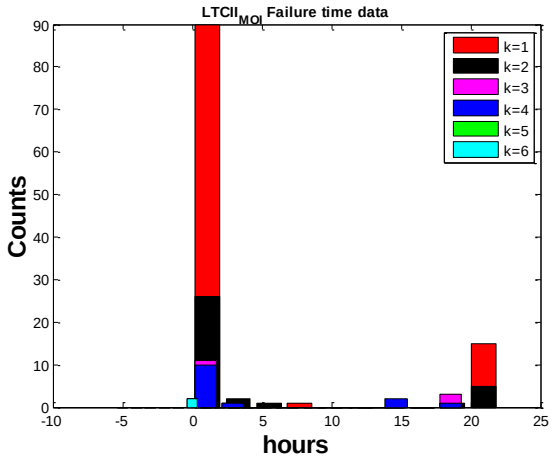

Fig. 3.5 Failure time data for each cluster

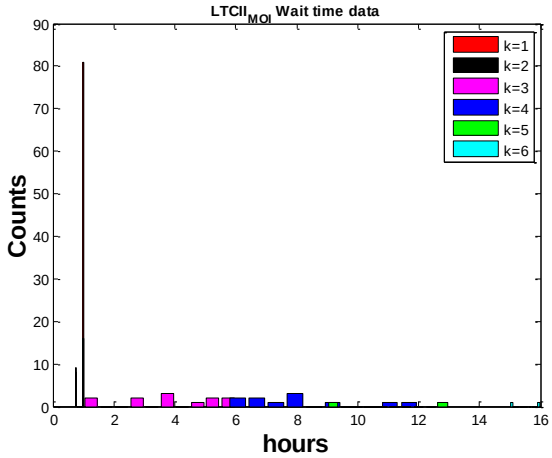

Fig. 3.6 Wait time data for each cluster

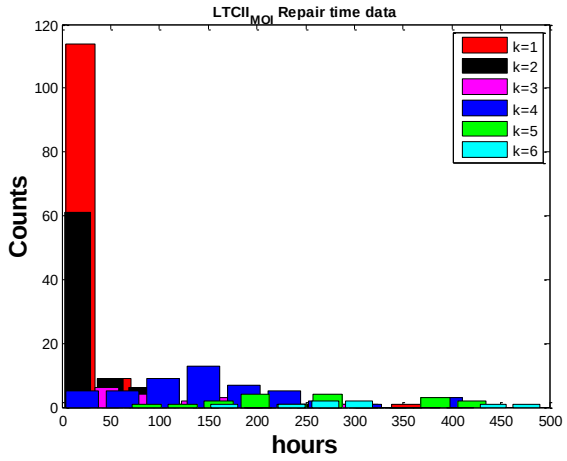

Fig 3.7 Repair time data for each cluster.

Cluster no.	C1	C2	C3	C4	C5	C6
L Range	<4.39	4.39 to 5.0234	5.0234 to 5.6568	5.6568 to 6.2903	6.2903 to 6.9237	>6.9237
p_f	<0.0249	0.0249 to 0.1172	0.1172 to 0.4080	0.4080 to 0.7816	0.7816 to 0.9489	>0.9489

Table 3.1: $LTCII_{MOI}$ discretized clusters and the corresponding range of outage probabilities

Cluster	Mean Failure time	Mean Wait time	Mean Repair time
C1	2.6264	0.99342	8.8459
C2	4.3869	0.90152	26.2252
C3	5.9605	1.825	71.31
C4	3.8904	6.3167	130.5399
C5	1	10	188.1839
C6	1	15.5	309.365

Table 3.2 Failure time, wait time and repair time means

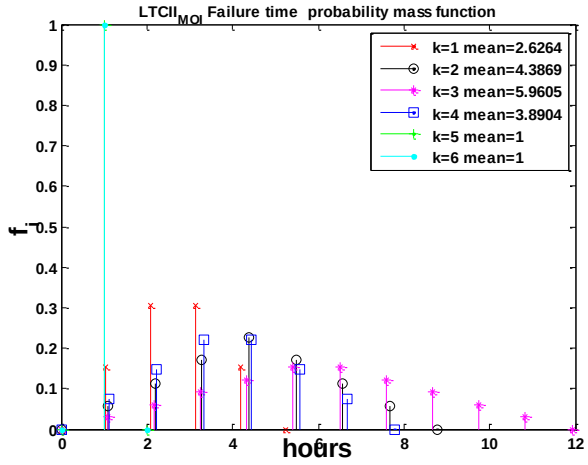

Fig 3.8. Failure time distributions for the $LTCII_{MOI}$ outage model

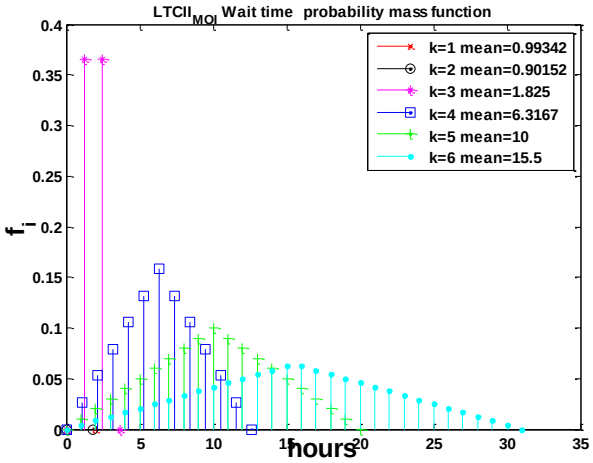

Fig 3.9. Wait time distributions for the $LTCII_{MOI}$ outage model

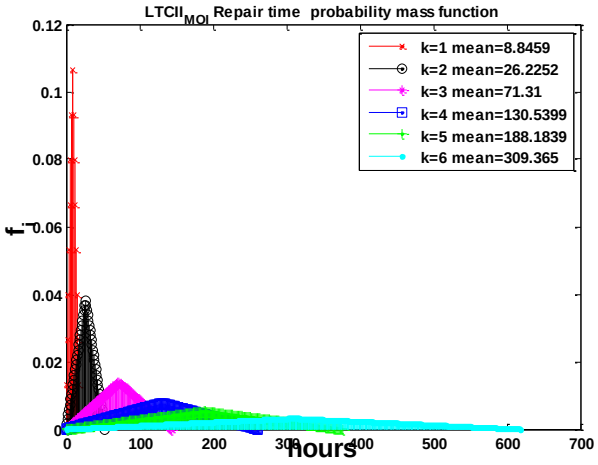

Fig. 3.10 Repair time distributions for the $LTCII_{MOI}$ outage model

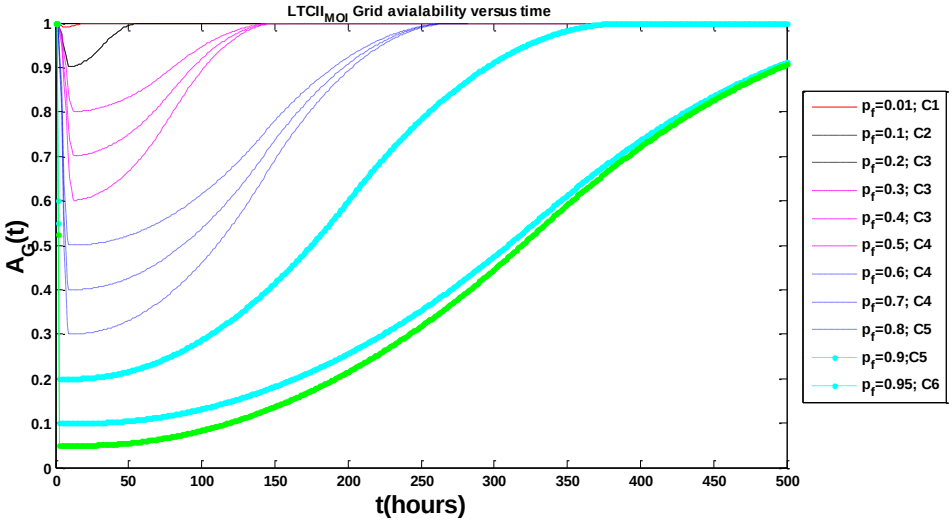

Fig 3.11 Grid availability versus time for various outage probabilities

Results for grid availability:

The availability of the grid at any location depends on the LTCII condition experienced by that location and the type of rate model used for the repair and failure rates. In order to find the grid availability based on the LTCII first decide which repair and failure function to use i.e. for a given location in question. In practice, if one wants to

know the availability of the grid under effect of a hurricane characterized with the inputs H, V, T and A (the normalized hurricanes actions storm surge height, maximum sustained wind speeds, exposure time and Area swept by the hurricane on land), the corresponding LTCII needs to be calculated and the failure and repair rate functions derived above for the range the LTCII belongs need to be used.

The procedure is detailed as follows,

1) Obtain H, V, T, and A for the location under consideration.

2) Compute the $LTCII_{MOI}$.

3) Calculate the failure probability p_f.

4) Find the cluster in which the computed $LTCII_{MOI.}$

5) Calculate the failure, wait and repair time distribution parameters for that cluster.

6) Find the failure and repair rate using the discrete hazard function (3.3).

7) Construct the transition probability matrix given in (3.5) and find the solution to (3.4).

8) Find the overall grid availability using (3.6).

From Fig. 3.11 it can be seen that the availability function of the grid for higher $LTCII_{MOI}$ is lower than that for lower values of $LTCII_{MOI.}$ These availability curves can be used as inputs for designing back up generation to improve overall power supply availability to the load.

CONCLUSIONS

This chapter presented a Markov chain model for calculating the availability of the grid during tropical cyclones. The model uses data from hurricanes from 2004 to 2008 to obtain the transition probabilities in the model for calculating the grid

availability. The hurricane intensity defined by the $LTCII_{MOI}$ was used to calculate the outage probability. It was seen that with a growing $LTCII_{MOI}$ value the grid availability worsens. This availability model can be used to design the backup system to improve the overall power supply availability at the load.

Chapter 4: Microgrid Distributed Energy Resources: Energy Sources, Storages and Renewables

This chapter discusses two main topics: a) the distributed energy resources of a microgrid and b) renewables energy sources and storage and their availability modeling with focus on PV systems.

DISTRIBUTED ENERGY RESOURCES IN A MICROGRID

Energy Sources

Renewables:

Renewable energy sources include photovoltaics, wind power plants, hydro power, bio fuels and geothermal power, photovoltaics and wind are two of the most popularly used [Song et al. 2013] and are also considered as prime candidates for their low green house emissions [Varaiya et al. 2011][Hatziargyriou and Zervos 2001]. Renewable energy sources are being considered for many microgrid application such as military bases [Sandia 2013] and telecommunication bases stations [NTT Docomo 2012][NTT 2013a]. Renewable energy sources, however, have intermittent power supply due to inherent variability present in the natural phenomena that govern their energy output [Kwasinski et al. 2012]. In the aftermath of the Japanese earthquake of 2011, Japanese telecom provider has started building green bases starting and resilient base stations [NTT 2013].

Micro-turbines, Diesel gensets and Portable generators

Micro-turbines, diesel gensets and portable generators are widely used distributed generation solutions especially as backup power supply. Micro-turbines can run on various types of fuels for example natural gas, biogas and propane [Capstone]. The efficacy and reliable use in improving power supply availability during natural disasters

is dependent on the type of natural disaster and the operating conditions imposed in the aftermath of the disaster. This is primarily because of the dependency on external infrastructure called lifelines. Lifeline interdependence is a wide area of research and it is critical in understanding the behavior of microgrid in normal operating conditions and in extreme events like natural disasters. During natural disasters, the dependency on lifelines increases due to the reduced power supply availability form the main grid. The lifelines impacted during natural disasters can be different depending on type of the disasters. For example in hurricanes like Gustav, extensive outages were prevented by using fixed natural gas generators which did not need refueling due to the presence of gas pipes which are largely unaffected during hurricanes [Kwasinski 2011b], however during earthquakes natural gas supply can be affected due to damage to gas pipelines [Kwasinski 2011b].

Fig. 4.1 DLC with small genset Hurricane Ike.

Fig. 4.2 DLC with temporary diesel genset installed after Hurricane Ike.

As mentioned before back-up power is extremely important during natural disasters. During the 2011 Japan earthquake, in the Tohoku region, there were 220 base stations out of service on March 11, the first day of the earthquake, with a rapid increase to 6270 in one day due to power supply issues, that is due to drained batteries resulting from extended power outages [NTT Docomo 2012]

Fig 4.3 A portable genset powering a base station near the town of Saichi [TCLEE 2012].

Portable generators are a useful solution for of deploying power for sites that have lost power during natural disasters. For example, NTT DoCoMo deployed 30 truck carried generators and about 400 portable gensets [TCLEE 2012] in the aftermath of the Japanese 2011 earthquake. For example, Fig. 4.3 shows a portable genset used to power a base station near the town of Saichi [TCLEE 2012].

Fuel cells

Fuel cells are another option that can be considered while choosing sources for microgrid applications. They have also been suggested as support or even replacements diesel gensets as backup power sources [Spink and Saathoff 2013,Gagge 2008]. Examples of fuel cells used during Hurricane Isaac in New Orleans and in Garden City in New York during Irene and Sandy shown in Figs. 4.4 and 4.5. With the diminishing use of nuclear power in Japan post the Japan earthquake of 2011, fuel cells are becoming a contender for possible power supply solutions[Fuel Cell today 2013].

Fig. 4.4 Fuel Cell deployed for DLC after Hurricane Isaac.

Fig. 4.5 Verizon CO fuel cell Irene Sandy

Storage

Energy storage maybe classified into the following types based on the mechanism of storage. However a particular type of technology might fit in more than one category.

1) Electrical storage which include batteries and ultra-capacitors
2) Mechanical energy storage which flywheels, compressed air.
3) Chemical energy storage which include natural gas, batteries, diesel, gasoline, fuel cells. Chemical energy storage mechanisms like fuel and batteries are some of the most common for DGs like diesel gensets, natural gas turbines and RESs like solar and wind.

Various storage devices can be compared using the Ragone plot [Ragone] given in Fig. 4.6.

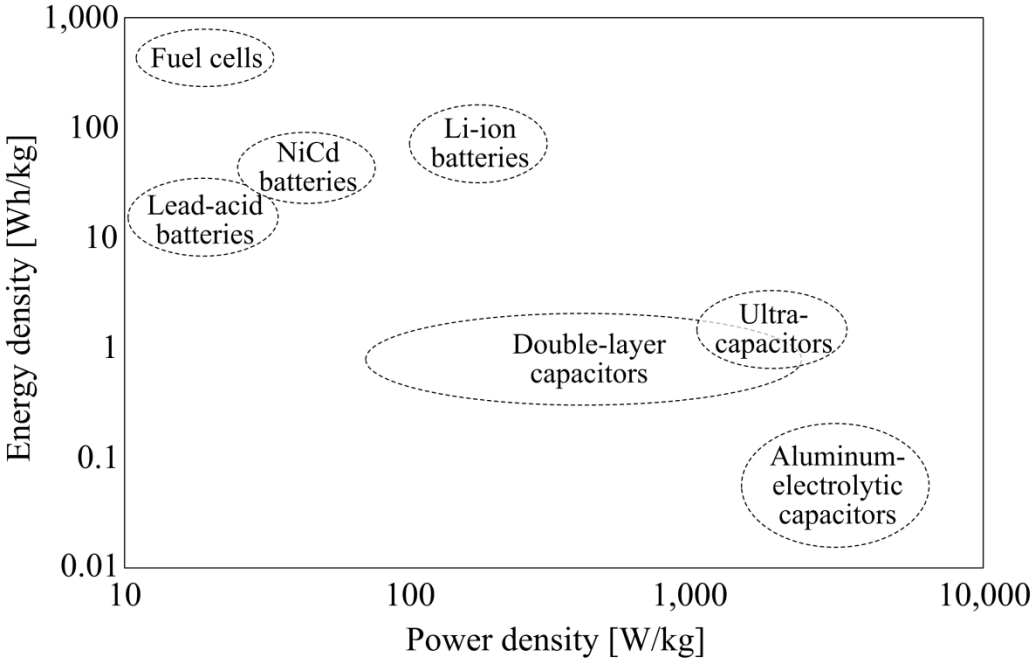

Fig 4.6 Ragone plot of various storage devices [Song et al. 2013.]

Operational and practical considerations for electrical energy storage

Storage is expected to decouple the microgrid from the dependence on external power. The availability of power to the microgrid itself serves as a measure of this dependency Storage is said to effectively decouple the external dependency of a microgrid on its lifeline if the availability of power supply to a microgrid from the DER is high even for a lifeline with low availability. In the following chapter that discusses the modeling of fuel supply to diesel genset; it will be shown that even for small availabilities of the lifeline the presence of any storage can improve the availability multifold. This improvement in availability is same in the case of DER without lifeline but with variable input like renewables. The availability improvement brought about by the storage is however dependent on the operation of the microgrid or the DER itself. In the case of diesel genset the fuel delivery could be dependent on the amount of fuel present in the tank or fuel orders could occur independent of the fuel state. Efficiencies of

the DER and the charging and discharging efficiencies of electrical storage affect the energy available to the load in the microgrid. Therefore during the design stage and during the operation of the storage, these practical aspects need to be considered while evaluating the availability,

AVAILABILITY OF RENEWABLES ENERGY SOURCES WITH STORAGE

Definition Renewable Energy Power Supply (REPS) system is the renewable energy source such as a PV or a wind turbine and generator along with its associated storage.

Availability of REPS system

Definition Availability *A(t)* at time *t* is defined as the probability that at time *t,* the load demand is met by the REPS. Unavailability is the probability that the load demand is not met i.e. *U(t)=1-A(t)*.In the absence of storage, the equation for availability of a REPS system with a collection of renewable energy sources and loads without energy storage is

$$A(t) = P(\sum_i X_{i(t)} \geq L(t)) \tag{4.1}$$

If the sum of the total energy produced by the sources is less than the load energy demand then some storage is required to support the loads for those times. Let B(t) be the energy content of a storage device supporting the load. The availability equation for the REPS system including the energy storage is

$$A(t) = P(\sum_i X_{i(t)} + \sum_i B_i(t) \geq L(t)) \tag{4.2}$$

Let $f_X(t)$, $f_B(t)$ and $f_{-L}(t)$ be the probability mass function of the source, battery SOC and the load demand at time *t*. Assuming that the load is independent of the fuel arrivals the availability is given by

$$A(t) = \sum_{g<0} f_G$$
$$f_G = f_X * f_B * f_{-L} \tag{4.3}$$

The assumption that the load and the PV input (insolation) can sometimes be invalid, which would mean that the convolution formula in (4.3) cannot be used. However this issue can be easily overcome by first obtaining the distributions f_B and finding f_G by simulation. For the remainder of this dissertation the PV input is assumed to be independent of the load.

RENEWABLE ENERGY SYSTEM OR RENEWABLE ENERGY POWER SUPPLY SYSTEM, AVAILABILITY MODELING

The equations for the energy transfer dynamics are as follows. Let X be the power output from the PV panel. Let L be the load. Then the energy transferred to and from the battery is given by

$$\Delta(t) = X(t) - L(t) \tag{4.4}$$

When $\Delta > 0$, energy is transferred to the battery i.e. the battery charges and when, $\Delta < 0$ energy is transferred out of the battery i.e. the battery discharges.

The battery state of charge evolves as follows

$$B(t+1) = B(t) + \Delta(t)$$
$$0 \le B(t) \le C \tag{4.5}$$

Efficiency and Degradation of Electrical storage: impact on availability modeling and sizing of storage

Charge and discharge efficiency

Charge and discharge efficiency plays an important role in the storage sizing. For non unity efficiencies the amount of energy lost per storage cycle can be high. For example suppose the $\Delta = 10$ J and the charging efficiency is $\eta_i < 1$ say 0.9 then the energy transferred to the battery is $= \eta_i \Delta = 0.9 \times 10 = 90$ and now let the energy demand

be 10 J and the discharge efficiency be $\eta_o < 1$ say 0.9, then the amount of energy drained out of the battery is $= (1/\eta_o)\Delta = 1/0.9 \times 10 = 11.111$ J

$$B(t+1) = B(t) + \eta_\Delta \Delta(t)$$
$$0 \le B(t) \le C \tag{4.6}$$

η_Δ is the charge/discharge efficiency, if the charging efficiency is η_i and discharge efficiency is η_o then for $\Delta > 0$, $\eta_\Delta = \eta_i$ and for $\Delta < 0, \eta_\Delta = 1/\eta_o$

Capacity degradation

Over the life of the battery the amount energy that can be stored in the battery decreases. There are a number of reasons which include corrosion and temperature.

An example of the geographical variation with battery life performance due to environmental conditions is given in Fig. 4.7 Song et al. 2013.

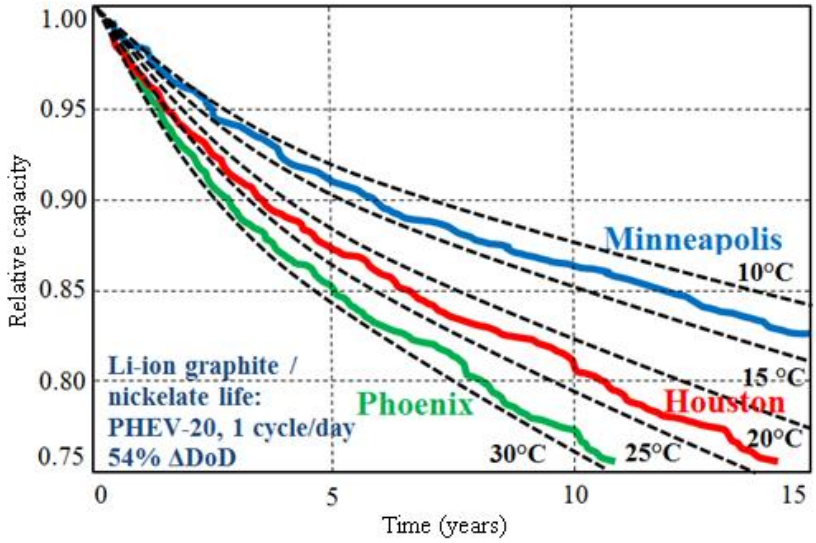

Fig. 4.7 Geographical impact on battery life due to temperature variation and humidity and atmospheric conditions and availability [Song et al. 2013]

In the Markov chain model for storage is given. First the degradation is ignored and the efficiency is set to unity.

Markov chain energy storage model for calculating availability

From (4.5) it can be seen that the future of the battery state of charge depends on the present value of the battery SOC which means that the changes in the battery SOC are Markovian in nature. The battery SOC change is completely governed by the value of Δ. Given the statistics of Δ the probability mass function for the battery SOC can be known. The statistics of Δ is given by the statistics of the PV and the load which is given next.

PV Statistics

Insolation for the PV panels is collected for 7 months in Austin, TX. The input power to the PV panel is given in Fig. 4.8. The corresponding histogram is given in Fig. 4.9. The panel is assumed to have an efficiency of 15%. With a total installed capacity of 10 kW. The mean PV input per unit area is 260 W/m^2. The area of the panel is adjusted such that the mean power output given the efficiency and capacity is 1.05 kW. The parameters for the installed PV array are given in table 4.1. The resulting PV output is given in Fig. 4.10.

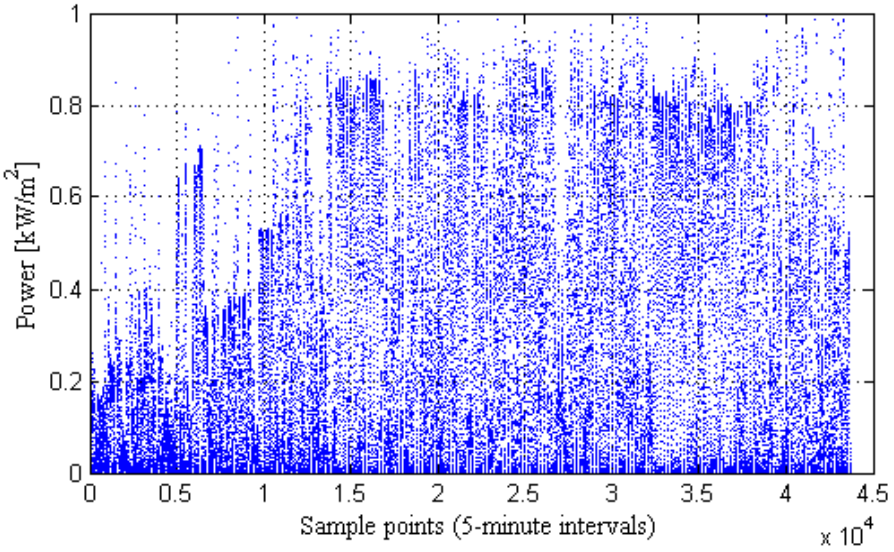

Fig. 4.8 PV Incident power collected from 7:00am to 7:00pm for 7 months. [Song et al. 2013]

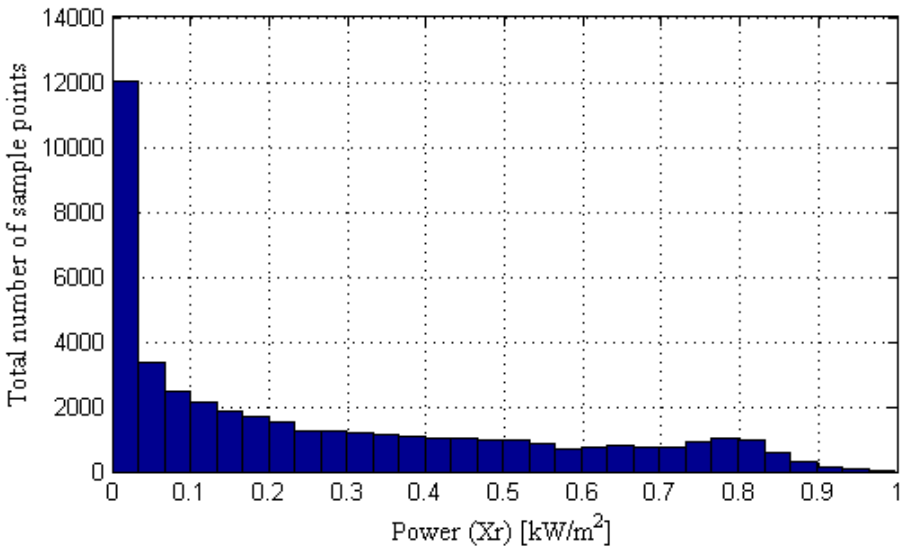

Fig. 4.9 Histogram of incident PV power [Song et al. 2013]

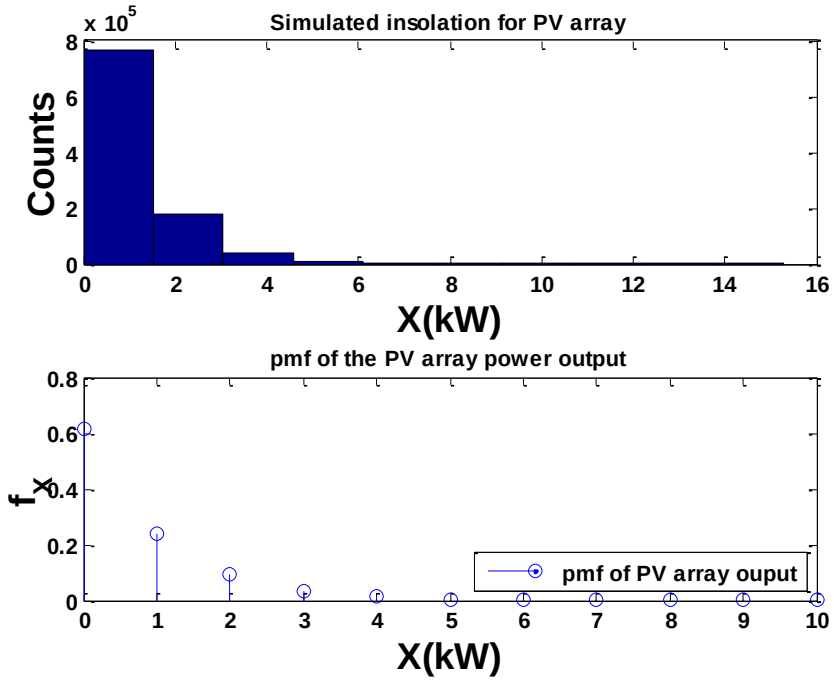

Fig. 4.10 Output of the PV panel with the insolation with parameters of Table 4.1

PV input exponential parameter	0.0038 W^{-1}
Total installed PV capacity	10 kW
Mean PV input per unit area	260 W/m^2
Panel conversion efficiency	15%
Area of array installed	26.67 m^2
Mean output of array	1.05 kW
Peak output of array	10 kW

Table 4.1 Photovoltaics and interface battery parameters

Load Behavior

Load statistics play an important role in determining the battery SOC. The load behavior can be complicated and load exhibit periodic behavior such as seasonality and day and night variation, i.e. the load can have very different distributions during different regimes like day time and night time and during different seasons like summer and winter. A plot of load observed from September 2011 to August 2012 is shown in Fig. 4.11. In this work the load considered here is assumed to be stationary in order to simplify the models.

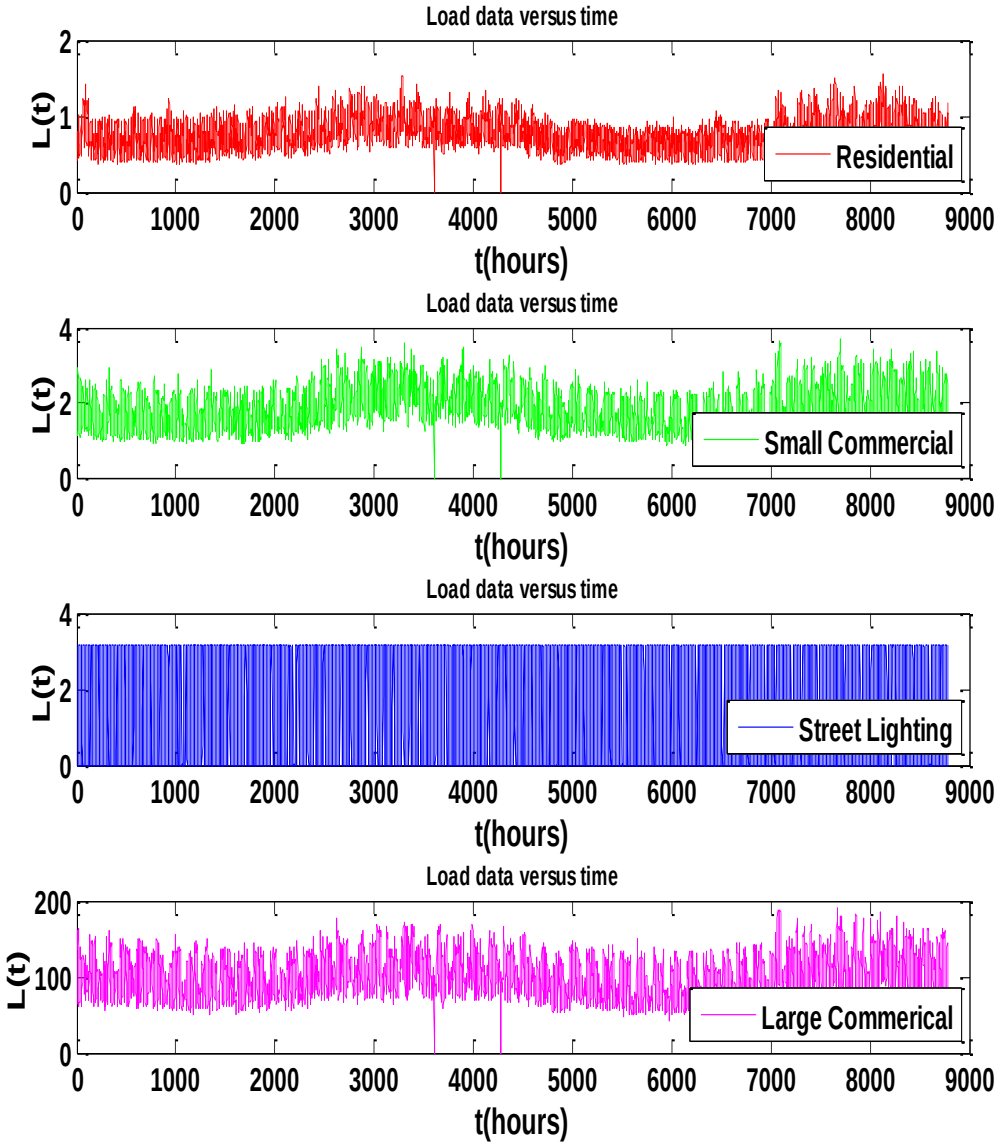

Fig. 4.11 Load versus time for September 2011 to August 2012.[NHEC 2012]

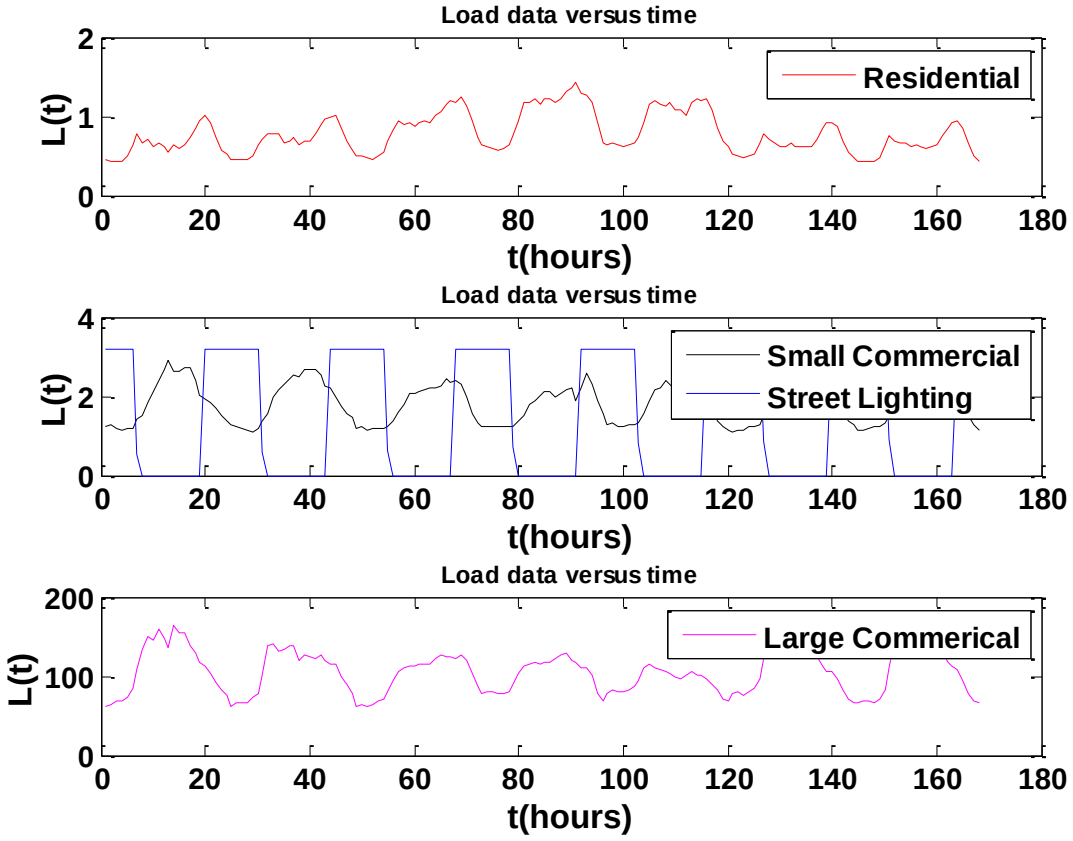

Fig. 4.12 Load variation over a week for the first week of September 2011.

The load versus time for the first week of September 2011 is shown in Fig. 4.12. The plots suggest that there exists some periodicity in the load statistics. Street lighting from Fig. 4.12 exhibits a very strict periodicity almost deterministic and takes two values. Therefore such loads could be considered deterministic but time varying. The load statistics for each of the load types is given in Fig. 4.13.

In the work described here, for simplicity, the Markov chains model presented assume that the load is stationary. If the load were assumed to be non stationary then each

of the terms corresponding to the load terms in the transition probability matrix for the evolution of the battery state of charge would also be time varying.

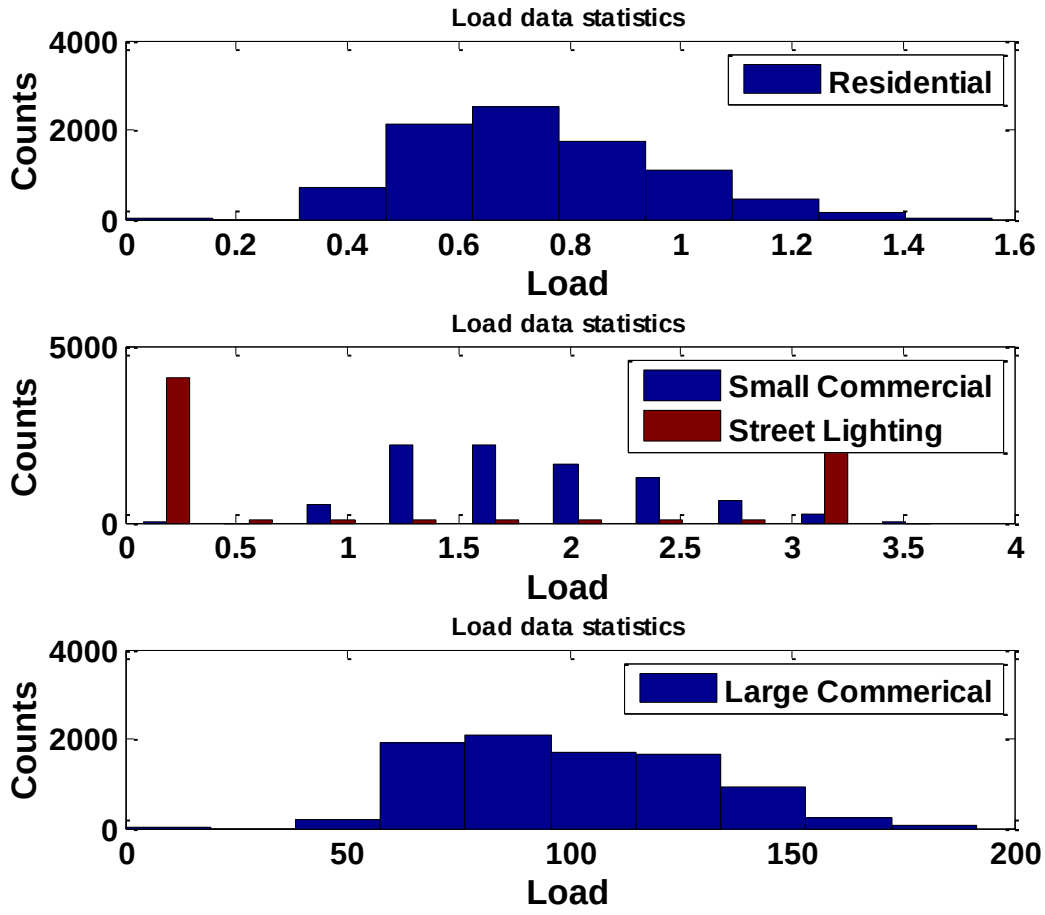

Fig. 4.13 Load Statistics observed from September 2011 through August 2012.

The loads used to exemplify the REPS availability model are assumed to be binomial with parameters given in the table 4.2. The plot for the distributions is shown in Fig. 4.14.

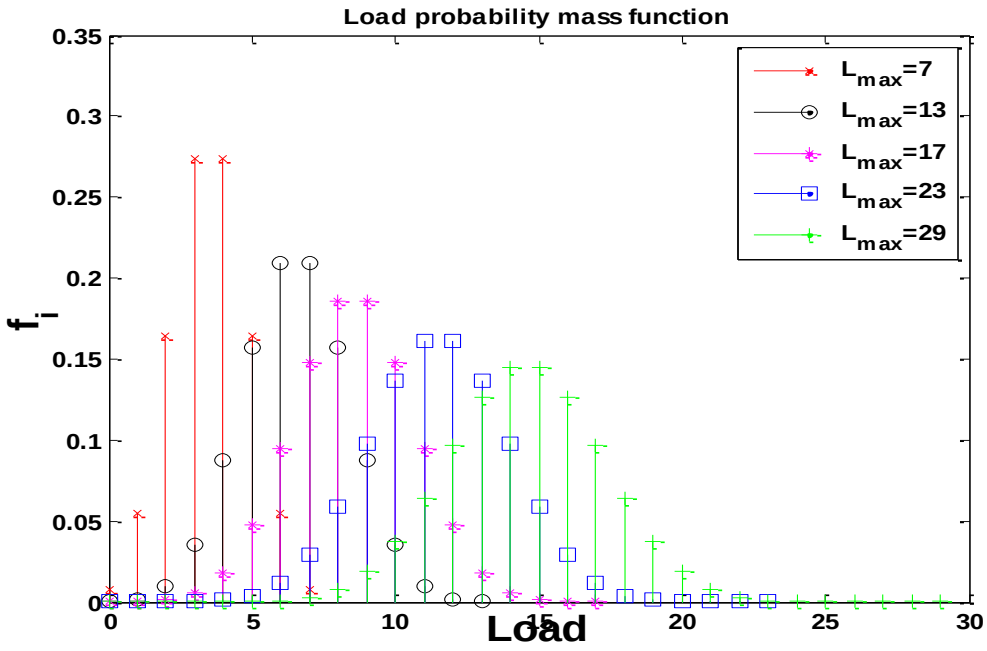

Fig. 4.14 Load probability mass function

Storage Behavior

Let the battery capacity be *C* in energy units. Divide the tank C into N+1 states from 0 to N. The state transition diagram for the Markov chain describing the transitions in the battery state of charge is given in Fig. 4.15.

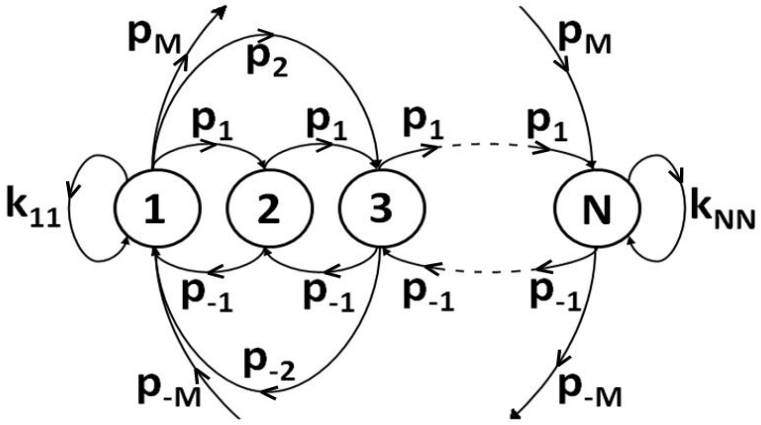

Fig. 4.15 State transition diagram for the battery state of charge

In practical purposes is usually the case that N >M which means that battery cannot be discharged from full capacity to empty in 1 time step. The transition probability matrix is

$$\mathbf{P_B} = \begin{bmatrix} K_0 & q_1 & q_2 & \cdots & & & \\ \tilde{p}_{-1} & q_0 & q_1 & \cdots & & & \\ \tilde{p}_{-2} & q_{-1} & q_0 & \cdots & & & \\ \vdots & \vdots & \vdots & \ddots & \vdots & \vdots & \vdots \\ & & & \cdots & q_0 & q_1 & \tilde{p}_2 \\ & & & \cdots & q_{-1} & q_0 & \tilde{p}_1 \\ & & & \cdots & q_{-2} & q_{-1} & K_N \end{bmatrix} \tag{4.7}$$

where the

$$\tilde{p}_{-i} = \sum_{k=0}^{M} q_k + \sum_{l=-i+1}^{-1} q_l \tag{4.8}$$

$$\tilde{p}_i = \sum_{k=0}^{M} q_{-k} + \sum_{l=i-1}^{1} q_l \tag{4.9}$$

$$K_0 = \sum_{k=0}^{M} q_{-k} \tag{4.10}$$

$$K_N = \sum_{k=0}^{M} q_k \tag{4.11}$$

As discussed before, the unavailability of the REPS system is given by the probability of the fitness function being negative i.e. the total energy difference between the REPS and Load for a given time step is

$$U_{REPS} = P(G < 0) = \sum_{g<0} f_G(g) \tag{4.12}$$

where, $f_G = f_\Delta * f_B$, also note that $f_\Delta = f_X * f_{-L}$ which is the distribution of the difference in the energy between source and load.

Optimal Energy Storage Size

Availability vs. energy storage capacity

The cost of storage can be high for highly available power supply as large amounts of storage might be needed. Additionally, over sizing the storage might be prohibitively expensive. Therefore storage size needs to be minimized in order to make capital costs low without sacrificing availability because a lower availability means larger downtime cost. It can be assumed that the cost of storage is non decreasing in capacity. Therefore smaller the storage in MWh, the lower will be the cost therefore while sizing the storage size, minimize the total storage cost for a given availability constraint i.e. find the smallest value of capacity *C* that will yield

$$U_{REPS} < U_{spec} \tag{4.13}$$

where U_{REPS} is found using (4.12)

Results

A plot of availability versus capacity is given for the various values of load in Fig. 4.16. If the availability requirement is 0.9 for a maximum load of size 13 then the minimum amount of storage required for satisfying the constraint is 20 kWh. When the REPs is used in a microgrid with diverse sources like diesel gensets, the overall availability can be further improved which is demonstrated in Chapter 6.

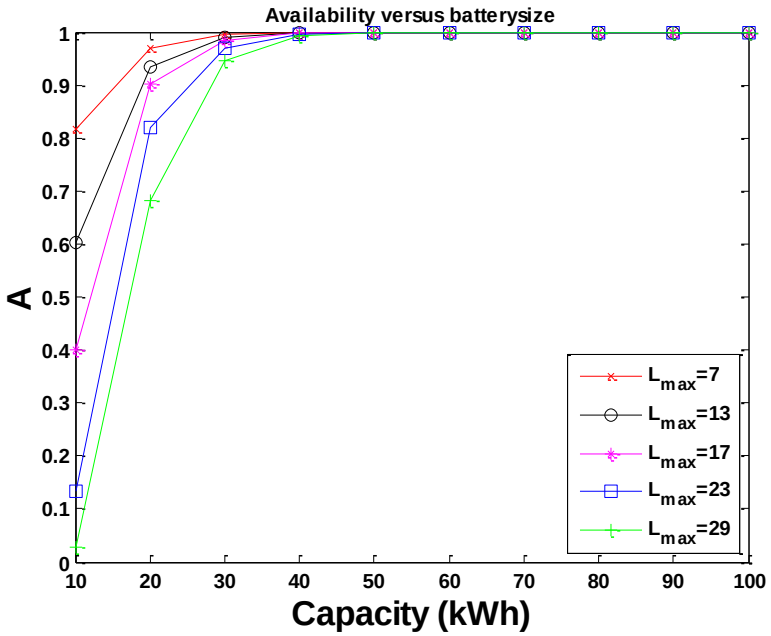

Fig. 4.16 Availability vs. Capacity for a PV system for various loads.

Load (kW)	1	2	3	4	5
P	0.5	0.5	0.5	0.5	0.5
N	7	13	17	23	29
mean	3.5	6.5	8.5	11.5	14.5
Max	7	13	17	23	29
variance	1.75	3.25	4.25	5.75	7.25

Table 4.2 Load parameters for the PV REPS

SUMMARY

This chapter discussed two main topics: the distributed energy resources of a microgrid and the availability modeling of a renewable energy power supply system with storage. The availability modeling for the renewable energy power supply systems with storage was discussed and the sizing of the storage was discussed.

Chapter 5: Microgrid Distributed Energy Resources: Diesel Gensets, Fuel Storage and Fuel Delivery Availability

Microgrid availability depends on the availability characteristics of its individual components which mainly fall into two categories, distributed generators and energy storage and their dependent infrastructure. However, since distributed generators such as diesel gensets depend on lifelines such as transportation networks, whose behavior during disasters affects the genset fuel delivery systems, the genset availability is dependent on the availability of the transportation network. Energy storage may be used to reduce the lifeline dependencies as demonstrated in [Kwasinski 2011a] and another option is to rely on renewable energy sources, such as photovoltaic modules or wind turbines that do not depend on a lifeline. Fuel cells have also been suggested as an addition in order to improve diversity [Spink and Saathoff 2013, Gagge 2008].

Diesel gensets, however, have been widely used for backups for telecommunication base stations [Kwasinski et al. 2012, TCLEE 2012]. They are also deployed as portable generators to power cell sites during hurricane and earthquakes [TCLEE 2012,Dueñas-Osorio and Kwasinski 2010] and are popular choice for local generation in microgrids [Krishnamurthy et al. 2008]. Diesel gensets are also the primary choice for power supply in remote areas [Tammam et al. 2012]. There are, however, many reliability issues with the use of diesel gensets even with the presence of the storage because the storage primarily depends on the lifeline to supply it with fuel. In standalone systems, where the diesel genset is the primary power system, the lifeline dependency is more pronounced. Energy storage sizing has been previously studied for such stand alone systems [Kwasinski 2011a, Zhao et al. 2013] and well as diesel systems

with renewables like wind [Gavaniduo et al. 1993, Yong-Hua 2009, Billinton and Karki 2001, Ying-Yi and Ruo-Chen 2012]. However, few works study the effect of transportation delays and storage and their effects on power supply availability [Kwasinski et al. 2012, Kwasinski 2011a].

The availability modeling of diesel gensets with storage and discontinuous fuel supply i.e. with delays in fuel delivery falls in the class of inventory management problems. This chapter presents models to calculate the power supply availability from gensets with discontinuous fuel supply and storage that can be used for gensets in various applications such as backup or in standby operation, in standalone mode, or as part of a microgrid which is the primary intention of the paper. It can also be used for these applications during extreme events like natural disasters or while supporting renewables like photovoltaic system and wind turbines. During natural disasters, the microgrids are in island mode and the power supply availability is predominately influenced by micro-grids DERs performance [Yokoyama et al. 2008, Tanrioven 2005, Li et al. 2010].

The availability of the genset is defined as the probability of the genset being able to meet the load demand. The gensets' ability to meet the load demand is in turn dependent on the amount of fuel available to the genset. In the absence of a continuous flow of fuel, the genset is dependent on its local storage such as a fuel tank for fuel. Therefore the availability of the genset can now be described in terms of the amount of fuel in fuel tank. The fuel in the tank is replenished by an external system of refueling that experiences lead times or delays. In order to find the probability of having a certain amount of fuel, Markov chains are used in order to describe the fuel consumption and refueling processes. Markov chain models have also been used for the modeling of other storage systems such as the modeling of the battery state of charge for renewables in Song et al. 2013. Markov and semi-Markov models are widely used in the modeling of

queuing systems and inventory management and control [Kashtanov 2010, Girtler 2013], which is similar to the approach presented in this chapter [Kwasinski et al. 2012, Song et al. 2013, Girtler 2013]. Delays and various logistical problems in transportation systems are also widely modeled using semi-Markov processes [Migawa 2013].

An important aspect regarding the fuel consumption is that the load that diesel gensets face could be also be stochastic which could be the result of optimization schemes applied to the load to consume minimal energy [Lalitha et al. 2013]. Therefore finding the amount of time the tank can supply the load is also studied in this chapter.

As mentioned before, the fuel arrivals are affected by lead times or delays which are stochastic in nature. The incorporation of these lead times in the power supply availability model is one of the primary contributions of this chapter.

The Markov chain models presented in this chapter can be used to analyze the availability characteristics of the diesel genset with storage and with discontinuous fuel supply in any off the above applications mentioned—standalone, standby or in a microgrid. A brief description of the application of the model in each case is given in the discussion section. Following are a few basic assumptions that are made while developing the models for the genset fuel supply availability.

A1. All events occur in discrete time.

A2. All physical quantities (fuel level in the tank, energy demand of the load) are discrete or discretized when using the models.

A3. When the refueling truck arrives the refueling is instantaneous and fills the tank completely and the truck leaves.

A4. Load is finite in size.

A5. Storage is finite in size.

A6. If the fuel truck delivery time is non-geometric then its distribution has finite support.

There are four models discussed here, model 1 is for fuel state independent fuel truck arrivals with deterministic constant load. Model 2 is for fuel state dependent fuel truck arrivals with deterministic constant load. Model 3 is for fuel state independent fuel truck arrivals with stochastic load. Model 4 is for fuel state dependent fuel truck arrivals with stochastic load.

LOAD AND FUEL STORAGE REPRESENTATION:

Let the fuel tank capacity be C in units of volume (say liters). Let σ be the smallest non zero unit of load or the fuel consumed over one time step, then the state space for the fuel in the tank is $S=\{0,1,2...N\}$ with each state i representing the presence of $i\sigma$ units of fuel being present in the tank. The tank capacity is $C=\sigma N$. Let $\boldsymbol{\pi}(t)$ denote the probability mass function (pmf) over the state space S i.e. the fuel level at time t and correspondingly $\boldsymbol{\pi}(0)$ is the initial state of the fuel tank and the long term, steady probability is $\boldsymbol{\pi}$.

MARKOV CHAIN MODELS FOR FUEL STORAGE AND FUEL DELIVERY SYSTEMS WITH DETERMINISTIC LOADS

Here the Markov chain tank models for state dependent and state independent fuel truck arrivals are described. Assumptions A1 to A6 hold with the additional assumption that the load is deterministic and constant. The load is normalized to be of size 1 since it consumes a constant value each time step.

Model 1: Deterministic constant load with fuel state independent fuel arrivals:

Formulation:

This the most basic model for the tank that is considered in this chapter. The fuel supply system is shown in Fig. 5.1a. The state space of the fuel tank has N states. Let $b(t)$ be the probability that a refueling event occurs at time t. This $b(t)$ is derived from the fuel tank arrival process indicated as point A (which is modeled separately as a two state process where the fuel delivery system is present or not present at the genset site at time t in the following section). This $b(t)$ represents the scheduling of the truck arrival. Now consider the changes in the fuel tank fuel level.

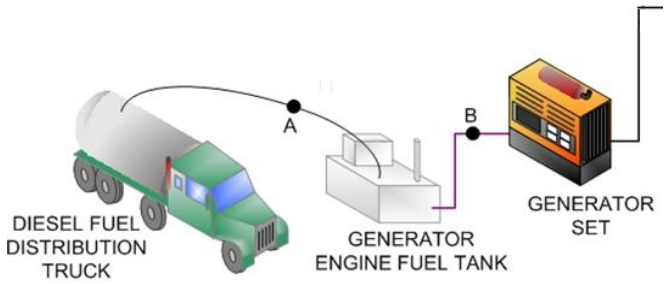

Fig. 5.1a Diesel genset and fuel supply system powered by trucks

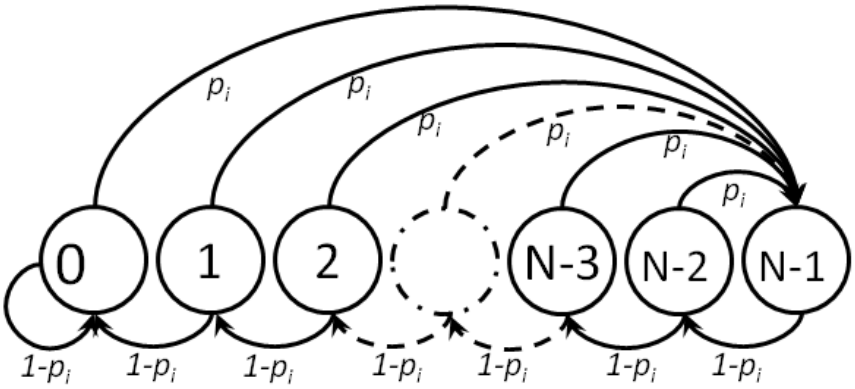

Fig. 5.1b Fuel tank state transition diagram for model 1

This is process is indicated by the flow of fuel indicated as B in Fig 5.1a. The change in the fuel tank occurs because of two events: refueling to full tank capacity or the consumption of the fuel by genset, which is one unit of fuel per unit time. This implies that there are only two transitions out of each state 1) a refueling event or 2) 1 unit fuel is consumed. Since the randomness of the refueling event is the only stochastic element (other than the restoration of grid when the model is applied to standby mode) in the genset operation, the *b(t)* alone is sufficient to characterize the transition in the fuel level at time *t*. The transition diagram at time instant *t* is given in Fig. 1b. Let **P**(t) be the transition probability matrix (TPM) that describes the change in the probability distribution $\boldsymbol{\pi}(t)$ on the fuel tank level at time *t* to then,

$$\boldsymbol{P}(t) = \begin{bmatrix} 1-b(t) & 0 & \cdots & 0 & b(t) \\ 1-b(t) & 0 & & 0 & b(t) \\ \vdots & & \ddots & \vdots & \\ 0 & 0 & & 0 & b(t) \\ 0 & 0 & \cdots & 1-b(t) & b(t) \end{bmatrix} \tag{5.1}$$

The distribution over the fuel tank state space is found by [Kulkarni 2010]

$$\boldsymbol{\pi}(\mathbf{t})=\boldsymbol{\pi}(\mathbf{t-1})\mathbf{P}(\mathrm{t}) \tag{5.2}$$

which yields the transient solution which needs to be found to find the probability of being in any tank state for each time instant. In order to numerically find the time varying $\boldsymbol{\pi}(t)$ for $t = [1,2,,...M]$ with $\boldsymbol{\pi}(\mathbf{t})=\boldsymbol{\pi}(\mathbf{t-1})\mathbf{P}(\mathrm{t})$ and given $\boldsymbol{\pi}(0)$. M is decided by the length of the operational interval of the genset over which the genset availability is to be found. When the refueling events are homogenous in time the probability that the system is refueling is independent of time i.e. *b(t)* =b, a constant which makes **P**(t)=**P**. If *M* is large enough then the equation $\boldsymbol{\pi}=\boldsymbol{\pi}\mathbf{P}$ (and the condition that the components of $\boldsymbol{\pi}$ add to 1) can be used to find the distribution $\boldsymbol{\pi}$, which yields $\boldsymbol{\pi}$ *=[(1-b)$^{N-1}$ b(1-b)$^{N-2}$ b(1-b)$^{N-}$*

$^{3\cdots}b(1\text{-}b)^{N\text{-}1}\,b]$. The unavailability U of the genset system is the probability of the fuel tank being empty π_0.

$$U = \pi_0 = (1-b)^{N-1} \tag{5.3}$$

Next a Markov chain model for calculating *b(t)*, the fuel delivery availability, is considered.

Fuel delivery model for calculating the value of *b(t)*:

The fuel delivery into the genset via the fuel storage (GFS) system can be represented by two distinct states, the presence of a fuel flow to the GFS system and the absence of the fuel flow, indicated as point A in Fig 5.1a. In this chapter, the discontinuous flow of fuel is considered wherein a fuel has to be delivered via trucks to the genset site. The fuel delivery system is said to be available when there exists a fuel truck at the site as shown in Fig 5.1a. From the assumptions A1 and A3, the instantaneous refueling allows the truck to be at the site for 1 time step unless the fuel delivery time distribution is such that two consecutive arrivals of the fuel truck can occur. The model considered here is such that two consecutive arrivals do not occur, which is the case in extreme events. However the model can be modified to incorporate the consecutive arrivals as well. The two state representation of the fuel truck delivery process is given in Fig. 2a. The states S_{NRF} and S_{RF} represent the absence and the presence of the fuel truck at the site respectively. The instantaneous (one step) arrival probability of the fuel truck is, however, time dependent (unless the arrival time of the fuel truck is geometrically distributed). Therefore the amount of time spent in the S_{NRF} state needs to be accounted for, which is done by creating the states 0_1 to 0_m. From A6, m is finite as the arrival time has a maximum value.

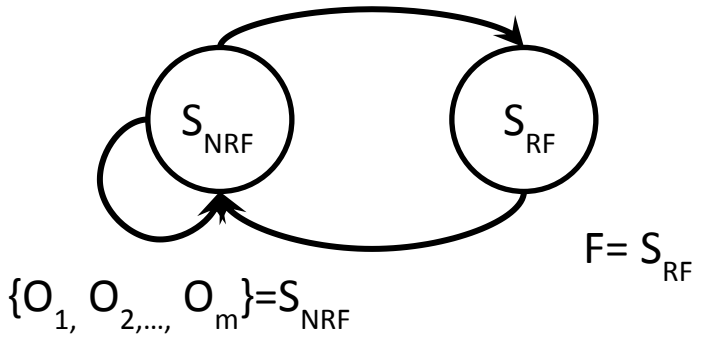

Fig 5.2a: Two state process representing the presence or absence of a fuel truck at the site for refueling

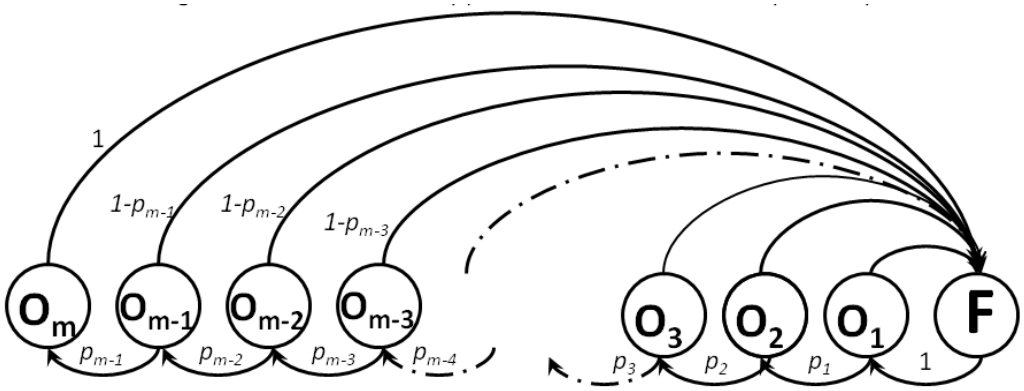

Fig 5.2b: State transition diagram for the fuel truck delivery clock states

The process now can be represented using the Markov chain given in Fig. 5.2b whose transition probabilities are derived using the instantaneous arrival probability equation (5.4) [Marshall and Olkin 2007] and the corresponding TPM is given in (5.5).

$$p_i = \frac{f_i}{1 - \sum_{j<i} f_j} \tag{5.4}$$

In case the refueling time is given as a continuous random variable, it can be discretized. The discretization of the fuel delivery function can be illustrated using an example for f_d. A triangular probability function and its discretized version are shown in Fig. 5.3. [Kwasinski et al. 2012]

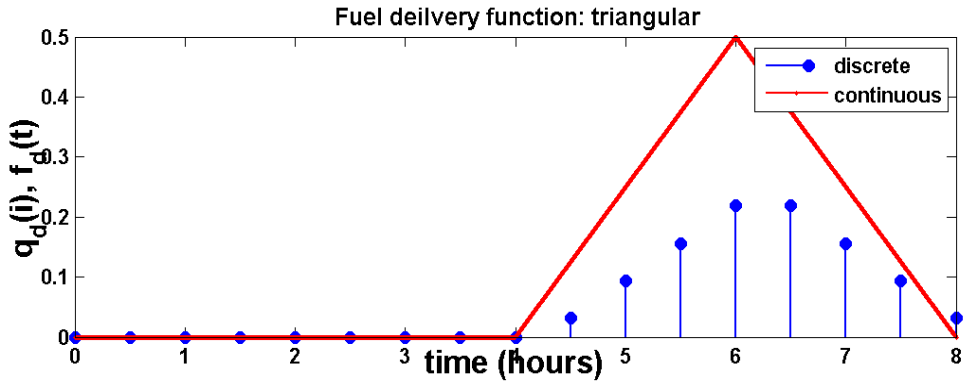

Fig 5.3 Discretization of the continuous time triangular probability density

$$\boldsymbol{P}_{\Psi} = \begin{bmatrix} 0 & 1-p_1 & 0 & & & 0 & 0 & p_1 \\ 0 & 0 & 1-p_2 & \cdots & & 0 & 0 & p_2 \\ 0 & 0 & 0 & & & 0 & 0 & p_3 \\ & \vdots & & \ddots & & & \vdots & \\ 0 & 0 & 0 & & 0 & 1-p_{m-1} & & p_{m-1} \\ 0 & 0 & 0 & \cdots & 0 & 0 & & 1 \\ 1 & 0 & 0 & & 0 & 0 & & 0 \end{bmatrix} \quad (5.5)$$

And $b(t) = \boldsymbol{\pi}_{\Psi}(N,t)$ the nth component of $\boldsymbol{\pi}_{\Psi}$, the distribution over the states in Fig. 5.2b calculated from $\boldsymbol{\pi}_{\Psi}(t+1) = \boldsymbol{\pi}_{\Psi}(t)\mathbf{P}_{\Psi}$ with initial conditions $\boldsymbol{\pi}_{\Psi}(N,0) = 1$. The steady state solution for $\boldsymbol{\pi}_{\Psi}$ is obtained as follows

$$
\begin{aligned}
&\pi_{0_1} = \pi_f \\
&\pi_{0_2} = \pi_{0_1}(1-p_1) \\
&\pi_{0_3} = \pi_{0_2}(1-p_2) \\
&\pi_{0_m} = \pi_{0_{m-1}}(1-p_{m-1}) \\
&\pi_f = \pi_{0_1} p_1 + \pi_{0_2} p_2 + \ldots + \pi_{0_m} 1 \\
&\pi_{01} + \pi_{02} + \pi_{01} + \ldots + \pi_f = 1 \\
&\pi_f = 1 - (\pi_f + \pi_f(1-p_1) + \pi_f(1-p_1)(1-p_2) + \ldots \\
&+ \pi_f(1-p_1)\ldots(1-p_{m-1}) \\
&\rightarrow \pi_f = 1 - \pi_f \Lambda
\end{aligned}
\tag{5.6}
$$

Where Λ is

$$
\Lambda = 1 + \sum_{i=1}^{m-1} \prod_{j=1}^{i} (1-p_j) \tag{5.7}
$$

On rearranging

$$
b = b(\infty) = \pi_f \frac{1}{2 + \sum_{i=1}^{m-1} \left(\prod_{j=1}^{i} (1-p_j) \right)} \tag{5.8}
$$

The above result in (5.8) can be derived in another way by considering the 2-state system to be a semi-Markov process. The long run distribution in state S_{RF} would be given by [Kulkarni 2010]

$$
b = \pi_f = \frac{E[T_{S_{RF}}]}{E[T_{S_{RF}}] + E[T_{S_{NRF}}]} = \frac{1}{1 + E[T_{S_{NRF}}]} \tag{5.9}
$$

However the method of (5.5) is useful in deriving the TPM for fuel state dependent truck arrivals. The representation of the fuel delivery system described here is also representative of a continuous fuel delivery system with failures and repairs that can occur homogenously in time.

The Markov chain can also be thought of as representing the transitions of a stop-clock keeping track of the fuel arrivals resetting on each fuel arrival, that is to say there is a one to one correspondence from the state of the Markov chain of Fig. 2b to that of a clock monitoring the arrival of the fuel truck. In the models that follow the clock states hence refer to the states of fuel delivery system as described by the state space of Fig. 5.2b.

Model 2: Deterministic constant load with fuel state dependent fuel order placements:

Formulation:

In this model, first the state space is constructed then the conditional probabilities for the transitions of the fuel level are derived depending on when the fuel orders are placed. Let the fuel tank start at time zero from the state of being full. It consumes one unit of fuel per time step and let the number of states be $N+1$. When the fuel level reaches state $\xi \leq N$, a fuel order is placed. The refueling truck arrives according to a fuel delivery time distribution f_d. In case the fuel delivery time distribution is continuous, a discretized version of that distribution is used. Let p_d be the discretized version of f_d. p_d gives the refueling probability at each time instants. Once the order is placed, the change is the fuel level in that 1 time-step is affected by the probability of arrival of the fuel truck in that time step. ξ is when the fuel delivery order is placed and that corresponds to $t=0$ for the fuel delivery time probability function. The fuel consumption occurs until the tank hits the state zero or refueling occurs. Until the point of hitting zero, the empty state, the state of the fuel tank itself accounts for the time (because the fuel tank level cannot be in that same state for more than one time-step because the generator is consuming fuel constantly) for which there was no fuel delivery but when the tank hits empty, the time

spent in zero for each time step needs to be tracked when there is no fuel delivery because the probability of fuel delivery is dependent on time. In order to keep track of the time states, zero is rewritten with some temporary states that account for the time spent in empty state. These states are labeled as $O = \{0_m, 0_{m-1}, \ldots, 0_1\}$ which indicate the state of the tank at empty for those time intervals. The state transition diagram for the Markov chain model is given in Fig. 5.4. The transition probabilities between states can be written using the above derivation in matrix form. The transition probability matrix has rows corresponding to the states in the following order $S = \{0_m, 0_{m-1}, \ldots, 0_1, 1, 2, 3, \ldots, \xi - 1, \xi, \xi + 1, \ldots, N - 1, N\}$.

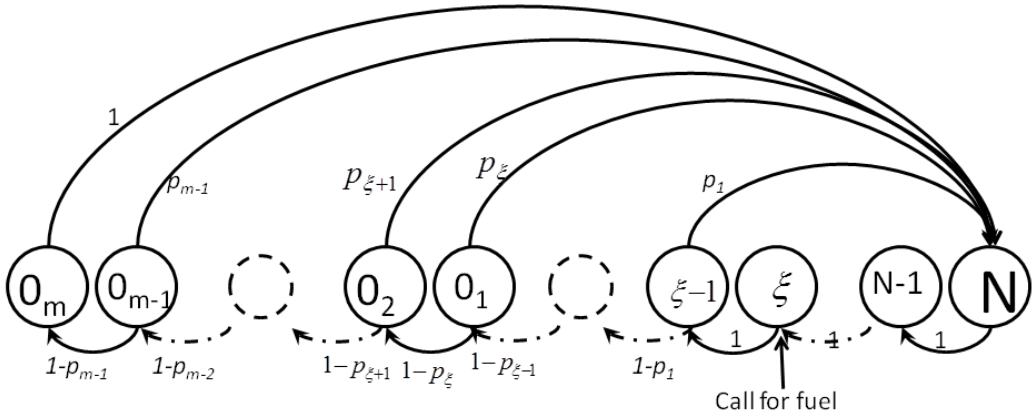

Fig. 5.4 State transition diagram for model 2

In order to make the constructing of the matrix easier, consider the following partition of the state space in two regimes $\Xi = \{0_m, 0_{m-1}, \ldots, 0_1, 1, 2, 3, \ldots, \xi\}$ and $Z = \{\xi + 1, \ldots, N\}$.

$$\mathbf{P}_{\Gamma} = \begin{bmatrix} \mathbf{\Gamma}_{\Xi\Xi} & \mathbf{\Gamma}_{\Xi Z} \\ \mathbf{\Gamma}_{Z\Xi} & \mathbf{\Gamma}_{ZZ} \end{bmatrix} \tag{5.10}$$

Where each $\mathbf{\Gamma}_{ij}$ are block matrices containing the transition probabilities from states in regime *i* to states in *j*.

$$\boldsymbol{\Gamma}_{\Xi\Xi} = \begin{bmatrix} 0 & 0 & \cdots & 0 & 0 \\ 1-p_{0_{m-1}} & 0 & \cdots & 0 & 0 \\ 0 & 1-p_{0_{m-2}} & \cdots & 0 & 0 \\ \vdots & \vdots & \ddots & \cdots & \vdots \\ 0 & 0 & \cdots & 1-p_{\xi-1} & 0 \end{bmatrix} \tag{5.11}$$

$$\boldsymbol{\Gamma}_{\Xi Z} = \begin{bmatrix} 0 & 0 & 0 & 1 \\ 0 & 0 & 0 & p_{0_{m-1}} \\ \vdots & \vdots & \vdots & \vdots \\ 0 & 0 & 0 & p_{\xi-1} \end{bmatrix} \tag{5.12}$$

$$\boldsymbol{\Gamma}_{Z\Xi} = \begin{bmatrix} 0 & 0 & \cdots & 1 \\ 0 & 0 & \ddots & \vdots \\ 0 & 0 & \cdots & 0 \\ 0 & 0 & \cdots & 0 \end{bmatrix} \tag{5.13}$$

$$\boldsymbol{\Gamma}_{ZZ} = \begin{bmatrix} 0 & 0 & 0 & 0 \\ \vdots & \vdots & \vdots & \vdots \\ 0 & 1 & 0 & 0 \\ 0 & 0 & 1 & 0 \end{bmatrix} \tag{5.14}$$

Where the entries $p_i, i = 1,2,3,..\xi$ and $p_{0_i}, i = 1,2,3,..m$ are calculated using formulae

$$p_{\xi-i} = q_i \quad i = 1,2,3..\xi \tag{5.15}$$

$$p_{0_i} = q_{i+\xi}\, i = 1,2,..m \tag{5.16}$$

Note that the total number of states including the temporary states N+ m.

The probability of being in the state space *S* is found as follows.

$$\boldsymbol{\pi}_{\Gamma}(\mathrm{t}) = \boldsymbol{\pi}_{\Gamma}(\mathrm{t}-1)\mathbf{P}_{\Gamma} \tag{5.17}$$

The probability of being in empty state is given by

$$\pi_f^0(t) = 1 - \sum_{i=1,2,..N} \pi_{\psi}^i(t) \tag{5.18}$$

The *i* in the superscript indicates the *i*th state. On solving

$$\boldsymbol{\pi}_{\Gamma} = \boldsymbol{\pi}_{\Gamma}\mathbf{P}_{\Gamma} \tag{5.19}$$

The steady state solution is obtained with the empty tank probability

$$\pi_f^0 = 1 - \sum_{i=1,2,..N} \pi_\psi^i \quad (5.20)$$

The fuel delivery availability can still be quantified using (5.8) and the power supply availability can be calculated for the given the fuel storage size.

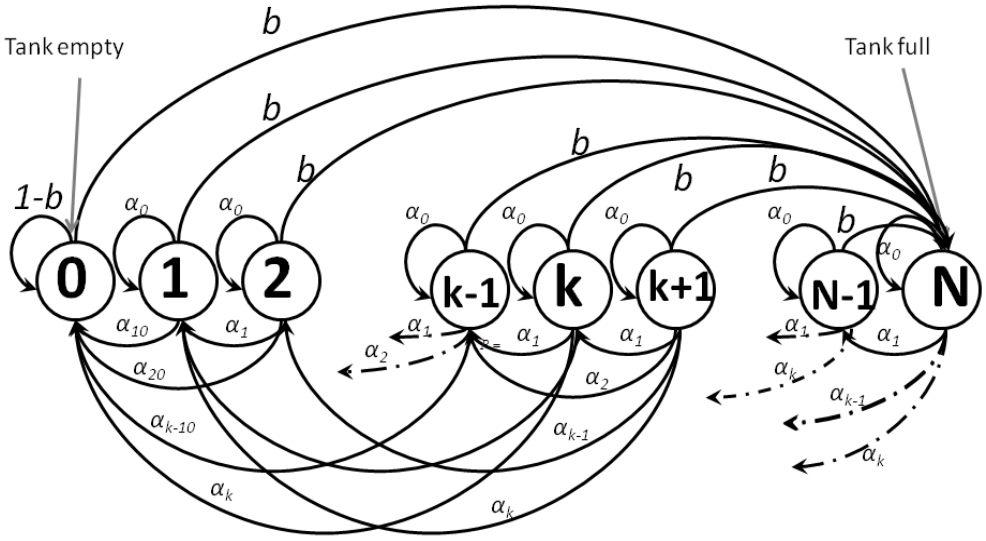

Fig 5.5 transition diagram for fuel tank Markov chain model 3

MARKOV CHAIN MODELS FOR FUEL STORAGE AND FUEL DELIVERY SYSTEMS WITH STOCHASTIC LOADS

In this section the models developed for deterministic loads are extended to include stochastic loads. All assumptions A1 to A6 hold with the additional assumption that the stochastic load is stationary.

Model 3: State independent fuel arrivals with stochastic loads:

In model 1, the load was characterized as constant while consuming 1 unit of fuel. The downward transitions hence in the markov chain occur only in adjacent states. In order to account for any varying of load the model can be extended as follows to incorporate stochastic loads. As mentioned before the load is assumed to be stationary with state space L={0,1,2,…K}with pmf $f_L=\{a_0,a_1,a_2,...a_K\}$. The state transition diagram is given in Fig.5.5. The TPM is given by

$$\boldsymbol{P}_{\Gamma} = \begin{bmatrix} 1-b & 0 & 0 & & & b & \\ \sum_1^K \alpha_i & \alpha_0 & 0 & \cdots & & b & \\ \sum_2^K \alpha_i & \alpha_1 & \alpha_0 & & & b & \\ & \vdots & & \ddots & & \vdots & \\ & & & & \alpha_0 & b & b \\ & 0 & & \cdots & \alpha_1 & \alpha_0 & b \\ & & & & \alpha_0 & \alpha_1 & b+\alpha_0 \end{bmatrix} \tag{5.21}$$

and

$$\alpha_i = (1-b)a_i \tag{5.22}$$

is the probability that *i* units of fuel are consumed given that there is no refueling event. The transient and steady state solution as before are calculated using

$$\begin{aligned} \boldsymbol{\pi}_{\Gamma}(\mathrm{t}) &= \boldsymbol{\pi}_{\Gamma}(\mathrm{t}-1)\mathbf{P}_{\Gamma} \\ \boldsymbol{\pi}_{\Gamma} &= \boldsymbol{\pi}_{\Gamma}\mathbf{P}_{\Gamma} \end{aligned} \tag{5.23}$$

The inputs to the model are $a_i=P(L=i)$ which is obtained from load data which for example could be a microgrid load and the refueling probability $b=P(F=S_{RF})$ also called the fuel delivery system availability can obtained from analysis of the fuel delivery system. And the fuel level pmf is $f_F=\boldsymbol{\pi}_F$ then, the availability is calculated as follows assuming that the load is independent of the fuel arrivals

$$U = \sum_{g<0} f_G = \sum_{g<0} (f_F * f_{-L}) \tag{5.24}$$

The refueling truck availability represented by $b=P(F=S_{RF})$ is long term fraction of time the fuel truck spends in the refueling state.

Model 4: Model for state dependent fuel ordering scheme with stochastic loads:

In this model, the fuel truck is called based on the level of fuel present in the tank similar to that of the model 2 except that the load is now stochastic. The general assumptions A1 to A6 still hold. In model 2 the load consumed/demand exactly one unit of fuel per time step which means that the time elapsed from the instant the fuel order was placed and the current time is directly encoded in the state, that is given the fuel state the amount of time from when the fuel order was placed is directly calculable. The only

condition under which the additional clock states were needed in model 1 was in when the tank was in the empty state. A key difference and complication introduced by the stochasticity of the load is that the time elapsed after placing the fuel order is not known from the state of the fuel tank alone. In order to keep track of the time elapsed, the clock state is also recorded. Therefore the state space for fuel level less than and equal to ξ is two dimensional. Each state is thereby represented by a pair *(x,y)* where *x* represents the clock state and y represents the fuel state. The resulting state transition diagram is given in Fig. 5.6.

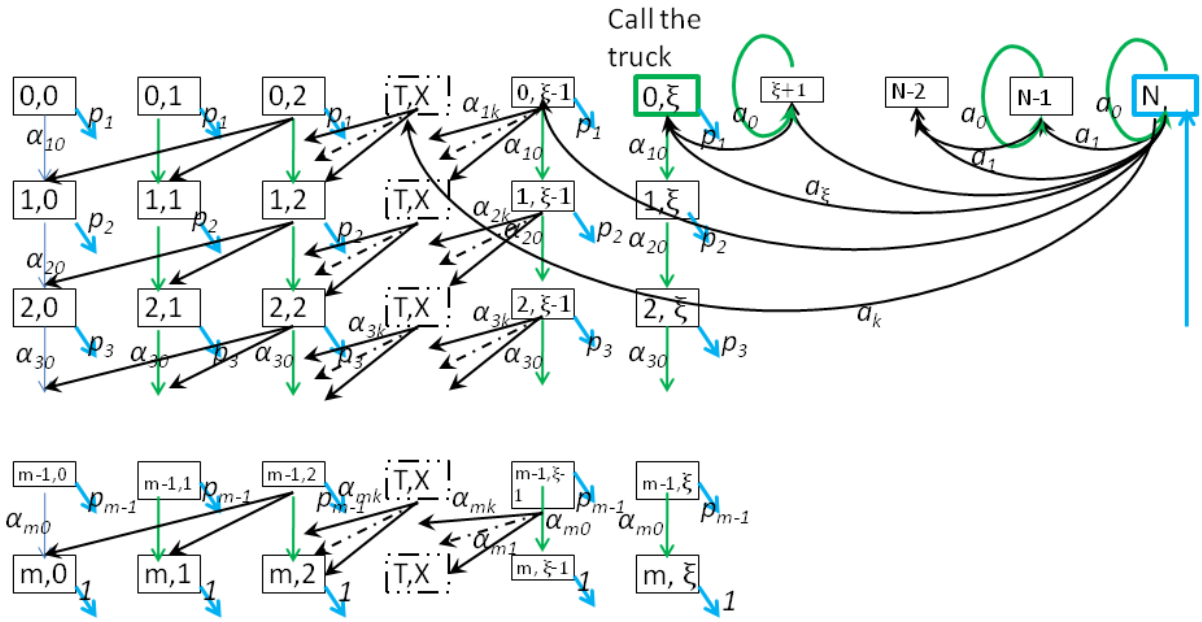

Fig 5.6. State transition diagram for fuel tank Markov chain model 4

The transitions in this model can be rather complicated however the transition probability matrix can be easily derived by making use of the some of the machinery already developed in fuel state independent model 3. In order to do so, first construct the state space for the 2D process over which the Markov chain is to be described. Let *X={0,1,2,..m}* be set of states the fuel delivery clock takes and let Y={0,1,2,…., ξ -1, ξ ,

ξ +1,…N-1,N} be the set of states the fuel in tank can be in. as before in model 3 define $\Xi=\{0,1,2,3,...,\xi\}$ and $Z=\{\xi+1,..,N\}$.The state space for the 2D Markov chain is $\Omega=\{X\times\Xi,Z\}$. Let $\mathbf{P_\Omega}$ be the transition matrix for Markov chain describing the evolution over Ω and the corresponding rows are given by the tuple (x, y) for x=1,…m and y < ξ. The downward transitions in Z partition of Ω are exactly the same as in model 3. $\mathbf{P_\Omega}$ is decomposed into 4 blocks, $\mathbf{\Omega_{\Xi\Xi}}$ is the block containing the transition within the states that correspond to the fuel tank have a fuel level less than or equal to ξ

$$\boldsymbol{P}_\Omega = \begin{bmatrix} \mathbf{\Omega}_{\Xi\Xi} & \mathbf{\Omega}_{\Xi Z} \\ \mathbf{\Omega}_{Z\Xi} & \mathbf{\Omega}_{ZZ} \end{bmatrix} \tag{5.25}$$

Note: ξ and the maximum value of load *K* govern the accessibility of the states in the 2D tank-truck state space transitions reached in 1 step with probability >0. Therefore these states appear only if the initial conditions give them a *p>0*. Consider first the transition probability matrix for the fuel tank given in model 3. Let $\mathbf{\Gamma_{\Xi\Xi}}$ be the downward transition block of the $\mathbf{P_\Gamma}$, the fuel tank transition matrix. Decompose $\mathbf{P_\Gamma}$ into the following blocks; $\mathbf{\Gamma_{\Xi\Xi}}$ contains the transition probabilities among the states Ξ in model 3 and $\mathbf{\Gamma}_{ZZ}$ contains the transition probabilities among the states; $\mathbf{\Gamma_{\Xi Z}}$ contains the transition from Ξ to Z and $\mathbf{\Gamma_{Z\Xi}}$ contains the transition from Z to. Ξ. Let $\mathbf{P_\Psi}$ be transition matrix for the fuel delivery system and let $\mathbf{\Psi_{00}}$ be the downward transitions block of $\mathbf{P_\Psi}$. Let $\mathbf{\Gamma}_{\Xi\Xi D}=\mathbf{\Gamma}_{\Xi\Xi}(1-b)$ with b=0 which yields the transitions (downward) within the tank state space in the absence of refueling. The transitions in the sub-ξ states (the state corresponding to the states which have a fuel level less than or equal to ξ) along with the fuel truck delivery clock states are now given by the Kroneckar product of the $\mathbf{\Gamma}_{\Xi\Xi D}$ and the $\mathbf{\Psi}_{00}$ i.e. The transitions between the states in $X\times\Xi$ is given by

$$\mathbf{\Omega}_{\Xi\Xi} = \mathbf{\Gamma}_{\Xi\Xi D} \otimes \mathbf{\Psi}_{00} \tag{5.26}$$

The transitions out of the sub-ξ tank and truck clock states when a refueling events occurs and the refueling fill the tanks by assumption A6. Therefore the transitions in the matrix $\mathbf{\Omega}_{\Xi Z}$ are all zeros except in the rightmost column of the matrix which is calculated by 1 minus the sum over the columns of $\mathbf{\Omega}_{\Xi\Xi}$. The formulae for the blocks of $\mathbf{P}_\Omega$ are summarized as follows

$$\begin{aligned} \mathbf{\Omega}_{\Xi\Xi} &= \mathbf{\Gamma}_{\Xi\Xi D} \otimes \mathbf{\Psi}_{00} \\ \mathbf{\Omega}_{\Xi Z} &= \begin{bmatrix} \mathbf{0} & 1 - \sum_j \mathbf{\Omega}_{\Xi\Xi} \end{bmatrix} \\ \mathbf{\Omega}_{Z\Xi} &= \begin{bmatrix} \mathbf{\Gamma}_{\Xi\Xi} & \mathbf{0} \end{bmatrix} \\ \mathbf{\Omega}_{ZZ} &= \mathbf{\Gamma}_{ZZ} \end{aligned} \tag{5.27}$$

The Markov chain on Ω hence described has some transient states i.e. states below ξ that cannot be reached in 1 step with probability >0 from states above ξ. Therefore these states appear in the realization if and only if the initial conditions are such that the chain starts from one of those states. The limiting probability distribution over Ω is given by

$$\boldsymbol{\pi}_\Omega = \boldsymbol{\pi}_\Omega \mathbf{P}_\Omega \tag{5.28}$$

In order to find the distribution over the state space of the fuel i.e. the marginal for the tank.

$$\boldsymbol{\pi}_{\mathrm{F}}^{\mathrm{T}} = \mathbf{M}_\Omega \boldsymbol{\pi}_\Omega^{\mathrm{T}} \tag{5.29}$$

Where $\boldsymbol{M}_\Omega = \begin{bmatrix} [\boldsymbol{I} & \dots & \boldsymbol{I}] & \mathbf{0} \\ \mathbf{0} & & & \boldsymbol{I} \end{bmatrix}$ is called the lumping matrix.

The unavailability is again found by

$$U = \sum_{g<0} f_G = \sum_{g<0} (f_F * f_{-L}) \tag{5.30}$$

Example: The above construction is exemplified using the following genset system which contains 5 tank states, 3 states for the fuel delivery clock and 4 states for the load whose state transition diagram is given in Fig.5.7. Using the same notation as above for the 2D tank truck system the parameters are a=[1/10,3/10,5/10,1/10] and

p=[0,2/10,5/8,1] with distribution on the tank states as $\boldsymbol{\pi}$=[0.2471,0.1376,0.2016,0.1034,0.3102]

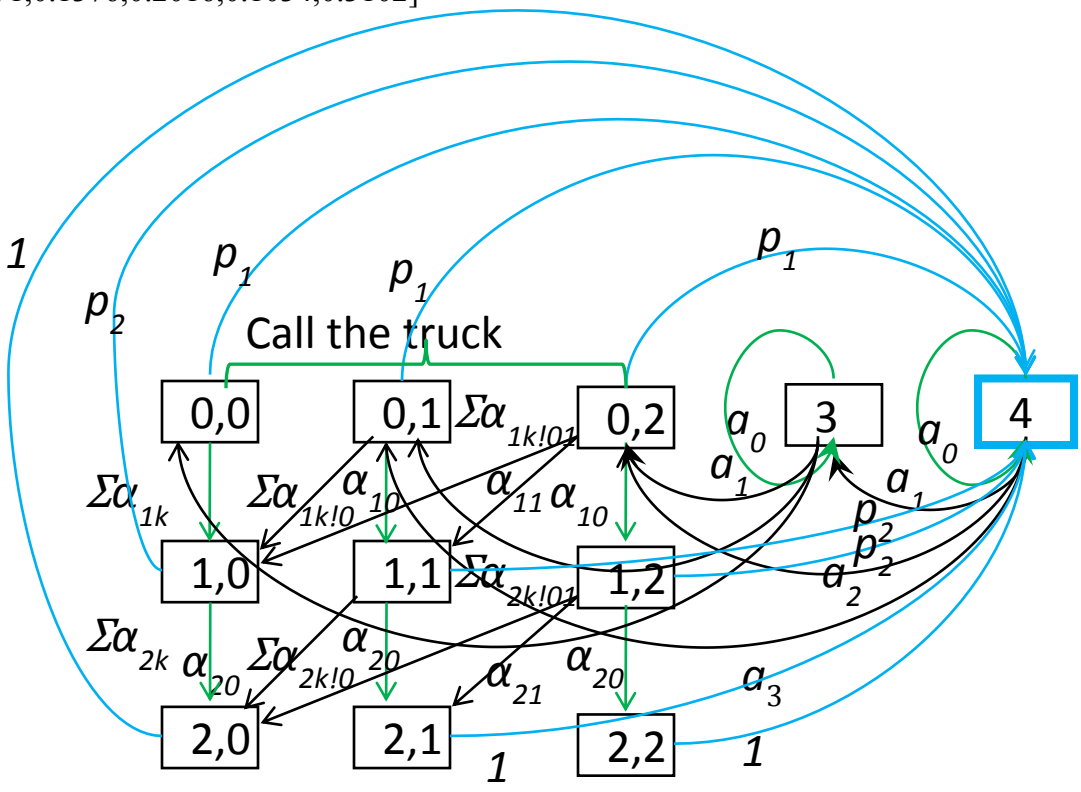

Fig 5.7 State transition diagram for the example of model 4

Load (kw)	L1	L2	L3	L4	L5
P	0.5	0.5	0.5	0.5	0.5
N	7	13	17	23	29
Mean	3.5	6.5	8.5	11.5	14.5
Max	7	13	17	23	29
Variance	1.75	3.25	4.25	5.75	7.25

Table 5.1: Load Parameters

Load (kW)	1	2	3	4	5
T_i	10	19	28	45	43
T_d	20	29	38	50	53
T_m	30	45	60	65	85
B	0.0465	0.0292	0.0203	0.0162	0.0127

Table 5.2: Fuel Delivery pmf Parameters Long

Load (kW)	1	2	3	4	5
T_i	8	11	13	15	17
T_d	11	15	17	20	24
T_m	15	18	23	26	30
B	0.077	0.0621	0.051	0.045	0.0399

Table 5.3: Fuel Delivery pmf Parameters Short

RESULTS, APPLICATIONS AND DISCUSSION

The diesel genset availability calculations for various values of load, fuel arrival pmfs and fuel tank capacity were calculated for models 1 through 4. Models 1 and 2 which consider deterministic constant loads are special cases of models 3 and 4 which consider the general case of stationary stochastic loads, therefore the results for the models 3 and 4 only are shown here. The load data used is given in table 5.1 and the fuel arrival pmf parameters are given in tables 5.2 and 5.3. The load pmfs used are binomial distributions for illustrative purposes shown in Fig. 5.8. The triangular densities are used for the fuel arrivals and these are discretized and used in the models for calculating the availability. Two sets of fuel arrivals pmfs are used. The first set represents long delays in

the fuel arrival whereas the second represents relatively shorter delays in the arrival of the fuel truck. The long delay densities are shown Fig. 5.9 and the short delay densities are shown in Fig. 5.10.

In order to use the models for practical calculations, the physical quantities such as fuel units and load values needs to be converted to the form as required by the models. For example, the energy content in diesel is 36 MJ/Litre [DOE], and the efficiency of diesel gensets are assumed to be around 40%. Let the smallest positive unit of load be 1 kW. Then for a time step of 1 hour, the number of units of fuel consumed in number of joules in 1 hour is 36 MJ. But since the efficiency is 40% and the volume of fuel consumed is 1/0.4 or the energy demand is 2.5x36MJ. Therefore the amount of fuel required to supply unit load for 1 time step is 2.5 liters or 1 unit of fuel tank corresponds to 2.5 liters of fuel. Using this method, the load is converted to the same units as the fuel consumed.

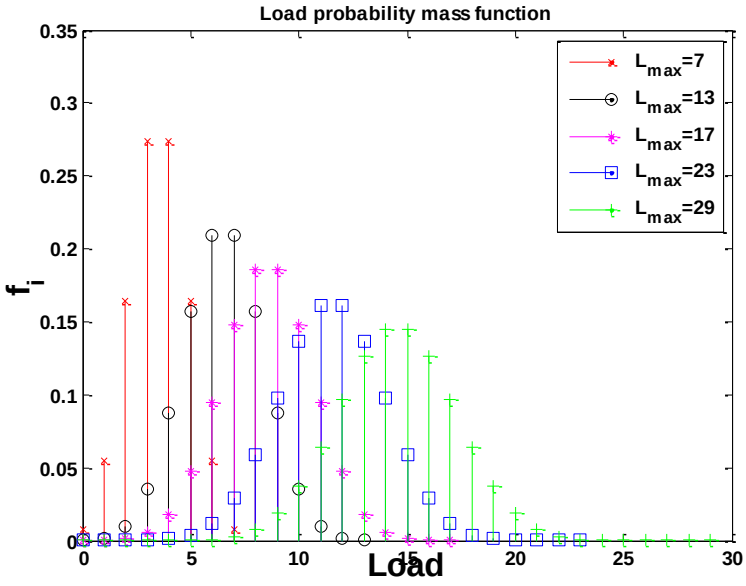

Fig. 5.8 Load Probability mass functions

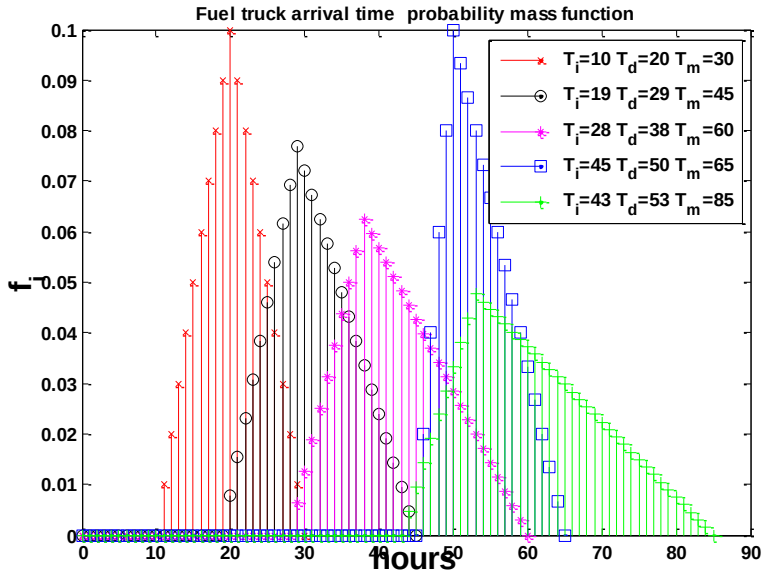

Fig. 5.9 Long Delays: Truck arrival density evaluated at 1 hour steps

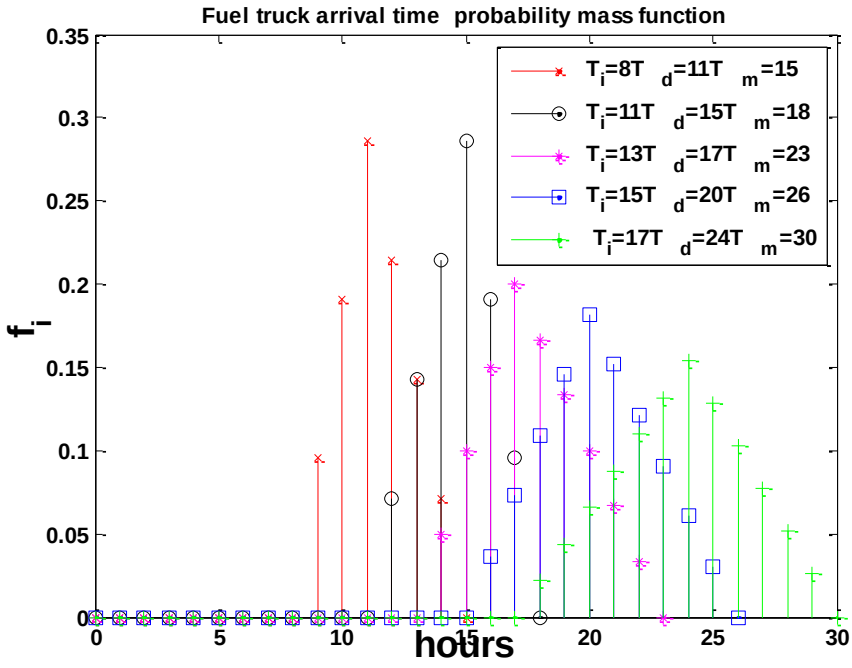

Fig. 5.10 Short delays: Truck arrival density evaluated at 1 hour steps

Availability versus Storage Capacity

Figures 5.11 to 5.14 show the plots of availability for models 3 and model 4 for long and short delays. Given a delay distribution for the truck it can be seen that the availability grows with increasing capacity of the tank. Model 3 which considers the fuel delivery availability directly as a refueling probability shows that even for low values of fuel delivery available like 0.0465, when a storage of capacity 50 units is introduced, for a mean load of 3.5 kW an availability of 0.5 is achieved, which corresponds to 2 orders of magnitude improvement in availability. The growth of availability with increase in storage at small values of storage is rapid i.e. when fuel supply availability is low the improvement in availability with additional storage improves the availability greatly. Figures 5.15 and 5.16 show the pmf of the fuel tank for tank capacity =80 units (200 liters for 1 unit =2.5 liters) for models 3 and 4 for long and short delays. It can be seen that peak probability occurs at the tank empty state for relatively longer delays and is indicated in both models. For model 4, ξ =0.5 was used in the plots. It must be noted that the fuel consumption rate can also depend on the rating of the generator [Diesel Service Chart].

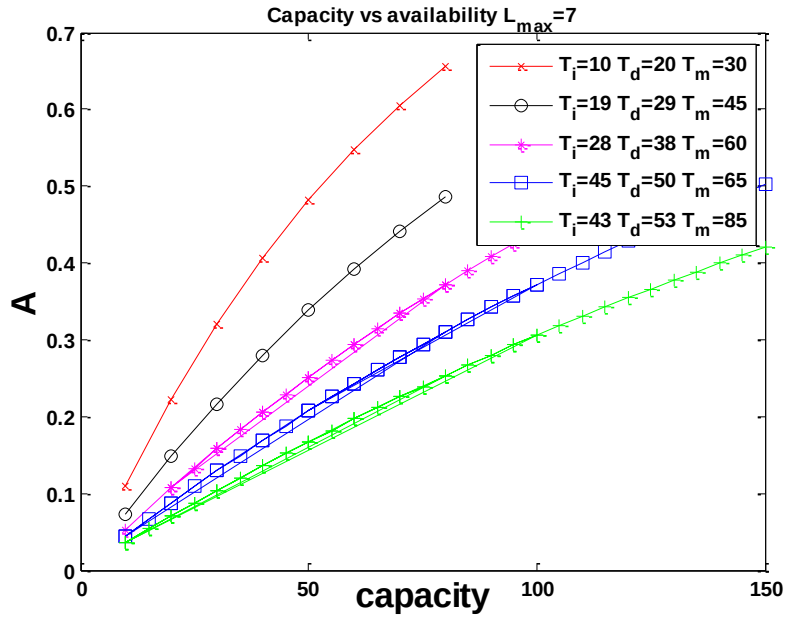

Fig. 5.11 Long Delays: Availability vs Capacity for model 3 for load L1.

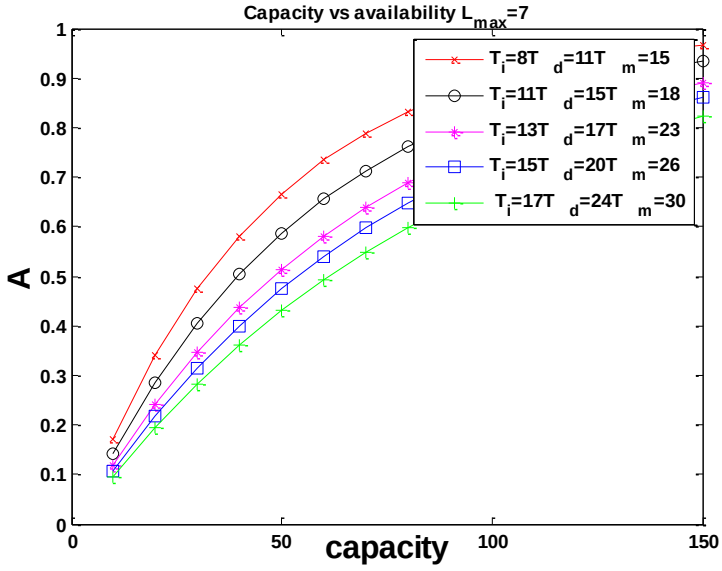

Fig. 5.12 Short Delays: Availability vs Capacity for model 3 for load L1.

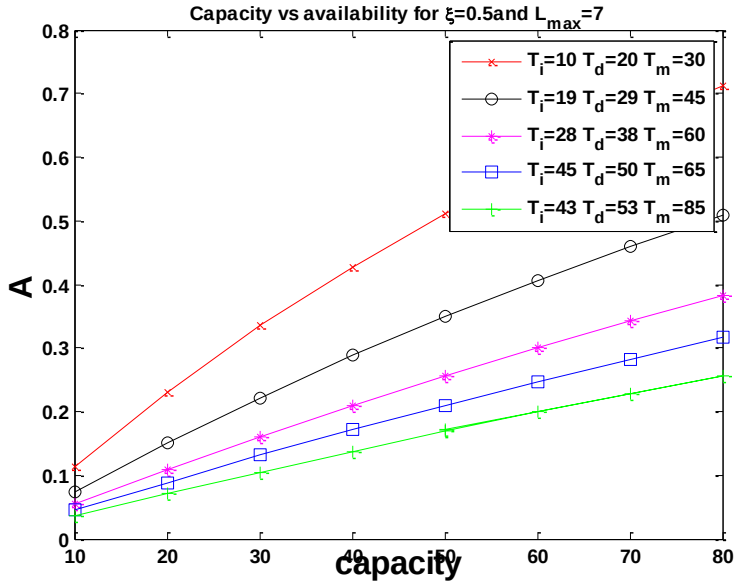

Fig. 5.13 Long Delays: Availability vs. Capacity for model 4 for load L1.

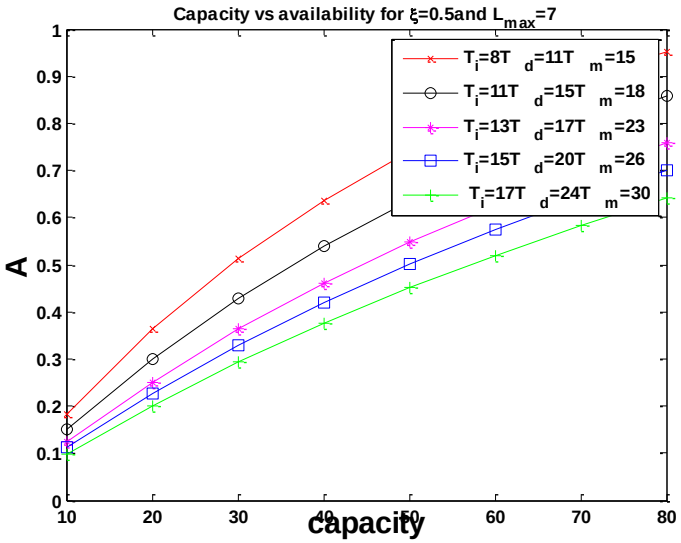

Fig. 5.14 Short delays: Availability vs. Capacity for model 4 for load L1.

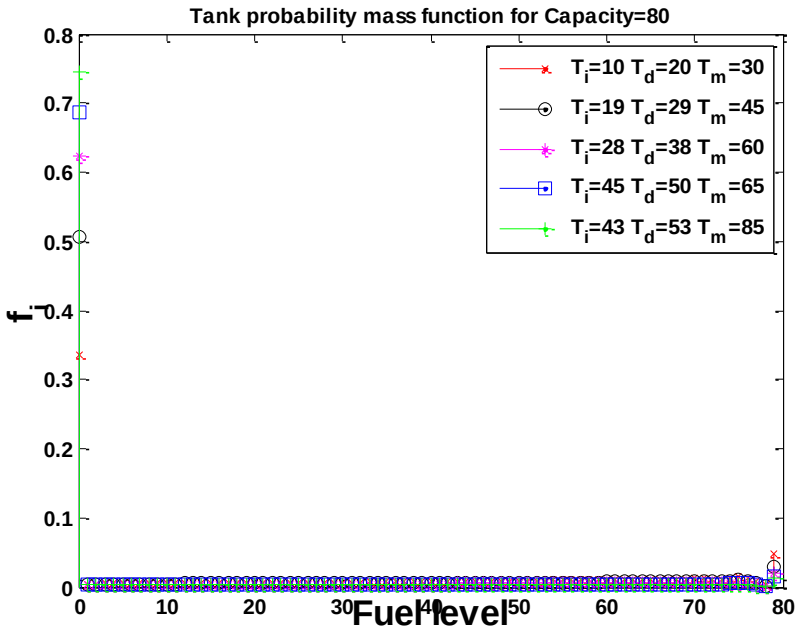

Fig. 5.15 Fuel tank pmf for model 3 for Load L_1 for capacity 80 units

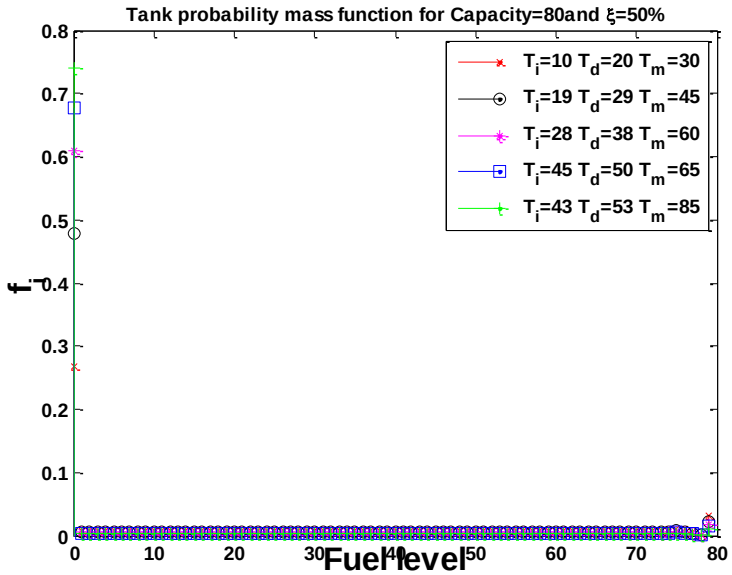

Fig. 5.16 Fuel tank pmf for model 4 for Load L_1 for capacity 80 units.

Availability vs ξ and optimal fuel order placement policy

The value of ξ controls the time at which the fuel order is placed in model 4. The value of ξ indicates the amount of time the controller waits before placing a fuel order. Smaller the value of ξ the more the controller waits to place an order. Also smaller the value of ξ longer is the time between running of out sufficient fuel and the refueling event, which reduces the overall availability of fuel to the genset. However waiting for long enough reduces the number of fuel orders placed over a period of time thereby reducing the cost incurred. Therefore, if an availability specification is mentioned then for a given feasible fuel capacity C, the value of ξ can be minimized in order to minimize the incurred cost of buying fuel. The optimization problem is described as follows.

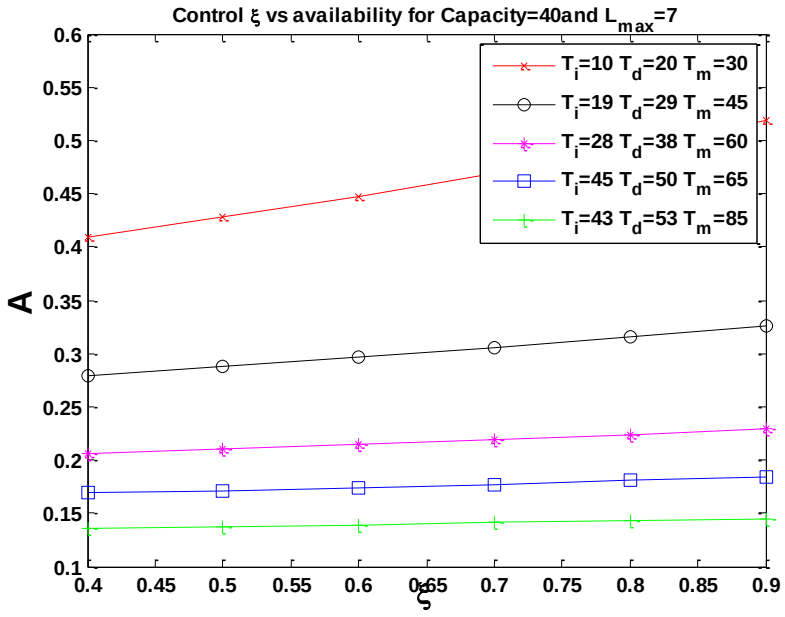

Fig. 5.17 Control vs Availability for capacity 40 and Load L_1.

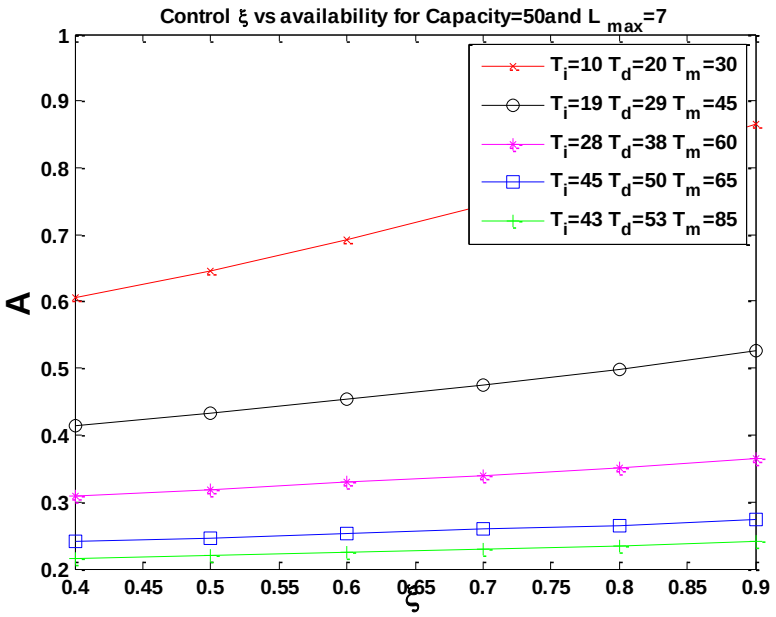

Fig. 5.18 Control vs Availability for capacity 50 and Load L_1

$$\min_{\xi} \xi$$
$$st \tag{5.31}$$
$$\sum_{g<0} \pi_F * \pi_{-L} \leq U_{\max}$$

A plot of ξ versus A is given in Fig. 5.17 and 5.18 for set of long delays arrivals for tank capacities of 40 and 50 units. The value of ξ is chosen at the point when the curve intersects the availability specification. The necessary and sufficient conditions that the TPM needs to satisfy for the of ξ falls within a broader class of problems [Arapostathis et al. 2003] which can form a basis for future work in optimizing the scheduling of fuel.

Nominal Tank Autonomy:

The nominal tank autonomy is defined as the amount of time taken for the fuel level to go from full to empty before a refueling event occurs. This time in markov chain terminology is the hitting time of the state 0 from state full. The markov chain in this

description has no upward transitions i.e. no refueling events. The Markov chain makes a transition every one step of time therefore the hitting time is the length of the path taken from the state F to state 0. The problem of finding the tank nominal autonomy now reduces to finding the path length distribution from node F to 0 in the directed graph of the state space of the fuel tank. However the self loops caused by the load= 0 makes the graph cyclic. In the cyclic graph the hitting time is unbounded, however an approximation can be made in order to change the graph into an acyclic graph and get an approximate nominal autonomy time distribution. Assume that that the probability of load being zero is zero or condition on L > 0, and the problem reduces to setting $a_0 = 0$ with new probability distribution $\boldsymbol{a}$ for the load, which makes the graph a directed acyclic graph. Let Θ be the set of all possible paths from state F to 0. Let R_i be the set of paths with path length i, the collection $\{R_i\}$ forms a partition of Θ. Let E_{ij} be the sequence of edges in path j of length i. Let e_{ijk} be the kth edge in path j of length i. Let q_{ijk} be the probability that e_{ijk} exists. Note that $q_{ijk}>0$ (edges with probability zero have weight 0 and therefore do not appear as edges in the graph and are not considered as part of a path). Therefore the product of the probability of the edges in the path gives the probability of that path being taken.

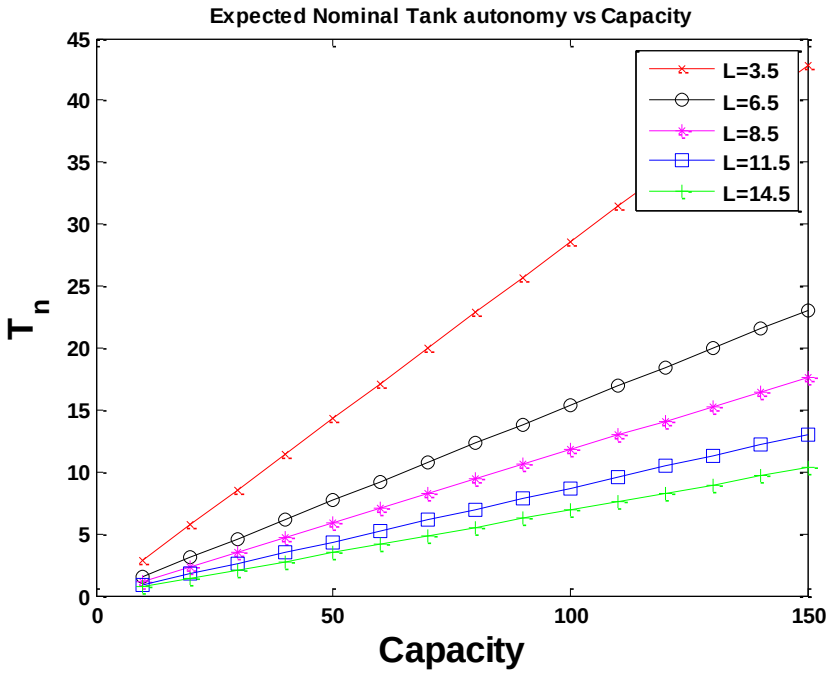

Fig. 5.19 Fuel tank nominal autonomy for mean load values in Table I

$$q_{ij} = \prod_{k=1}^{|E_{ij}|} q_{ijk} \tag{5.32}$$

Now since the paths taken are mutually exclusive their probabilities can be added,

$$q_i = \sum_{j=1}^{|R_i|} q_{ij} \tag{5.33}$$

The set of q_i is the hitting time/ path length distribution and $i=\{0 \text{ to } N-1\}$. Note that since the graph is acyclic and finite. The maximum time to hit the empty state is $N-1$. In the original case where $a_0>0$ the time is not bounded above but the expected value of the tank autonomy time is finite because the of the Markov chain property that a finite a periodic irreducible markov chain is positive recurrent. This method of path enumeration is also however computationally intensive. In some cases the number of paths maybe of the order of n!, which makes the calculation intractable for even modest values of n. In practice is easier to estimate the tank autonomy using the mean value of the load to get

the mean nominal autonomy. For example consider the case of the tank capacity of 100 units and with load L_1. It has a mean value of 3.5kW and the time step is 1 hour. The expected nominal tank autonomy is calculated as 100/3.5= 28.57 hours i.e. the time taken to empty the tank when the mean load is applied. The results for the mean nominal tank autonomy for the loads considered are given in Fig. 5.19. Using Fig. 5.19 with Fig. 5.13 and 5.14 the availability for a given tank autonomy can be calculated for various fuel delivery delays.

Stand alone operation and microgrid operation:

In the standalone operation and in the microgrid operation of the genset, the models are directly applicable and the steady state solution can be directly used if the pmfs do not change with time. The load values is the load allocated to the genset issued in the availability calculations.

Fuel supply availability back up gensets standby during grid outages:

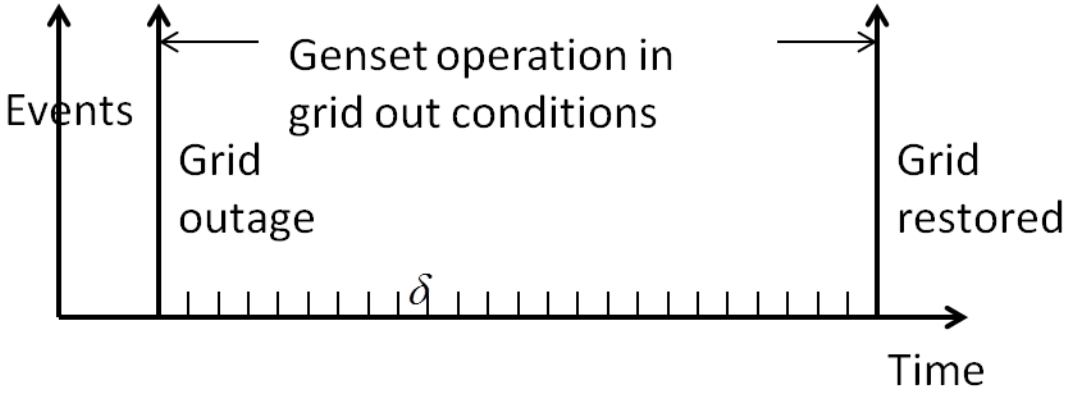

Fig. 5.20: Timeline of events for the genset refueling system

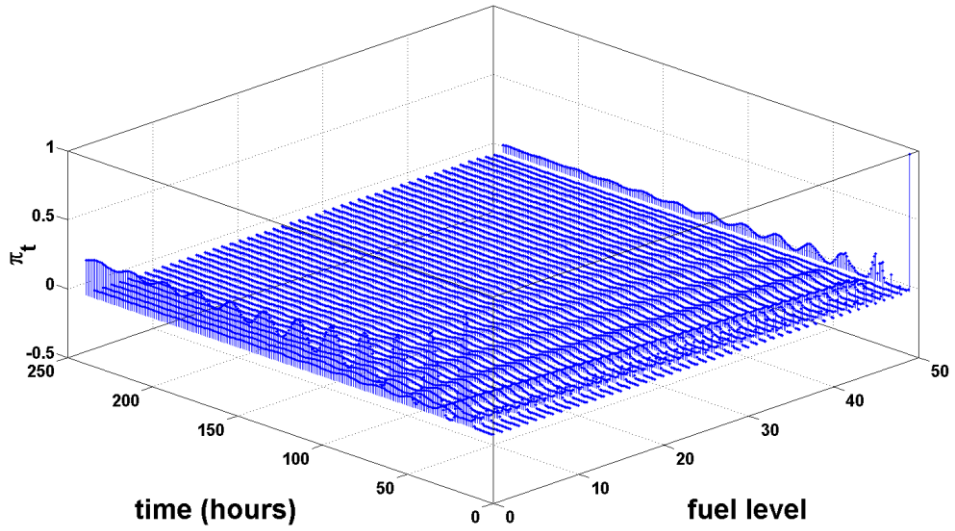

Fig. 5.21 Fuel tank pmf evolution over a period of 10 days for model 4

In the case of standby operation of the genset a timeline of events for the standby operation of the genset is given in Fig. 5.20. Consider a load supplied by the main grid with a back up diesel genset with tank capacity *C*. Let a grid outage occur at time t=0 and the genset is brought into operation. Consider the case when the genset starts (an event which occurs with some genset start probability say ρ_{GS}) when the grid outage occurs and the genset is in standby mode with the tank full. Let the restoration time for the grid be T_r. Let T_r be measured in hours. In case of grid outage caused by extreme events like tropical cyclones or earthquakes the outages could last for days to weeks [Krishnamurthy and Kwasinski 2013]. For example, let T_r =240 hours which corresponds to a restoration time of 10 days. For finding the genset availability in the time interval $[0,T_r]$ the transient solution is found. The transient solution for the fuel tank is given in Fig. 5.21. Note that this standby description can also be extended to a microgrid which has a grid connected

to it and is facing a grid outage. Thus transient solution can be calculated for the duration of a grid outage in the microgrid case.

CONCLUSIONS

This chapter presented four models for deriving the power supply availability of diesel gensets with discontinuous fuel supply. The presence of storage was considered and its effect on fuel supply availability was analyzed for long and short delays in the fuel delivery process. The models for the fuel tank were developed for both deterministic and stochastic loads with fuel state independent and independent arrivals. The effect of controlling the fuel level at which the fuel order is placed was also found. The nominal tank autonomy was calculated for various load values. It was seen that with increasing storage, the genset availability increased thereby reducing the dependency on the fuel truck delivery system. The improvement in availability was large for an increase in storage for small values of installed capacity.

Chapter 6: Microgrids distribution and interfaces

As mentioned before, microgrids can themselves have the availability issues [Kwasinski et al. 2012, Kwasinski 2010, Kwasinski 2011c] for many distributed energy resources (DERs). The microgrids however have an advantage because of the existence of diversity in its sources. Diversity reduces the dependency on any single source which in turn reduces the dependency on any external lifelines [Kwasinski 2010]. Storage is another mechanism via which the life dependency can be reduced and it improves availability [Kwasinski et al. 2012, Kwasinski 2010, Song et al. 2013]. For diesel gensets, storage is in the form of fuel tanks and sometimes in terms of inertial storage like flywheels [Zhao et al. 2012]. For renewables, storage options include batteries Song et al. 2013 and ultra capacitors [Song et al. 2010].

A number of approaches have been tried in terms of evaluating on the impact of microgrid as well various techniques of using microgrids more useful have been studied[Varaiya et al. 2011, Dialynas and Hatziargyriou 2007, Xioahong et al. 2010, Falahati et al. 2012]. Renewables are expected to be a major contributor of energy especially photovoltaics and wind generators. References [Huang et al. 2011] [Mitra et al. 2012] studied the reliability of a microgrid with photovoltaics and wind generators. References Song et al. 2013, [Bahramirad et al. 2012] and [Kakimoto 2012] studied methods to find the optimal storage sizing for a given reliability constraint for microgrids with renewables. But the methods are either limited to simulation based techniques or the microgrid is limited to specific type of source for example photovoltaics i.e. a lack of diversity. The effect of CHP integration into microgrids has been studied by [Basu et al.

2010] and the integration of a highly reliability distribution system has been studied in [Khodayar et al. 2012].

Energy storage plays an important role in improvement of power supply availability. In the evaluating the energy storage's capability to supply energy, Markovian techniques are becoming popular in modeling the evolution of battery state of charge. Such techniques have been employed in renewables Song et al. 2013 [Theristis and Papazoglou 2014] which is also employed in this chapter.

The distribution system of the microgrid is essential is transporting power reliably and integrating the various DERs. Various methods of selecting optimal configurations for smart microgrids [Erol-Kantarci et al. 2011, Kwasinski 2011d ,Hadjsaid et al. 2010] and in this chapter their availability characteristics are studied.

MICROGRID COMPONENTS

In chapter 1 Microgrids are defined as locally confined and independently controlled electric power grids in which a distribution network with a given architecture integrates distributed energy resources with the loads. The components of the microgrids can be broadly classified into four categories; 1) sources 2) loads 3) energy storage 4) interfaces. The sources in a microgrid include the main grid, micro turbine, gas gensets, diesel gensets and renewable energy sources like photovoltaics and wind turbines. The loads, however, are dependent on the specific application under which the microgrid is employed which could be hospitals, military bases, ships, remote communities, telecommunication systems and campuses. Energy storage includes batteries, fuel tanks, compressed air, flywheel and ultra capacitors. Interfaces can comprise of power electronics interfaces and protective equipment like circuit breakers in the network. The

availability of the microgrid is defined as the probability of being able to serve the demand by the DERs given the architecture of the distribution system.

Behavior of microgrid components influencing availability:

Sources:

A main contributor of to the availability of power supply is the variation in the power output of the sources which are due to a number of reasons depending on the source. Sources like gensets depend on lifelines such as pipes and transportation networks whose availability affects the fuels delivery to the genset that makes the power available from genset variable. In case of renewables the natural phenomena make the power supply variable [Kennedy and Marden 2009].

Energy Storage:

Energy storage is used to address the stochastic nature in the case of the lifelines as well as the variability present in renewables, the energy available from the storage is also variable because of the stochastic nature of the sources feeding the storage and well as the stochastic nature of the load consuming energy from the storage and other phenomena such as leakage and degradation [Song et al. 2013].

Interfaces :

Circuit breakers (CBs) are used as protection equipment in a microgrid and power electronics interfaces are used for controlling the power flow as well as a measure of protection. However they are also subject to failure and repairs. But their availability is generally very high in the range of 5 to 6 nines[Kwasinski 2011c].Additionally, the reliability of CBs have increased due to the evolution of technology, from air blast, oil

minimum, SF6 dual pressure into SF6 single pressure type CBs. Power electronic interfaces also have the added advantage of built in redundancy. Power electronics interfaces can be configured in a *n+1* redundancy or in general an *n+m* redundancy which means *n* components are minimum required for the interface to function and an additional *m* are added. For a given *m* as *n* grows the availability reduces [Kwasinski and Krien 2007]. The redundancy works when the components are relatively uncorrelated in their failures. The circuit breaker availability can be calculated using a following continuous Markov chains representation showing in Fig. 6.1.

The availability of the circuit breaker with the conductor in series is calculated as the probability of being state 11 (both conductor and breaker being in a working state) in the state transition diagram of Fig. 6.1. The state transition rate matrix is

$$\mathbf{Q}_{CB} = \begin{bmatrix} -(\mu_B + \mu_C) & \mu_B & \mu_C & 0 \\ \lambda_B & -(\lambda_B + \mu_C) & 0 & \mu_C \\ \lambda_C & 0 & -(\lambda_C + \mu_B) & \mu_B \\ \rho\lambda_C & (1-\rho)\lambda_C & 0 & -\lambda_C \end{bmatrix} \tag{6.1}$$

where μ_B is the breaker repair rate, μ_C is the conductor repair rate, λ_B is the breaker failure rate, λ_C is the conductor failure rate, and ρ is the breaker failure to open probability

Using typical specifications for highly available circuit breakers [Military Reliability Handbook] the failure rates and the repairs rates for the conductor as circuit breaker are $\mu_B = \mu_C = 4.2e-3$ and $\lambda_B = \lambda_C = 1.68e-9$ with $\rho = 0.01$ which yields and availability of 6 nines.

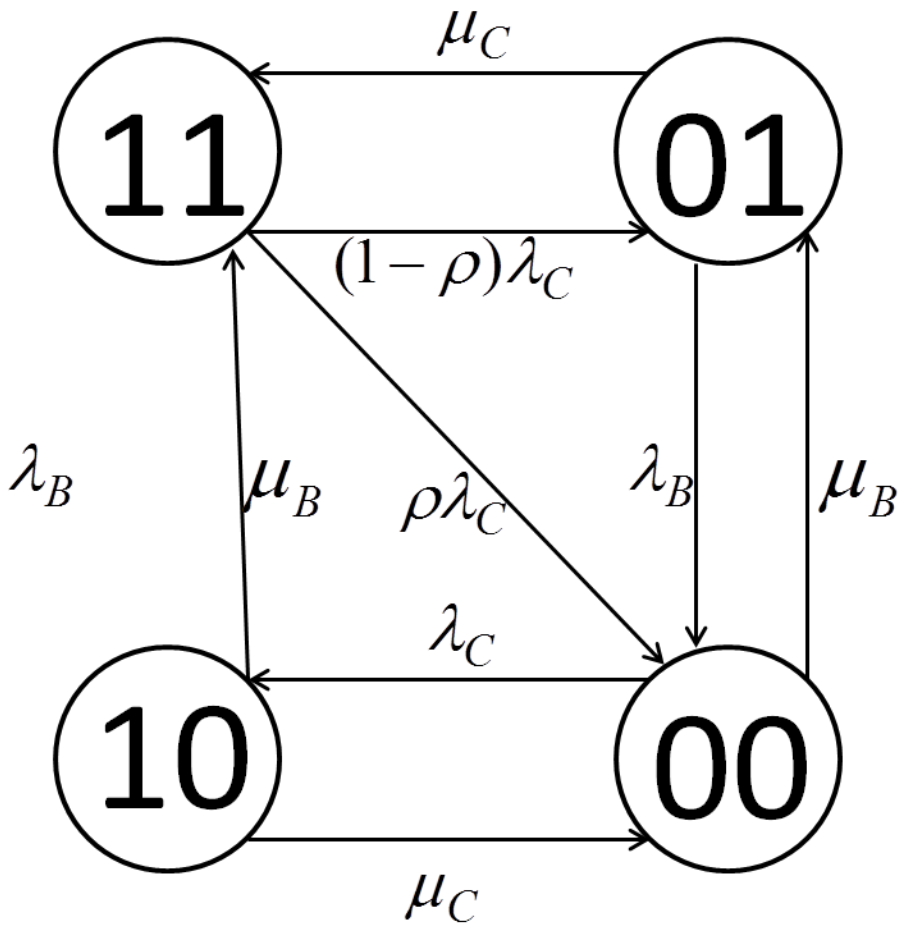

Fig. 6.1 Circuit breaker availability model state transition diagram.

The CBs and power electronics interfaces can be collectively labeled as interfaces in the microgrid for the calculation of availability. The availability of these interfaces is important as their availability becomes a scaling factor at each connection of a source in a microgrid distribution network. That is, a source is available only if the interface connected to it is functional. Therefore while calculating the availability the interface availability are used as scaling factor of availability because of the only if they work for the power flows from the source, or power flows into a load. The faults in the interfaces are the ones considered as failures in the distribution network for example,

short circuit failure modes of CBs and the failure of power electronic interfaces. It is also assumed that the failure of the interfaces is independent of each other.

Availability of the microgrid

The availability of the microgrid is defined as the probability of serving the load demand by the microgrid resources. Therefore a failure to supply any load is considered a failure. In other words, the unavailability can be measured as the amount of energy deficiency of the system. This energy present of the system can be represented via a fitness function defined as follows.

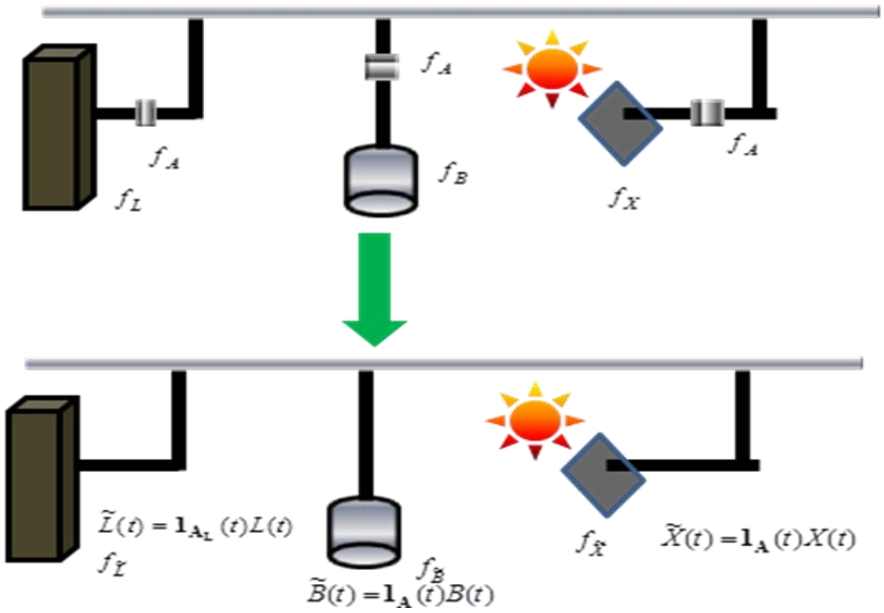

Fig. 6.2 Renewables and energy storage with interfaces, an equivalent representation for availability calculations

Consider a basic setup as shown in Fig. 6.2 wherein a source is powering a load supported by a storage unit Let $X(t)$ be a energy available at source at time t and $B(t)$ be the energy available from the storage at time t and $L(t)$ be the load at time at time t then the fitness function $G(t)$ at time t is defined as

$$G(t) = X(t) + B(t) - L(t) \tag{6.2}$$

The availability is defined as when the total energy $X(t)+B(t)$ available is greater than or equal to the load i.e. $X(t)+B(t) \geq L(t)$ or $G(t) \geq 0$. Therefore availability of the system in Fig. 6.2 is the probability that $G(t) \geq 0$. If $f_X(t)$ $f_B(t)$ $f_L(t)$ are the distributions of $X(t)$, $B(t)$ and $L(t)$ at time t then,

$$A(t) = P(G(t) \geq 0) = \sum_{g \geq 0} f_G(t) = \sum_{g \geq 0} (f_X * f_B * f_{-L})(t) \tag{6.3}$$

In order to compute $f_G(t)$ the distributions $f_X(t)$ $f_L(t)$ and $f_B(t)$ are needed .The $f_B(t)$ depends on $f_X(t)$ and $f_L(t)$ which is to be derived given the type of source. In the next section the modeling of the microgrid DERs is given. Also, note that the fitness function shown in (6.1) has no interfaces. The definition can be extended in order to incorporate the interfaces which are given in the next section.

MICROGRID DERS MODELS

In this chapter three sources are considered to be present in the microgrid: the main grid, diesel gensets and photovoltaics. The probabilistic behavior of the power output of each of these sources need be to calculated. Each source can come with its own associated energy storage.

Source characteristics with interface:

Let X be the power output of the source and let $\mathbf{1_A}$ be an indicator random variable such that the interface is in a working state. Then the power output at the interface terminal is $\tilde{X} = \mathbf{1_A} X$. Let f_A and f_X be the probability mass functions (pmf) of the interface and the source respectively. The pmf of $\tilde{X}$ denoted by $f_{\tilde{X}}$ is given by the following formula:

$$f_{\tilde{X}}(x) = \begin{cases} f_X(x) f_A(1) & x \neq 0 \\ f_X(0) f_A(1) + f_A(0) & x = 0 \end{cases} \tag{6.4}$$

Renewables and energy storage with interfaces:

The energy storage model with PV is derived from the work in Song et al. 2013 and extended to include the interface. The energy storage dynamics without interfaces is given by the following equation Song et al. 2013.

$$B(t+1) = \max\left[0, \min\left[B(t) + X(t) - L(t), B_m\right]\right] \tag{6.5}$$

This is equation is linear in the interval $[0, B_m]$ however when interfaces are included using (4) the equation becomes,

$$B(t+1) = \max\left[0, \min\left[B(t) + \mathbf{1}_{\mathbf{A_B}}(t)\tilde{X}(t) - \mathbf{1}_{\mathbf{A_B}}(t)\tilde{L}(t), B_m\right]\right] \tag{6.6}$$

The above process is represented by a Markov chain similar to the one in [Song et al. 2013], the transitions in the battery state. For calculations, here it is assumed that the battery SOC distribution $f_B(t)$ is already known which can be calculated using the method in [Song et al. 2013] with the modification required for the interfaces as indicated in (6.5). The state transition diagram or such a Markov chain is shown in Fig 4.15. The focus of this chapter is to calculate the availability in the presence of a distribution network. Note that in (6.1), the calculation of the fitness function, the storage element is treated like a source. Then the output of the battery along with its interface is $\tilde{B}(t) = \mathbf{1}_{\mathbf{A_B}}(t)B(t)$ with the pmf calculated using (6.4).

Diesel gensets with interfaces:

Diesel genets depend on a fuel supply for generating power. In extreme conditions, the fuel supply to the diesel genset is discontinuous. The genset can supply power only if there is sufficient fuel being supplied to the genset via some mechanism whether it is a pipeline or a fuel tank. The discontinuity of fuel supply is mitigated by the presence of storage, but the tank needs to be refueled by a refueling system usually composed of trucks. There, however, is a lead time or delay associated with each refueling instance from the time when it is demanded. The evolution of the fuel tank

states as in the case of the battery state of charge is modeled using a Markov chain but with lead times. In case of fuel state independent truck arrivals, this could be the case when multiple diesel generators are involved, as in the case of a microgrid, the fuel supply availability is taken as the refueling probability. The refueling probability denoted as *b* in the state transition diagram for the Markov chain of the fuel tank in Fig. 5.5. In a standalone diesel genset system powering the load the fitness function for the diesel genset and load is

$$G(t) = F(t) - L(t) \tag{6.7}$$

Where $F(t)$ is the energy proportional to the volume of fuel in the fuel tank. For evaluating the output of the diesel genset with an interface the $F(t)$ is replaced with $\widetilde{F}(t) = \mathbf{1}_{W_{CBF}} F(t)$ and the fitness function becomes

$$G(t) = \widetilde{F}(t) - L(t) \tag{6.8}$$

The distribution for the energy output for the genset can be calculated with (6.4).

Model of the main power grid

The model for the grid under tropical cyclones was derived in Chapter 3. The availability function can be directly used here which is given by

$$A_{grid}(t) = p_f\,(p_A(t) + p_D(t)) + 1 - p_f \tag{6.9}$$

The capacity of the grid is assumed to be infinite i.e. if there is a grid then any and all of the load may be supported by it as a long as there is a path to the load from the grid tie point via the distribution network. In order to make the calculations of the availability via the fitness function, two approaches are possible while considering the presence of the grid. The first approach is, the grid capacity is set to the sum of the maximum load. Therefore

$$f_{grid}(t) = \begin{cases} \sup \sum_i L_i & A_{grid}(t) \\ 0 & 1 - A_{grid}(t) \end{cases} \tag{6.10}$$

The second approach is to condition on the absence of the grid i.e. the grid being out and calculate the microgrid availability. The total microgrid availability using the second method is:

$$A = A_{nogrid} U_{grid} + A_{grid} \tag{6.11}$$

However, the above formula needs to be used according to the type of distribution network used to connect the microgrid. The second approach is the simpler of the two and is used while considering the radial and ladder distributions because it simplifies the calculation whereas for the ring distribution the first approach is used as the formula needs to account for which leg of the ring the grid is connected to which increases the number of terms in the equation. In next the section, effects of architectures are discussed in calculating the overall microgrid availability. Also, note that the time variable in (6.11) is omitted for ease of notation. The availability equations are nonetheless to be calculated for each time *t*. In the flowing section the suppressed notation is used and it is to be understood that all availability equations derived in Section IV are functions of time

MICROGRID ARCHITECTURES

Microgrids are generally connected using one of the three architectures, radial, ring and ladder [Kwasinski and Krien 2007]. Radial architecture is one of the most popular architectures used [Guerrero 2013] owing to its simplicity. The microgrid availability is largely dependent on the configuration of the connections of the various sources and grids via interfaces. This section derives availability formulae for the microgrid for each of the microgrid distribution architectures.

Radial Microgrid:

The radial architecture is commonly used as distribution architecture for microgrids. Consider a general radial architecture in Fig. 6.3. The loads get power only if the interfaces at the load are all working. Let a_i be the availability of the ith interface and W_{CBL} the set of working states of the load interface. The set of working states is a singleton with all the interfaces working.

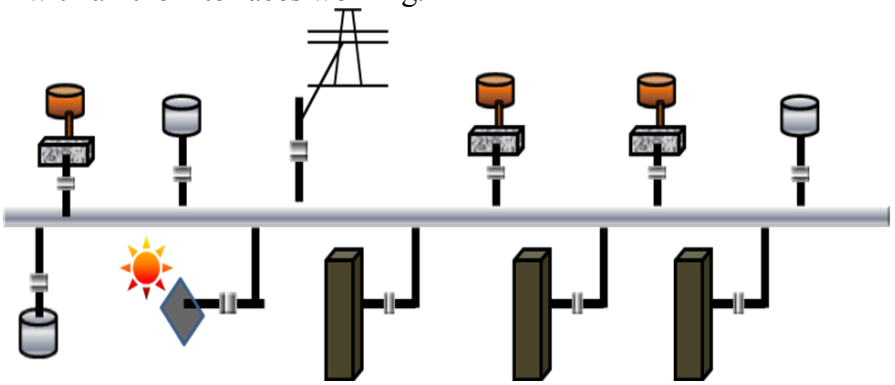

Fig. 6.3 Schematic of a Radial microgrid with 3 loads, 1 PV with 3 batteries and 3 diesel genset and a grid tie

The radial microgrid formula is:

$$A_{\mu G}(radial) = P\left(\mathbf{1}_{W_{CBL}}\mathbf{1}_{G(t)\geq 0} = 1\right)$$

$$= P\left(\mathbf{1}_{W_{CBL}} = 1\right)P\left(\mathbf{1}_{G(t)\geq 0} = 1\right) = A_{CBL}A_G \tag{6.12}$$

$$A_{CBL} = a_{CBL_1}a_{CBL_2}\ldots a_{CBL_N} \tag{6.13}$$

$$A_G = P(G(t) \geq 0) = P\left(\sum_i 1_{W_{CBi}}X_i - L \geq 0\right) = f_{\tilde{X}} * f_{-L} \tag{6.14}$$

$$\tilde{X} = \sum_i 1_{W_{CBi}}X_i \tag{6.15}$$

In the microgrid it is assumed that the genset is called into action only when the PV and the batteries are insufficient to serve the load i.e. the diesel genset is only used to serve the part of the load that cannot be served by the PV and the battery. Therefore, while calculating the diesel genset pmf, the load seen by the genset is:

$$L_{gs}(t) = \{X_{PV}(t) + B(t) - L_{Total}(t)\}^{-} \tag{6.16}$$

When the fitness function is calculated all similar sources are lumped. The diesel genset are lumped together and the photovoltaics are lumped together and the loads are lumped together. Once lumped, the $f_{\tilde{F}}$, $f_{\tilde{X}_{pv}}$ and $f_{\tilde{B}}$ are used to find the overall microgrid availability. In the presence of the grid the radial availability formula is

$$A_{\mu G}(radial) = A_{CBL}A_G U_{grid} + A_{CBL}A_{grid} \tag{6.17}$$

Ring Microgrid

Consider the ring microgrid in Fig 6.4. As in the radial case the loads get power only if the interfaces at the load are all working. Let a_{CBL_i} be the availability of the interface at the *i*th load. Let X_l be the set of sources for the left leg of the ring and X_r the set of sources for the right leg of the ring X_x be the set of all sources. Similarly, let L_l, L_r and L_x be the set of loads for the left leg the right leg and all loads respectively.

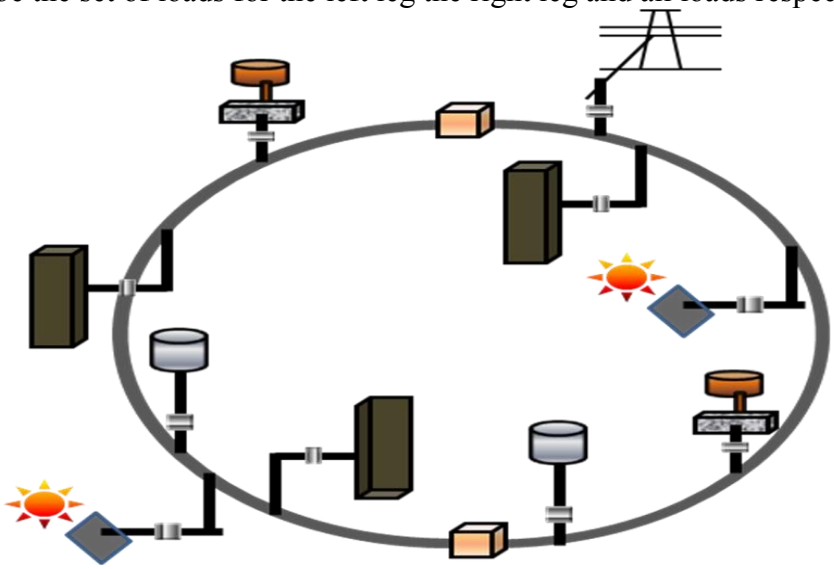

Fig. 6.4 Schematic of a Ring microgrid with 3 loads, 2 PV with 2 batteries and 2 diesel genset and a grid tie

The connectivity of the ring is primarily controlled by the states of the interfaces on the bus, e_1 and e_2. If either one of them is working then each load can be served by

each source therefore the purpose of availability calculation the distribution network is similar to the radial network. When both e_1 and e_2 are both failed then the left and right legs of the ring get separated and the fitness function of each leg has to be considered and the availability under the condition of the ring being separated and the condition when both legs are working i.e. the probability that the fitness function of the left and right legs are non negative. The ring availability formula is therefore

$$A_{\mu G}(\text{ring}) = P\left(1_{W_{CBL_X}}\right)P(G_x(t) \geq 0)P(\mathbf{1}_{W_{CBB}} = 1) + P(\mathbf{1}_{W_{CBB}} = 0)P(1_{W_{CBL_r}})P(G_l(t) \geq 0)P(1_{W_{CBL_r}})P(G_r(t) \geq 0) \quad (6.18)$$

The probability of both bus interfaces being off is the product of the unavailability of the bus interfaces which $U_{CBB} = u_{e_1}u_{e_2}$ and the probability of either one being on is $A_{CBB} = 1 - U_{CBB} = 1 - u_{e_1}u_{e_2}$ .Then`

$$A_{\mu G}(\text{ring}) = P(1_{W_{CBL_X}})P(G_x(t) \geq 0)(1 - U_{CBB}) + U_{CBB}P(1_{W_{CBL_r}})P(G_l(t) \geq 0P(1WCBLr)PGrt\geq0 \quad (6.19)$$

The total load interface availability is the product of the availability of the interfaces at the load

$$A_{CBL_x} = a_{CBL_1}a_{CBL_2} \dots a_{CBL_N} \quad (6.20)$$

The load interface availability for the left leg and right legs are

$$\begin{aligned} A_{CBL_l} &= a_{CBL_1}a_{CBL_2} \dots a_{CBL_K} \\ A_{CBL_r} &= a_{CBL_{K+1}}a_{CBL_{K+2}} \dots a_{CBL_N} \end{aligned} \quad (6.21)$$

Therefore,

$$A_{\mu G}(\text{ring}) = A_{CBL_x}P(G_x(t) \geq 0)(1 - U_{CBB}) + U_{CBB}A_{CBL_l}P(G_l(t) \geq 0ACBLrPGrt\geq0 \quad (6.22)$$

The fitness function for the full ring is

$$G_x = \sum_{i\in X_x} 1_{W_{CBi}}X_i - \sum_{i\in L_x} L_i \quad (6.23)$$

The fitness functions for the left and right legs are

$$G_l = \sum_{i \in X_l} 1_{W_{CBi}} X_i - \sum_{i \in L_l} L_i$$
$$G_r = \sum_{i \in X_r} 1_{W_{CBi}} X_i - \sum_{i \in L_r} L_i \quad (6.24)$$

Also note that $G_x = G_l + G_r$ which means that that once f_{G_l} and f_{G_r} are known f_{G_x} can also be evaluated as $f_{G_x} = f_{G_l} * f_{G_r}$.

Let

$$A_x = P(G_x \geq 0) \ , A_l = P(G_l \geq 0), A_r = P(G_r \geq 0) \quad (6.25)$$

then the ring microgrid availability formula is

$$A_{\mu G}(ring) = a_{CBL_1} \ldots a_{CBL_N}((A_x + u_{e_1} u_{e_2}(A_l A_r - A_x)) \quad (6.26)$$

In ring microgrids the load seen by a given storage element is dependent on its location. Consider a very simple case, with one PV, one battery and one load on each leg of the ring. When at least one of the bus interfaces are in the on state, the batteries share the load L_l and L_r but when the bus interfaces are off the load on B_l is L_l and the load on B_r is L_r. In this case, two separate markov chains need to calculated for this condition alone for each of the batteries which increases the complexity of the problem, however if the probability of the for highly available interfaces the probability of not sharing the load is low. Therefore, when the buses are separated it can then be assumed that the batteries have an energy sharing proportional to their capacity.

Ladder Microgrid:

The availability calculation of a ladder microgrid is also similar to the radial microgrid. The basic schematic is given in Fig. 6.5. Consider the interfaces connecting the DERs and loads to the buses as shown in Fig. 6.5. In order for the load to be served or the DERs to remain connected to the rest of the system at least one of the interfaces on the leg needs to work. This is the case for every leg. Therefore for the purpose of availability calculations the two interfaces can be replaced by a single interface with an availability corresponding to an equivalent condition that at least one of the interfaces is

working as shown in Fig. 6.6. The replacement is done as follows. Let a_l and a_r be the availability of the left and right interface. The availability of the equivalent interface a_e is

$$a_e = 1-(1-a_l)(1-a_r) = a_l + a_r - a_r a_l \tag{6.27}$$

Replacing the interfaces on each leg of the ladder by their equivalent interface with a single bus in the distribution the problem reduces to finding the availability of the equivalent radial network shown in Fig.6.7.

$$\begin{aligned} &A_{\mu G}(ladder \mid a_l a_r) = A_{\mu G}(radial \mid a_e) \\ &= A_{CBL} P(\sum_i \mathbf{1}_{W_{CBi}} X_i - L \geq 0) \end{aligned} \tag{6.28}$$

$$\text{where } A_{CBL} = a_{CBL_1} a_{CBL_2} \ldots a_{CBL_N} \tag{6.29}$$

are the equivalent interfaces availabilities and the set of working states W_{CBL} are such that the equivalent interfaces are working.

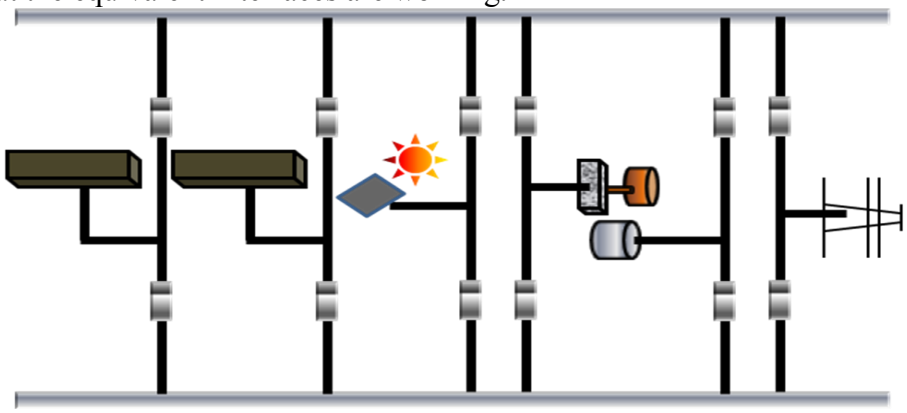

Fig. 6.5 Ladder microgrid

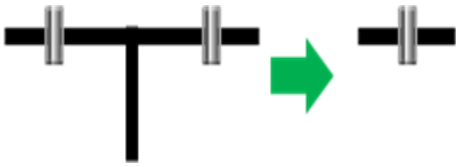

Fig. 6.6 Interface connection equivalent representation

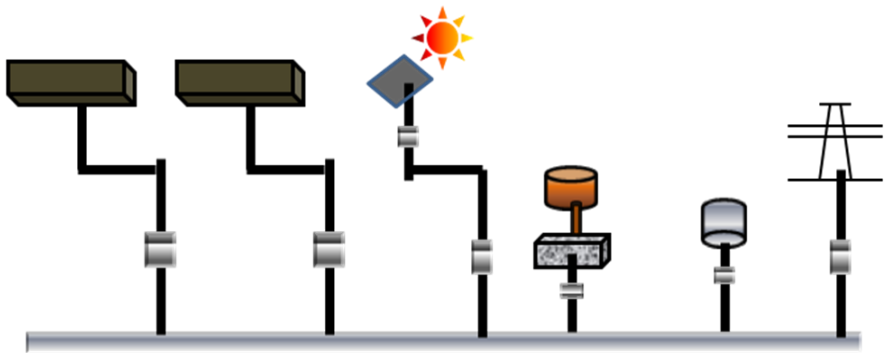

Fig. 6.7 Equivalent radial representation of a ladder network for availability calculations

RESULTS AND DISCUSSION

The equations derived in the previous section are at all time dependent, however each of the DERs operate at different times scales. This is especially true during extreme events like natural disasters like tropical cyclones and earthquakes. During tropical cyclones and earthquakes grid outages can last for days and weeks whereas the diesel gensets and PV resources and load evolve in much smaller times scales. Compared to the grid restoration the DERs are assumed to be in their steady state operation. Therefore the only time dependence of the availability is of the main grid when the microgrid availability with the grid is considered. Typical failure time, wait time and repair time parameters for the grid are given for triangular densities in table 6.2. These are discretized and used in the formula for calculating the grid availability. The grid outage probability is assumed to be 0.75 which corresponds to a value of $L=6.4$ which correspond to areas like Suffolk in New York during Super-storm Sandy [Krishnamurthy and Kwasinski 2013]. The plot for the grid availability versus time is given in Fig. 6.8 for the parameters in Table 6.1.

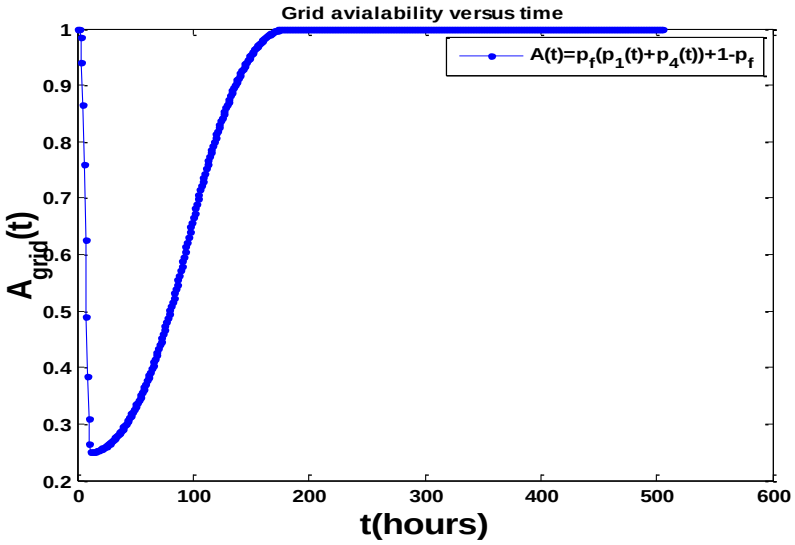

Fig. 6.8 Time dependent grid availability during tropical cyclones with grid outage probability 0.75.

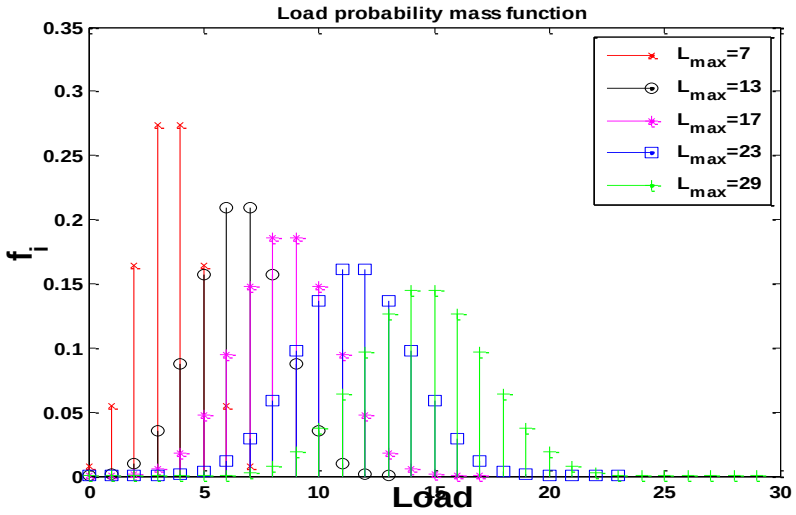

Fig. 6.9 Load Probability mass function

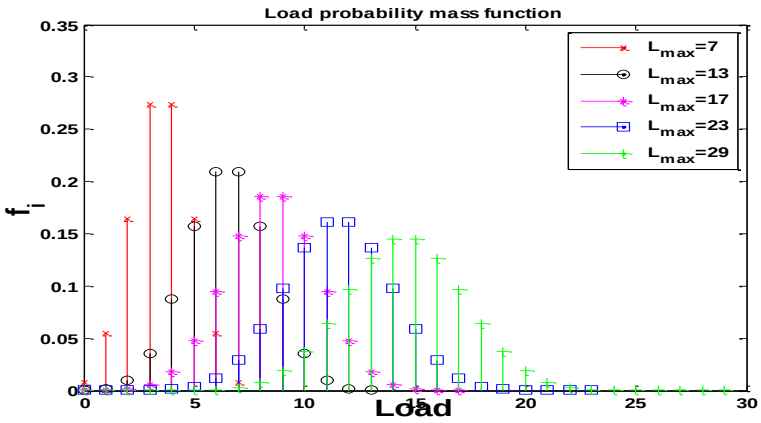

Fig. 6.10 Load seen by the microgrid with load interface availability of 6-nines

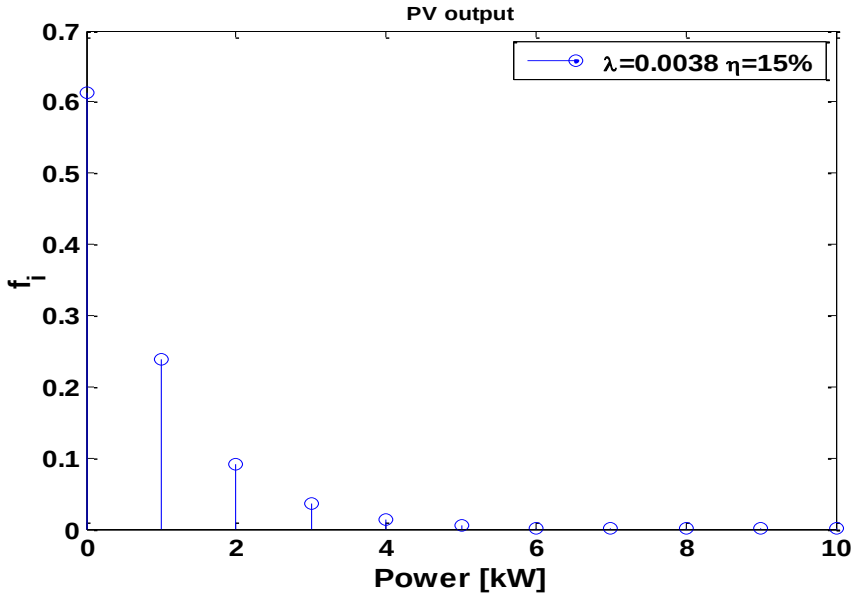

Fig 6.11 PV output probability mass function for parameters in Table II.

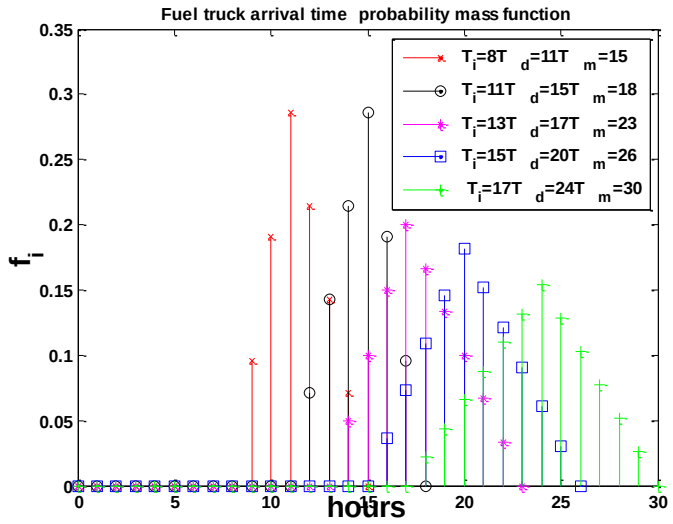

Fig. 6.12 Truck arrival density evaluated at 1 hour step

(Hours)	Fail time	Wait time	Repair time
T_i	0	0	0
T_d	5	6	72
T_m	10	10	240

Table 6.1: Grid Parameters

Load (kw)	1	2	3	4	5
P	0.5	0.5	0.5	0.5	0.5
N	7	13	17	23	29
Mean	3.5	6.5	8.5	11.5	14.5
Max	7	13	17	23	29
Variance	1.75	3.25	4.25	5.75	7.25

Table 6.2: Load Parameters

PV input exponential parameter	0.0038 W^{-1}
Total installed PV capacity	10 kW
Mean PV input per unit area	260 W/m^2
Panel conversion efficiency	15%
Area of array installed	26.67 m^2
Mean output of array	1.05 kW
Peak output of array	10 kW
Circuit breaker/PE. Interface availability	0.999999[Maish 1999]

Table 6.3: Photovoltaics and interface battery parameters

(Hours)	1	2	3	4	5
T_i	8	11	13	15	17
T_d	11	15	17	20	24
T_m	15	18	23	26	30

Table 6.4: Fuel Delivery pmf Parameters

The insolation data used here was collected in Austin, Texas, from 7 am to 7 pm for 7 months from Song et al. 2013. A typical 250 W PV panel from [Solar tech Data Sheet] has 15.3 % efficiency and 1.51 m^2 are used for the calculations. The PV array hence constructed has the parameters given in Table 6.2. The load is assumed to be binomial with parameters given in Table 6.3 and whose pmfs without and with interfaces are given in Figs. 6.9 and 6.10 respectively. The PV output pmf is given in Fig. 6.11. The

interfaces in general are assumed to have an availability of 6-nines as derived for the circuit breakers [Kwasinski 2011c].

The fuel delivery arrivals are calculated using triangular densities whose parameters values and the refueling probabilities are given in table IV. The plot of the fuel truck arrival densities are given in Fig. 6.12.

Using the above data for the microgrid DERs, the availability for each of the architectures radial, ring and ladder are calculated for various configurations of sources, interfaces, storage and loads. The results for the radial, ring and ladder are presented to discuss the effects of the various DERs and architecture on the availability of the microgrid.

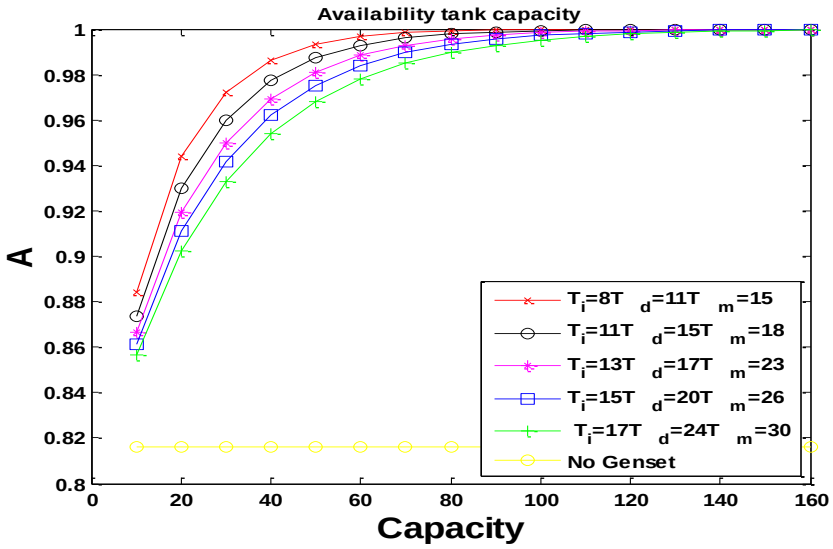

Fig. 6.13 Radial microgrid without grid availability vs tank capacity with PV with battery size Battery size 10kwh for load L_1

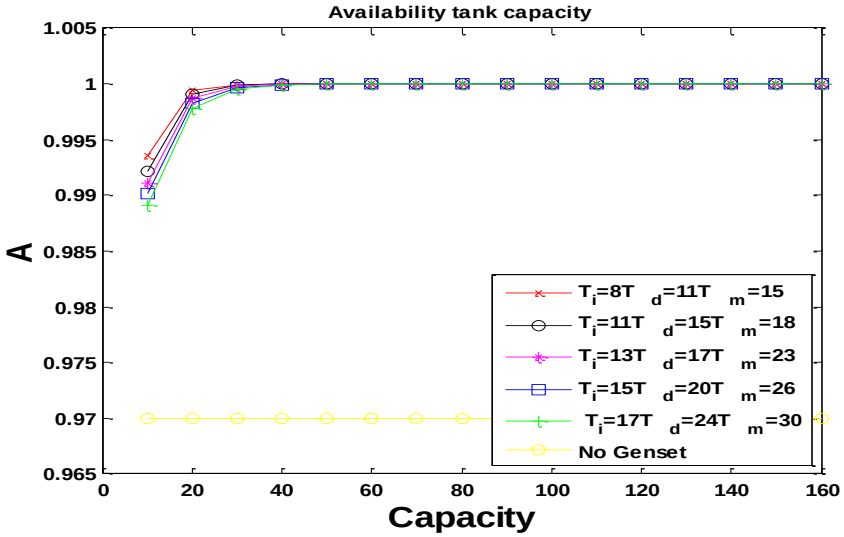

Fig. 6.14 Radial microgrid without grid availability vs tank capacity with PV with battery size battery size 20kwh for Load L_1

As mentioned before the PV sources are lumped together and the genset sources are lumped together. The diesel genset supports the portion of the load that the PV and the battery are not able to serve. For the radial configuration, in the absence of the grid the availability of the PV with a battery of capacity 10 kWh for load L_1 is 0.81598 and the same PV system with a battery of capacity 20 kWh for load L_1 is 0.96991. On the introduction of a diesel genset with a tank of capacity 40 kWh and a refueling probability or fuel delivery availability of 0.081 The availability improves to 0.9985 for the battery of 10kWh and to 0999994 for the battery of size 20 kWh. The plot of the availability versus tank capacity for the radial microgrid for the PV with 10 kWh battery capacity for load L_1 is given in Fig. 6.13 for various fuel delivery arrival time densities. It is seen that even for very low fuel delivery availabilities there is a significant improvement in availability by the addition of a genset with a fuel tank. A similar plot of availability versus tank capacity is shown for a battery of 20 kWh in the same system in Fig. 6.14. The improvement in availability, for a mean fuel arrival time of 11.33 hours, which is the

highest fuel delivery among the ones considered, beyond 100 kWh is small with a minor change only in the 8th decimal places. The results indicate that microgrid with the lower fuel delivery availability responds better to an increase in storage compared to a microgrid with higher fuel delivery availability. This can be seen from a closer scrutiny of the curves for availability vs. tank capacity for the radial microgrid in Fig. 6.13 and 6.14. The results indicate that increasing the storage produces greater improvement in availability for smaller values of fuel delivery availability. For example, for the microgrid with the 20 kWh battery, increasing the tank capacity from 100 kWh to 110 kWh for the second fuel delivery functions with mean 14.66 hours produces an improvement of 1 nine. The improvement in the availability demonstrates that the presence of storage can improve the availability of the microgrid as well the added diversity improves the availability.

A similar argument can be made for the case of incorporating renewables in a microgrid which has primarily depended on diesel gensets for improving the availability of the microgrid power supply to its loads.

The microgrid availability is limited by the availability of the interfaces in the microgrid. In specific the microgrid availability is bounded above by term A_{CBL} which is the product of the availability of the circuit breakers connected at the load when the load is more dispersed (more load units for the same total load) the overall availability reduces due to the reduction in value of A_{CBL} however the grouping of the load leads to increasing the single point of failures with the microgrid system at the load interface. Therefore in order to obtain better design of a highly available system, choices need to be made in how to configure the placement of the load within the microgrid distribution.

The ring microgrid for the same set of sources as above can be connect in a number of configuration by choosing the bus for connection for each microgrid

component. If everything is connected to the same bus then the availability is equal to that of a radial architecture as seen from the ring availability formula. The worst case or the case with the lowest availability is when all the DERs are on one bus and all the loads are on the other bus. The results for availability versus tank capacity with a PV with battery of 20 kWh are shown in the Fig. 6.15 with bus circuit breakers having 6 nines availability.

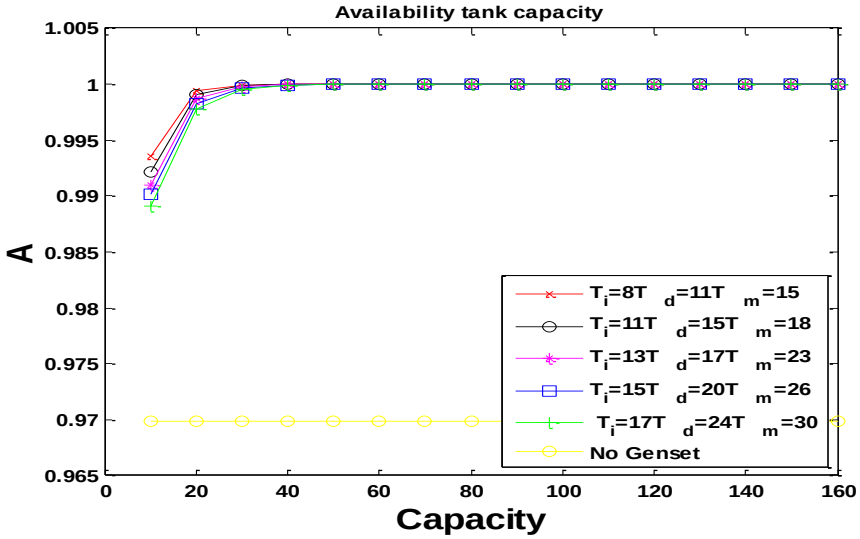

Fig. 6.15 Ring microgrid without grid availability vs tank capacity with PV with battery size battery size 20kwh for Load L_1

The ladder network calculations are exactly the same as the radial network when the interfaces on each leg are replaced by their equivalent. The presence of the additional interfaces improves the interface availability in each leg of the ladder network. This behaves like the redundancy for the power electronics interfaces with n=1 and m=1. For the interfaces considered here the left and right legs interface have $a_l = a_r = 0.999999$ i.e. 6-nines. The equivalent interface availability a_e is $a_e = 1-(1-a_l)(1-a_r)$ which is 12 nines. Now consider a microgrid with the same components as the radial microgrid in the previous example but connected in a ladder configuration. The resulting plots for the tank

capacity versus ladder microgrid availability without the grid are shown in Fig. 6.16. At tank capacity 40 kWh the availability is 0.9999954. It can be seen that the amount of resources required can be large to improve availability by 1 nine depending on the component and its function in the microgrid.

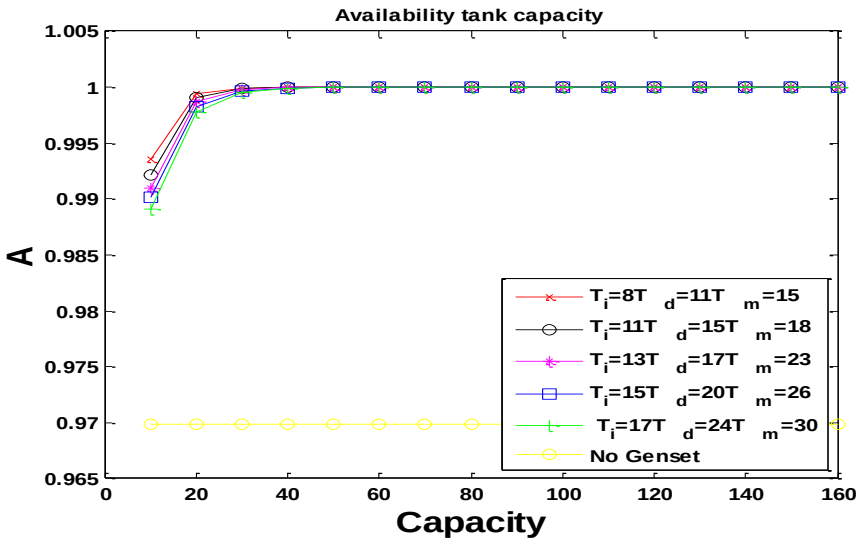

Fig. 6.16 Ladder microgrid without grid availability vs tank capacity with PV with battery size battery size 20kwh for Load L_1

Comparison of radial, ring and ladder architecture in the presence of interfaces:

The equivalent availability graph for radial and ring distribution architecture are shown in Fig. 2.21. As seen, the graphical availability representation which is the model for calculating the performance from the ring network is different from its electrical network representation. In the graph the edges are the interfaces and the nodes are the buses, DERs and loads. Therefore under the condition that loads and DERs are disconnected, availability drops. However, the benefits of the ring architecture might be further analyzed when the failures and repairs among the various components of the microgrid become correlated; i.e. in the case there are others benefits that could arise from separating the loads from the DERs, which is a topic for further research. When

comparing the numerical availability results for radial, ring and ladder architectures for the same set of sources and load it was observed, as expected, that the ladder has better availability that than of the ring and radial. The comparison is done using an islanded microgrid with the PV, 20kWh battery, 40 kWh fuel storage serving load L1. The better performance of the ladder is due to the presence of a redundant interface for each DER and load. When comparing the ring and radial network, it can be seen that in the best case, the ring can do as well as the radial network i.e. their availabilities are equal, and in the worse case the ring availability reduces, their values are given in Table 6.5 for bus circuit breakers availabilities of 4 and 6 nines respectively.

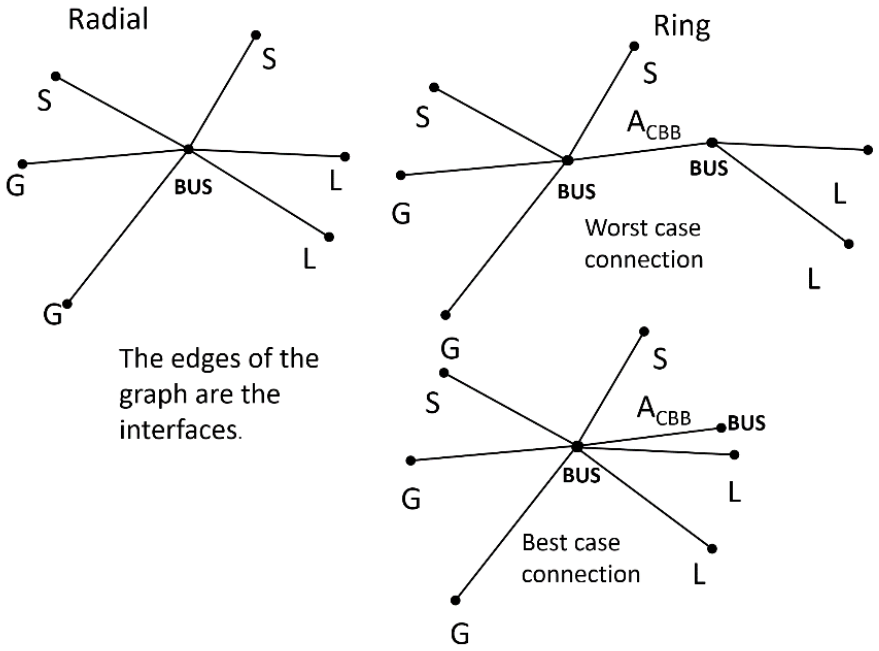

Fig. 6.17: Availability graph representation of radial and ring networks for the case of 2 generators 2 storage and 2 Loads for the availability model of the distributions architectures with interfaces each edge represent an interface connection. Buses, sources, storage and loads are indicated by the nodes.

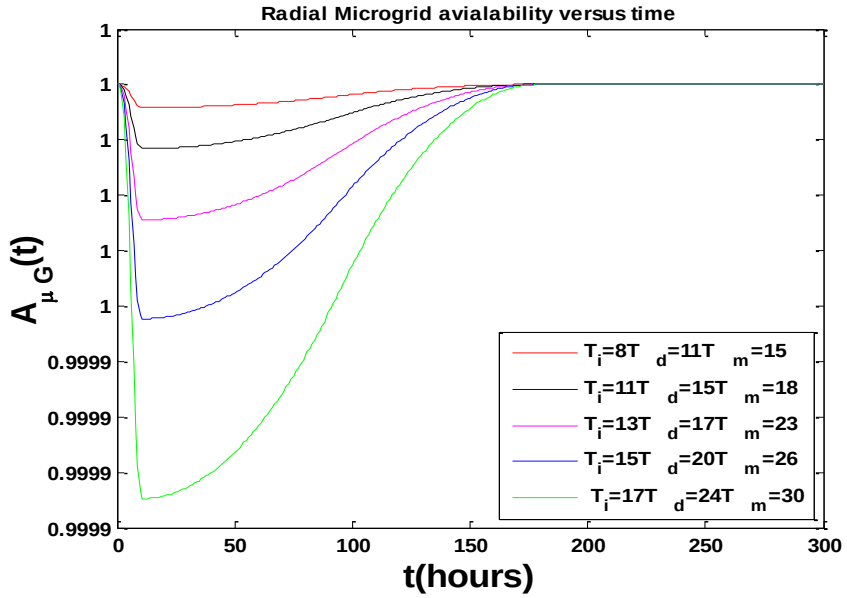

Fig. 6.18 Radial microgrid with grid availability vs time with PV with battery size 20kwh and tank capacity 40 kWh for Load L_1

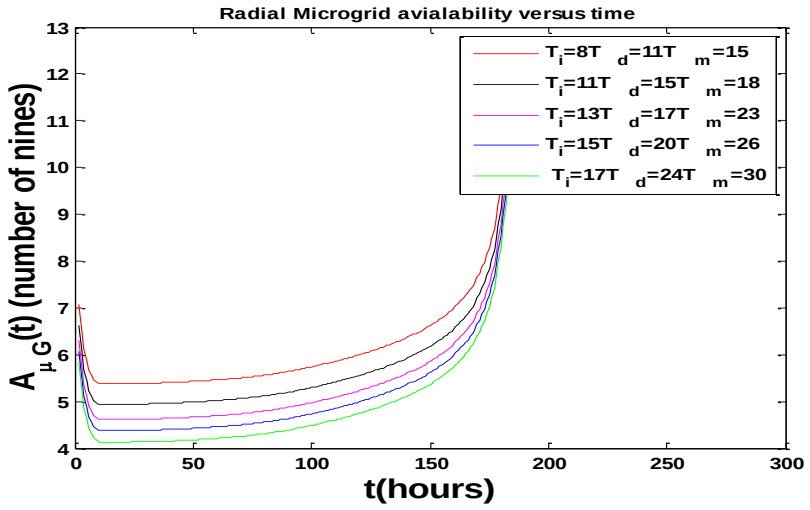

Fig. 6.19 Radial microgrid with grid availability in number of nines vs time with PV with battery size 20kwh and tank capacity 40 kWh for Load L_1

The above calculations have been so far limited to considering the grid absent. The grid is now incorporated by using the grid availability formula. The resulting time dependent availability function is given in Fig. 6.18. The same result but in terms of number of nines is given in Fig. 6.19. On comparing Fig. 6.8 and Fig. 6.19 it can be seen that the incorporation of diverse energy sources like renewables and diesel gensets the load can be supported with sufficient availability during extreme events. The type of source and the amount of storage that is required for each source is dependent on external life lines. But it can be seen that the presence of storage reduces the dependency on the lifeline by increasing availability even when the availability of fuel from the lifeline is quite low as indicated in table 6.4.

On comparing the availability results for radial, ring and ladder architectures for the same set of sources and load it was observed, as expected, the ladder has better availability that than of the ring and radial. The comparison is done using an islanded microgrid with the PV, 20kWh battery, 40 kWh fuel storage serving load L1. The better performance of the ladder is due to the presence of a redundant interface for each DER and load.

Architecture type	Interface availability	Bus a_{CB}	Microgrid Availability
Radial	6 nines	NA	5.2218 nines
Ring	6 nines	6 nines	5.2217 nines
Ring	6 nines	4 nines	5.2211 nines
Ladder	6 nines	NA	5.337 nines

Table 6.5: Microgrid availability by architecture, for Load L_1, battery capacity 20 kWh, Tank capacity 40 kWh.

On comparing the ring and radial network, it can be seen that in the best case, the ring can do as well as the radial network i.e. their availabilities are equal, and in the worse case the ring availability reduces, their values are given in Table 6.5 for bus circuit breakers availabilities of 4 and 6 nines, respectively. However, for very highly availability interface availabilities the difference in the availabilities between the infrastructures is minute. This is because relative to the contribution of the storage, lifeline and renewable system the interface availability for computational purposes is essentially 1. In fact, in the next chapter where the ICT site availability case studies are presented, the interface availability is assumed to be 1 to simplify the analysis.

CONCLUSIONS

This chapter discussed the microgrid availability modeling for quantifying the availability of microgrid with interface and three distribution architectures. The microgrid availability formulae for typical microgrid distribution architectures like the radial ring and ladder architectures were derived. A diverse set of sources in renewables, diesel genset and the main grid were considered in the availability calculations in the presence of storage and discontinuous fuel supply. It was found that the radial availability formula can be used as a building block in order to derive the formulae for the ring and ladder networks. The power supply availability was calculated for typical values of grid failure and restoration characteristics observed during tropical cyclones. It was seen that the incorporation of storage and a diverse set of sources in the form of a microgrid can greatly improve power supply availability during extreme events like tropical cyclones when the microgrid goes into island mode.

The next chapter uses the developed availability framework and studies ICT facilities availability during three major hurricanes namely Katrina, Ike and Sandy that affected the United States this past decade.

Chapter 7: Case Studies: Empirically validated availability model of information and communication technologies facilities under hurricane conditions

INTRODUCTION:

This chapter presents cases studies studying the performance of power infrastructure for information and communication technology (ICT) sites during hurricanes with the aid of the models developed in the previous chapters. Information and communication technology sites are selected because they represent an important example of a critical load that is not considered as such by electric utilities even when numerous federal and state agencies, such as the DHS, have identified communications as a critical service and national infrastructure. Most of the past works on this topic tend to describe performance of communication networks without including availability models or quantifying information and communication technology (ICT) sites performance with actual data collected in past events. Furthermore, although there exists a good number of studies realizing availability models of communication facilities power plants under normal operating conditions, these models present significant gaps even in basic critical components. For example, models of standby diesel generators exclude the impact of the fuel delivery process using a transportation network—which is, then, defined as a lifeline for the ICT site—on the diesel generator availability. That is, past models of standby gensets consider fuel supply with a perfect availability or with an unrealistic model. This chapter uses the models developed in the research to analyze the ICT sites performance during hurricanes and in their aftermath. The use of the developed models in the research presents the following novel aspects to the study of the ICT site behavior during hurricanes. Using the model for the diesel fuel delivery and tank, the effect of lifelines

such as roads and transportation infrastructure performance on overall availability of the ICT plant can be calculated. The field damage assessments enable the validation of the model and the data used. The impact of the energy storage on availability can also be studied using the models developed. The characterization of hurricane intensity presented in the earlier reports enables how a particular ICT system is affected.

The focus of this study is the ICT sites during hurricanes Katrina (2005), Ike (2008) and Sandy (2012). The data for which is obtained from NOAA, the utilities and network operators in the region affected by these hurricanes and field assessments. Of the regions surveyed, the coastal regions were affected the most during these hurricanes due to storm surge, high winds and high exposure time. Next an overview of hurricane history for Katrina, Ike and Sandy is given and observations from the field damage assessments exemplified using photographs taken in the immediate aftermath of the hurricane in the affected region. Following this, the mathematical availability framework developed in the previous chapters is adapted to study the behavior of ICT sites during hurricanes.

ICT SITES DURING HURRICANES

Hurricane history:

Katrina

Hurricane Katrina originated in the Atlantic Ocean near the Bahamas and made multiples landfalls in the United States of America, first in Florida and second the state of Louisiana as category 2 hurricane [Kwasinski et al. 2009]. The most affected parishes were Plaquemines, New Orleans St. Bernard, Jefferson parishes and areas along Lake Ponchartrain. ICT site damages during Katrina were located mostly near the coastal areas with very little sites actually experiencing complete physical damage. Most sites primarily lost power due to damaged batteries and the loss of the mains power supply.

These outages were worsened due fuel supply disruption. Poor construction practices like not placing equipment on raised platforms were also a common issue. [Kwasinski et al. 2009]. This chapter uses the model to calculate ICT site availability for various locations given the characteristics of the fuel supply disruption using the methods of chapter 5.

Ike

Hurricane Ike made landfall in the United State of America in Galveston Bay, TX in 2008. The coastal areas in Chambers county and Galveston County were the hardest hit with wind speeds in the excess of category 2 hurricane. Thousands of people lost power all the way from the Gulf coast to the interior of Texas. An important observation from field damage assessments was that the damage distribution confined mostly distribution system of the grid was spatially inhomogeneous. As in the case of Katrina, many ICT sites experienced power supply issues due to fuel starvation and drained batteries.

Sandy:

Sandy made land fall in the United States of America in the east coast of the United States of America as a category 1 hurricane [NOAA]. Sandy threatened many states in the northeast as it moved towards the coast with a total wind swath area of 1.4 million square miles in the ocean [Wunderground 2012]. However, it did considerably diminish as it made landfall on the New Jersey and New York coast.

ICT Site Behavior:

The ICT sites considered here are Central offices, Cell sites and Digital Loop Carriers (DLCs). The failure modes primarily observed during these ICT site outages are due to power supply issues. This is true not only during hurricane but other disasters such

as earthquakes [Dueñas-Osorio and Kwasinski 2012]. Power issues have been identified as the predominant cause of ICT site loss of service. Additionally, field observations during Katrina, Ike and Sandy indicate that due to long refueling times that in those places with heavy flooding and blocked roads, ICT sites with gensets as backup lost power due to running out of fuel [Kwasinski 2011b]. Examples of some central offices, cell sites and DLC affected during Katrina are shown in figures 7.1, 7.2 and 7.3. Flooding issues were a common cause of ICT site damages. Many facility doors were not water tight which lead to failed batteries [Kwasinski et al. 2009]. These flooding issues were present in the other hurricanes as well.

Fig. 7.1. Central office during Katrina with diesel fuel tank

Fig. 7.2. Cell site in New Orleans after Katrina

Fig 7.3. DLC system powered by genset after Katrina.

Figure 7.4 shows one of the few cell sites that survived in Bolivar peninsula. Most of the infrastructure we completely wiped out due to the extremely large storm surge with range greater than 10 feet. Most communication infrastructure if not destroyed lost power due to loss of mains power supply. DLCs were powered by portable gensets if they could be reached given the conditions of the transportation network as shown in Fig.7.5. However many cell sites and DLCs that were on the coast were destroyed as sown in Fig. 7.6 and 7.7.

Fig 7.4. Cell site in Bolivar peninsula during Hurricane Ike [Kwasinski 2008a]

Fig. 7.5. Failed DLC during Hurricane Ike due to loss of power [Kwasinski 2008a]

Fig 7.6. Hurricane Ike , Sabine TX, Central office destroyed[Kwasinski 2008a]

Fig. 7.7 Destroyed Cell site and DLC Hurricane Ike [Kwasinski 2008a]

Flooding issues were again seen during Sandy, for example, a central office during Sandy is shown in Fig. 7.8. Fig. 7.9 shows crews pumping flood water out of a central office in Manhattan in New York City. Fig. 7.10 shows a cell site located on top of the building with generators on the bottom, which is one of many sites wherein there was no cabling so that a portable generator maybe connected during the loss of power supply. Additional cable shad to be run down the building in order to keep the cell site operational [Kwasinski 2012].

Fig. 7.8 Flooded central office after hurricane Sandy [Kwasinski 2012a]

Fig. 7.9. Water being pumped out of the central office in Manhattan after Sandy [Kwasinski 2012a]

Fig. 7.10. Rooftop cell site in Rockaway Peninsula, New York

In the analysis that follows, the areas where in the ICT site performance is studied, the areas are classified into various zones for each hurricane. These zones indicate the amount of delay experienced by the fuel trucks that deliver fuel to the ICT site. It must be noted here that the delay time is a random variable. Therefore, each ICT

site experiences a delay independent of other ICT sites that maybe present in the zone. The triangular delay model is used for the fuel truck delivery time distribution in this chapter as done in Fig. 5.4. For each zone, the ICT sites experience the same delay characteristics. The analysis is conducted for only the first fuel delivery cycle, which is the most important cycle because the longest delays are expected during this period and grid power can be out during this period.

The schematic of a typical ICT site power supply system given below, in Fig. 7.11. The basic components are the mains power, genset and tank, the fuel delivery truck, rectifiers, battery and load. During hurricanes the availability of the rectifiers compared to the rest of the component is relatively very high. Therefore, for the case study presented here the rectifiers can be assumed to operating at availability 1. This assumption simplifies the analysis. The energy consumption of an ICT site can be variable and it is dependent on traffic [Lorincz et al. 2012] and the exact capacity information in terms of energy stored might not be available. However, the storage elements can be represented using their autonomy times. Each ICT site has a specific fuel tank autonomy depending on the type. The battery back up values can vary based on type and location of the ICT site. In both cases, battery and fuel tank, the autonomy time is considered as a measure of capacity (in case capacity in terms of state of charge or volumes of fuel is given, the autonomy can be calculated using the methods outlined in chapter 5 for calculating autonomy). The models for the case study are given next.

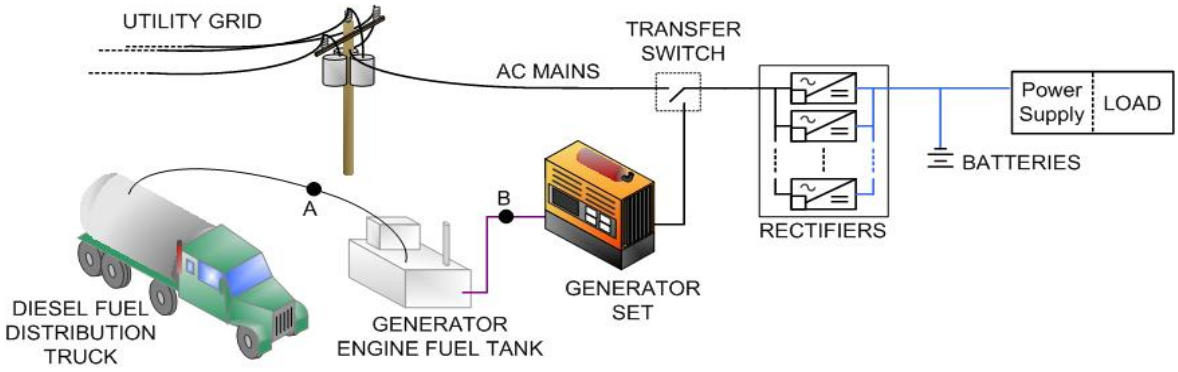

Fig. 7.11 ICT site power supply schematic

MODELS FOR ICT SITE POWER SUPPLY COMPONENTS

Main power grid

Probability of failure of the power grid to an ICT site at can be estimated via the fraction of customers losing power. If n out of m customers have lost power in a given area the probability that a given ICT site has lost power is n/m. This is due to the fact the most ICT site are connect at the distribution level. Therefore the probability of losing power from the grid for an ICT site can be found as the fraction of customers losing power in that county or parish. Therefore the grid availability is

$$A_{grid} = 1 - p_f = 1 - 0\%_{\max} \tag{7.1}$$

Diesel fuel delivery availability

In chapter 1, the models for fuel delivery and fuel tank were derived using markov chains. The availability of the truck was represented by $b=P(F=S_{RF})$ the long term fraction of time the fuel truck spends in the refueling state characterized by the triangular arrival density. However, here the unavailability of the genset system is calculated for the first cycle, therefore the unavailability of the whole genset system is the probability that the fuel is depleted before the truck arrives. Therefore the overall power supply availability of the genset is

$$U_{gen} = P(T_{truck} > T_{TC})$$

$$U_{gen} = P(T_{truck} > T_{TC}) = 1 - F_{T_{truck}}(T_{TC}) = 1 - \int_{[0,T_{TC}]} f_{T_{truck}}(\tau)d\tau, \quad (7.2)$$

$$f_{T_{truck}}(t) = Tri(t, T_i, T_D, T_M)$$

Batteries:

Typical ICT sites are also equipped with a battery backup. Given that there is no power available from the mains grid and the diesel genset, the batteries provide the additional autonomy. Thus under such a condition, the unavailability of the power supply system will be the probability that the batteries are drained before diesel genset or the mains grid comes back online. The unavailability is thus the probability that the ICT site power supply is under the condition that there is not enough fuel in the tank to support the load and the battery autonomy time is less than the fuel delivery time when the grid is off given that there is no mains grid and. The unavailability without the grid is therefore

$$U_{bat} = P(T_{T_{truck}} > T_{TC} + T_{bat}) \quad (7.3)$$

The above formula is sufficient in the present analysis to calculate the unavailability of the genset plus battery under the original assumption of the highly available rectifier. In the case the rectifier availability is also to be included to improve the availability estimate, the following modification needs to be done in order to calculate the unavailability. Let T_r be the restoration time of the grid and let T_f' be the fuel arrival time. Now define, the variable $T_{r,gen}$ which measures the time that some power is available to the load other than the battery (either the genset or grid

$$T_{r,gen} = \min(T_r, T_f') \quad (7.4)$$

Then unavailability is

$$U_{SYS} = 1 - A_{rectifier}\, A_{Grid+genset} P\left(T_{r,gen} < T_{bat}\right) \quad (7.5)$$

Where the CDF $P(T_{r,gen} < T_{bat})$ is calculated using the following formula (3.6), if T_r and $T_{f'}$ are independent.

$$P(T_{r,gen} < T_{bat}) = \int_0^t f(\tau)d\tau = F_{T_{r,gen}}(T_{bat}) = (F_{T_r}(T_{bat}) + F_{T_f'}(T_{bat}) - F_{T_r}(T_{bat})F_{T_f'}(T_{bat})) \quad (7.6)$$

The above analysis is derived using models from [Kwasinski et al. 2012, Kwasinski 2011] wherein the power supply availability for an ICT site in standby mode was developed. The analysis here is a simplified version of the models developed in those papers as it considers only the first refueling cycle for the genset in the various zones after the hurricane. From [Kwasinski 2011], the overall system availability under constant repair and failure rates for the ICT site shown in Fig. 7.11 is

$$U_{sys} = p_{gridfailed} e^{a_D(T_D+T_{bat})} + U_{SYS,nobat} e^{a_F T_{bat}} \quad (7.7)$$

Where $p_{gridfailed}$ is the probability that grid is in a failed state, a_D is the overall rate at which the power supply going from a state of having a grid failure with rectifiers and genset working where as a_F is the overall repair rate of the system i.e. the sum of the transition rates from the set of failed to working states. In (7.7) T_D is the fuel tank autonomy and T_{bat} is the battery time. The complete details of the Markov chain model for the derivation of (7.7) are in [Kwasinski 2011].

As mentioned before, in this report, the calculations are restricted to the first refueling cycle, and for only the highly available rectifier with the assumption $A_{rectifier}$ =1 in order to illustrate the effect of the infrastructure dependency for the standby genset. From the grid model developed in chapter 2 and data observed form previous hurricanes, it was seen that grid outages can extend for several weeks and in the first cycle of the fuel delivery. Therefore, it is highly likely that if the ICT site was experiencing a grid outage, then the grid outage would have existed during the time of the first refueling cycle. Therefore, for the grid model, it can be assumed the grid is failed with the probability p_f

obtained by the grid failure probability equation (7.1). Therefore, overall unavailability including the grid for the first cycle is found as

$$U_{SYS} = U_{grid}U_{bat} = p_f P(T_{T_{truck}} > T_{TC} + T_{bat}) \quad (7.8)$$

Where U_{bat} is the probability that the fuel in the tank and the battery are drained before a fuel arrival (found using (7.3)) and the U_{grid} is the probability that there is a grid outage (found using (7.1)). The data for p_f is given in table 7.1. The data for the tank capacity T_{TC} and battery capacity T_{bat} is given in table 7.2.

Results and Discussion: ICT site availability

The zones for Katrina, Ike and Sandy are shown in Figs 7.12, 7.13 and 7.14. The delay parameters for the fuel truck delivery time are given in table 3.1 and the corresponding triangular fuel arrival densities are plotted in Fig. 7.15, 7.16 and 7.17 indicating each zone. The fuel tank and battery data for the ICT sites types namely Central office, cell sites, and DLC are given in Table 7.2. The grid outage probabilities for each zone are derived from historic data obtained county-wise/ parish-wise for each of these hurricanes as shown in table 7.3. These values are used for calculating the grid unavailability. Using the formulae discussed above, the unavailability, zone wise for each hurricane, for each ICT site type are given in table 7.4 for Katrina, table 7.5 for Ike and table 7.6 for Sandy.

Among the zones, zone 1 has the most intense outages with longest restoration times for any infrastructure present in the area. The long delay zones are typically located on the coastal regions where the storm surge action is maximum, which results in flooded roads and submerged lines making logistics difficult. The high delays are also generally restricted to coastal counties in these three hurricanes such as Plaquemines and St. Bernard during Katrina. Central offices in zone 3 and 4 do better and have relatively

lower unavailability for the first cycle of fuel delivery. In zone 1, the unavailability for all ICT site infrastructure without grid power is 1. This is because of the extremely long delays experienced by the fuel trucks trying to access these zones. In fact, the fuel and battery back times are in some cases an order of magnitude apart as shown in Table 7.1 and 7.2. In various zones the battery back time can vary as seen in Table 7.2. Therefore, the unavailability, U_{batmin} and U_{min} are calculated when the smallest battery capacity is used and correspondingly U_{batmax} and U_{max} when the maximum is used. For any ICT site with any other battery capacity in the range [T_{batmin}, T_{batmax}], the unavailability of the system with only batteries and genset will be between the $U_{batmin,}$ and U_{batmax} and the overall unavailability including the grid will be between U_{min} and $U_{max.}$.

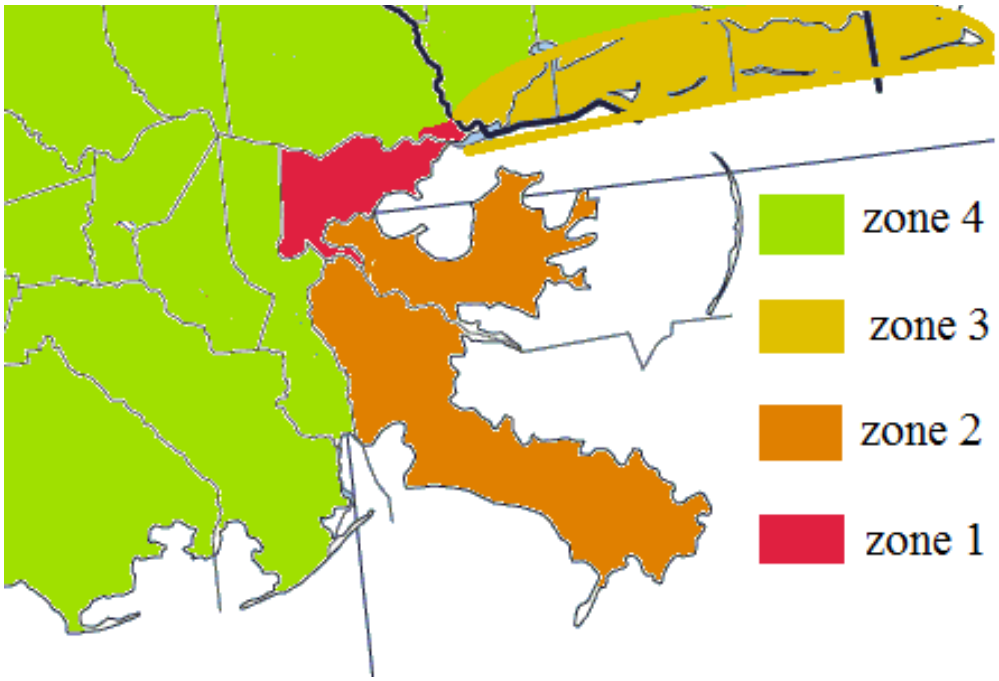

Fig. 7.12. Katrina: Louisiana, Zonal classification for various fuel delivery delays. Delays given in Table 7.1

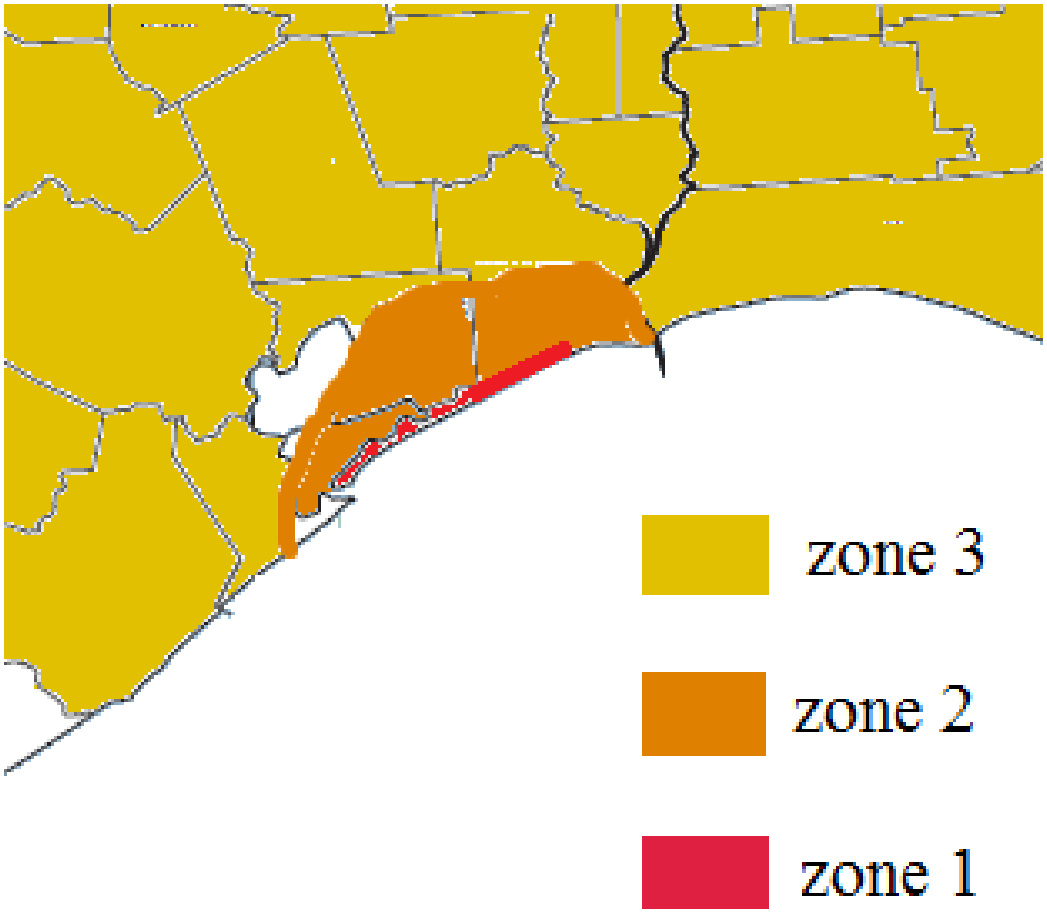

Fig. 7.13 Ike, Texas, Zonal classification for various fuel delivery delays. Delays given in Table 7.1

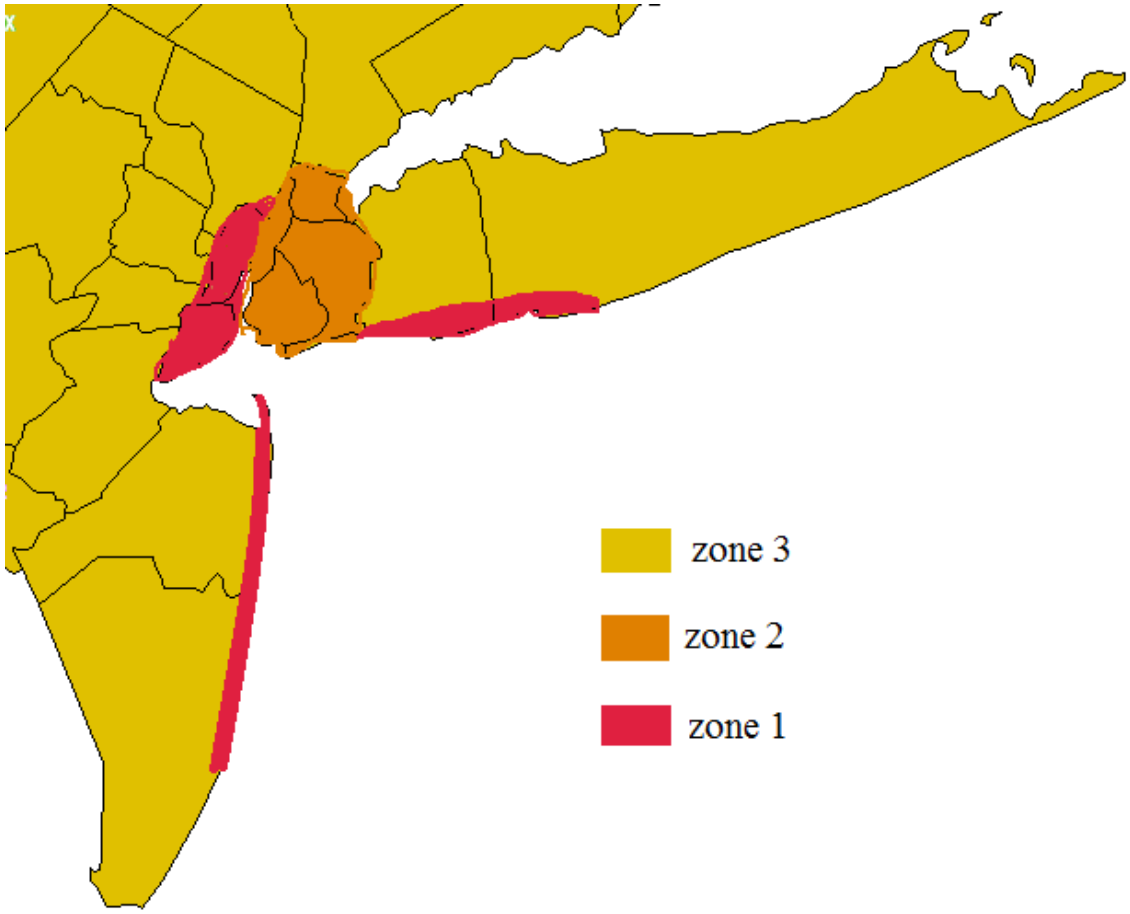

Fig. 7.14 Sandy, New Jersey and New York, Zonal classification for various fuel delivery delays. Delays given in Table 7.1

Hurricane	zone	Ti(days)	Td(days)	Tm(days)	Mean delay	p_f
Katrina	1	20	30	45	31.67	1
Katrina	2	7	15	30	17.33	1
Katrina	3	2	5	10	5.67	0.99
Katrina	4	2	3	7	4	0.99
Ike	1	7	15	30	17.33	1
Ike	2	2	4	7	4.33	1
Ike	3	1	2	3	2	0.97
Sandy	1	2	4	7	4.33	0.93
Sandy	2	1	3	5	3	0.76
Sandy	3	1	2	3	2	0.5

Table 7.1: Fuel truck delivery delay distribution parameters and zonal grid outage probability

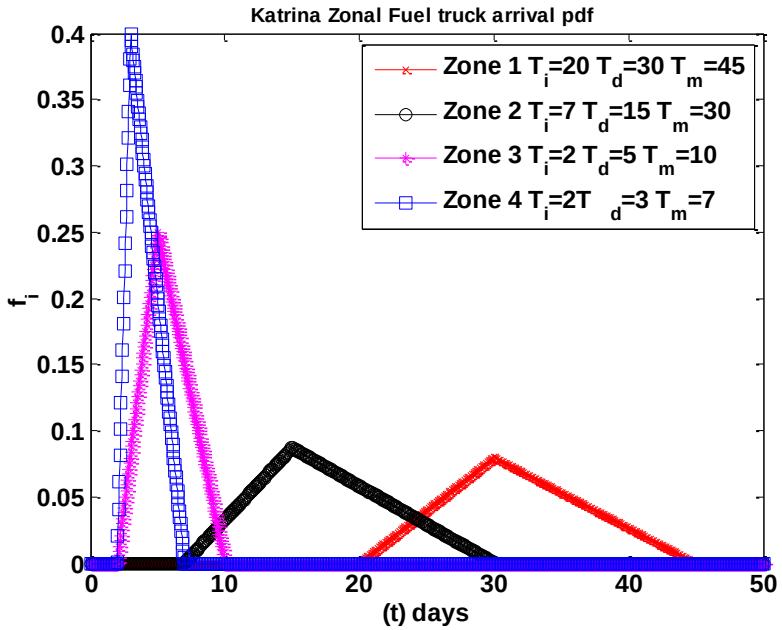

Fig. 7.15 Fuel delivery truck delay distribution for Katrina

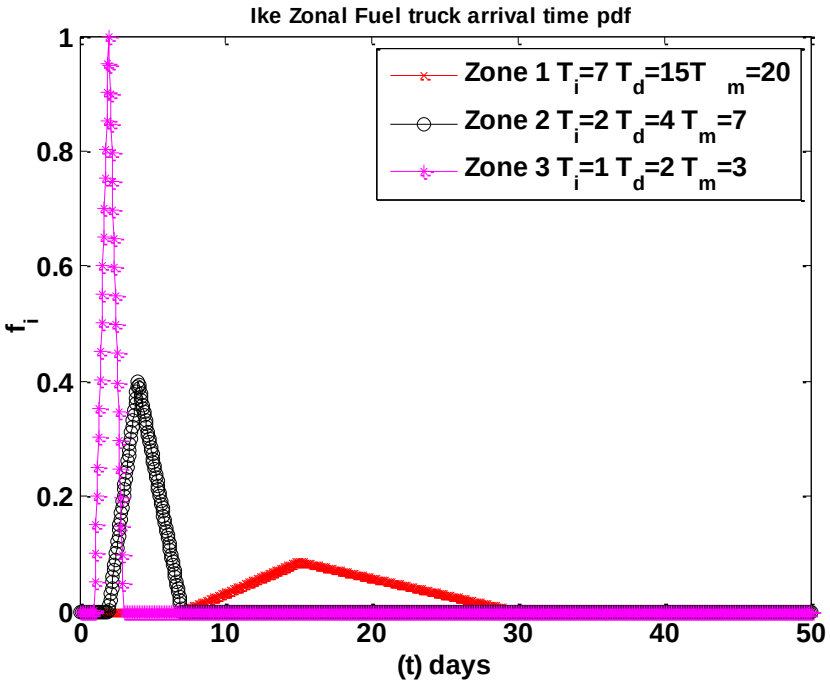

Fig. 7.16 Fuel delivery truck delay distribution for Ike

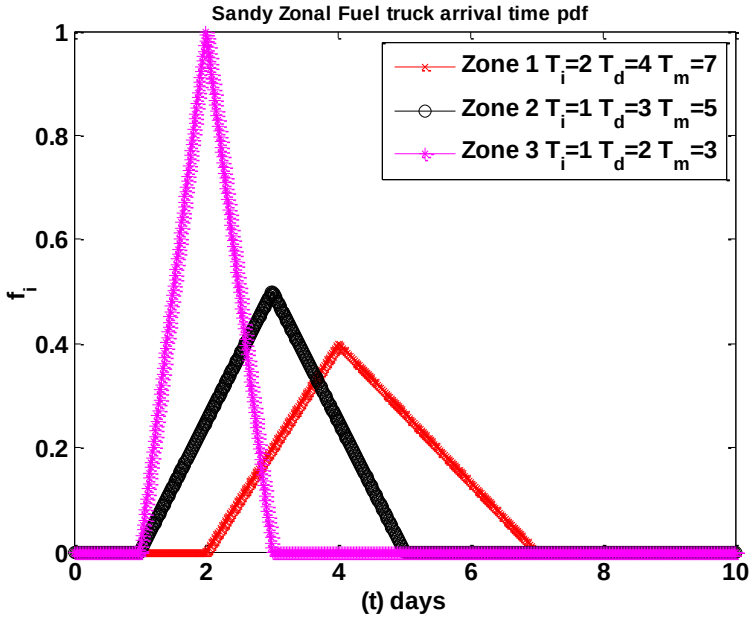

Fig. 7.17.: Fuel delivery truck delay distribution for Sandy

ICT site type	T_{TC} (hours)	Tbatmin (hours)	Tbatmax (hours)
CO	72	6	12
CS	24	4	8
DLC	24	4	8

Table 7.2: Fuel tank and Battery sizes for various ICT site type

Hurricane	County	Zone	p_f	T_r (days)
Katrina	Plaquemines	1,2	1	45
Katrina	St. Bernard	2	1	45
Katrina	Orleans	1	1	45
Katrina	St Tammany	3,4	0.8943	45
Katrina	St John	4	0.9944	45
Ike	Chambers	1,2	1	19
Ike	Jefferson	1,2	1	10
Ike	Harris	3	0.9787	18
Ike	Orange	3	1	9
Ike	Galveston	2,3	0.9065	45
Sandy	Nassau	1,2	0.93	15
Sandy	Suffolk	1,2	0.76	14
Sandy	Manhattan	2	0.40	5
Sandy	Queens	2	0.18	13
Sandy	Staten island	1	0.70	9

Table 7.3: Grid Outage Probabilities and Restoration times in various locations

Zone	site	T_{TC}	T_{batmin}	T_{batmax}	U_{gen}	U_{batmin}	U_{batmax}	U_{min}	U_{max}
1	CO	72	6	12	1	1	1	1	1
1	CS	24	4	8	1	1	1	1	1
1	DLC	24	4	8	1	1	1	1	1
2	CO	72	6	12	1	1	1	1	1
2	CS	24	4	8	1	1	1	1	1
2	DLC	24	4	8	1	1	1	1	1
3	CO	72	6	12	0.9583	0.9349	0.9063	0.925551	0.897237
3	CS	24	4	8	1	1	1	0.99	0.99
3	DLC	24	4	8	1	1	1	0.99	0.99
4	CO	72	6	12	0.8	0.7031	0.6125	0.696069	0.606375
4	CS	24	4	8	1	1	1	0.99	0.99
4	DLC	24	4	8	1	1	1	0.99	0.99

Table 7.4: Katrina Zonal Unavailabilities for various ICT site types

Zone	site	T_{TC}	T_{batmin}	T_{batmax}	U_{gen}	U_{batmin}	U_{batmax}	U_{min}	U_{max}
1	CO	72	6	12	1	1	1	1	1
1	CS	24	4	8	1	1	1	1	1
1	DLC	24	4	8	1	1	1	1	1
2	CO	72	6	12	0.9	0.8438	0.775	0.8438	0.775
2	CS	24	4	8	1	1	1	1	1
2	DLC	24	4	8	1	1	1	1	1
3	CO	72	6	12	0	0	0	0	0
3	CS	24	4	8	1	0.9861	0.9444	0.956517	0.916068
3	DLC	24	4	8	1	0.9861	0.9444	0.956517	0.916068

Table 7.5: Ike Zonal Unavailabilities for various ICT site types

Zone	site	T_{TC}	T_{batmin}	T_{batmax}	U_{gen}	U_{batmin}	U_{batmax}	U_{min}	U_{max}
1	CO	72	6	12	0.9	0.8438	0.775	0.784734	0.72075
1	CS	24	4	8	1	1	1	0.93	0.93
1	DLC	24	4	8	1	1	1	0.93	0.93
2	CO	72	6	12	0.5	0.3828	0.2813	0.290928	0.213788
2	CS	24	4	8	1	0.9965	0.9861	0.75734	0.749436
2	DLC	24	4	8	1	0.9965	0.9861	0.75734	0.749436
3	CO	72	6	12	0	0	0	0	0
3	CS	24	4	8	1	0.9861	0.9444	0.49305	0.4722
3	DLC	24	4	8	1	0.9861	0.9444	0.49305	0.4722

Table 7.6: Sandy Zonal Unavailabilities for various ICT site types

Effects of cooling infrastructure on ICT site availability

In Fig. 7.11 it can be seen that the connection of the cooling infrastructure in the power supply chain of the ICT site is before the batteries. This is usually the case in many ICT site facilities [Kwasinski et a. 2009][Ospina et al. 2014]. The additional autonomy

provided by the battery is therefore unavailable to the cooling infrastructure. Therefore an additional failure mode exists wherein the failure of power to cooling infrastructure might lead to overheating of the facility and a failure may occur before the battery runs out of charge. This problem has been studied in past work such as [Kwasinski and Krien 2007][Kwasinski 2008]. Since batteries are not powering the cooling infrastructure, the probability of failure of the power to the cooling infrastructure is calculated by setting Tbat to zero in (7.8). However failure of the air conditioner does not lead to an instantaneous failure of the telecommunication system due to overheating because of thermal inertia that is there is some time before the equipment overheats. The probability of failure of the ICT site due to failure of cooling infrastructure can be calculated if time to failure due to overheating time is known. Therefore the failure of the telecommunication equipment can occur at a time less than $T_{TC} + T_{bat}$, therefore the unavailability estimate of (7.8) is a best case estimate of the telecommunication unavailability for the first refueling cycle. A more accurate calculation can be performed given the overheating time of the telecommunication equipment in the ICT facility. Let Toh be the failure due to overheating time then the unavailability of the ICT site considering the overheating for Toh < Tbat is

$$U_{sys} = U_{grid}U_{ac} = p_f P(T_{truck} > T_{TC} + T_{oh}) \tag{14}$$

Where Uac is the unavailability of the cooling system without the grid.

Summary:

This chapter presented case studies for the models developed for diesel genset fuel supply to study the characteristics of the ICT site power supply during hurricanes. Data and field observations form Katrina, Ike and Sandy for central offices, cells sites and DLCs were used in order to evaluate their performance based on the location and

operating condition the ICT sites were subjected to. In accordance with field observations, the ICT sites in the coastal regions result in high unavailability due to fuel starvation and battery depletion caused by long delays times in the fuel delivery. This indicates that present communication infrastructure equipped with traditional standby systems are not equipped to be resilient to hurricanes of the like of Katrina, Ike and Sandy. Microgrids can be suitable solutions for improving power supply availability by providing a set of diverse sources and energy storage for the ICT site to use [Kwasinski et al 2012]. The models for microgrids have been developed to quantify the availability of microgrids in the presence of renewable energy sources such as photovoltaics and wind and diesel gensets with discontinuous fuel supply. Results from these models indicate that the power supply systems with high availability specifications are possible for critical loads such as ICT sites. The highly available microgrid planning is made feasible by these models as they quantitatively evaluate the microgrid availability under various operating conditions. Using these availability models and the microgrid framework the ICT site availability might be improved.

Chapter 8: Summary, Conclusions and Future Work

SUMMARY AND CONCLUSIONS

This dissertation presented models for evaluating the availability characteristics of various microgrid DERs in the presence of storage and lifelines dependencies. Chapter 2 discussed the characterization of hurricane-caused power systems outages through localized tropical cyclone intensity indices. The analysis used an empirical statistical approach based on data from the 2004, 2005 and 2008 hurricane seasons. Four outage metrics are defined for each county or parish: maximum outage incidence, 95% restoration time, 98% restoration time, and average outage duration. For each four indices , namely, the $LTCII_{MOI}$, $LTCII_{Tr95}$, $LTCII_{Tr98}$ *and* $LTCII_{AOD}$ and for each outage metric $O\%_{max}$, $T_{r,95\%}$, $T_{r,98\%}$ and M respectively derived. Using this data, Chapter 3 went on to derive the grid availability model during tropical cyclones wherein for each intensity of tropical cyclones the time dependent availability function of the grid was derived.

Next, in Chapter 4, following a survey of various DERs of a microgrid the availability modeling of PV systems was discussed and the optimal storage sizing for a given availability constraint was presented using Markov chains models.

Using similar Markov chains modeling ideas for storage, chapter 5 presented four models for deriving the power supply availability of diesel gensets with discontinuous fuel supply. The presence of storage was considered and its effect on fuel supply availability was analyzed for long and short delays in the fuel delivery process. The models for the fuel tank were developed for both deterministic and stochastic loads with fuel state independent and independent arrivals. The effect of controlling the fuel level at which the fuel order is placed was also found. The nominal tank autonomy was calculated for various load values. It was seen that with increasing storage, the genset

availability increased thereby reducing the dependency on the fuel truck delivery system. The improvement in availability was large for an increase in storage for small values of installed capacity.

Using the models developed for the grid and for each of the DERs with storage developed from chapters 3 to 5, chapter 6 discussed the microgrid availability modeling for quantifying the availability of microgrid. The microgrid availability formulae for typical microgrid distribution architectures like the radial, ring and ladder architectures were derived. A diverse set of sources which include renewables, diesel genset and the main grid were considered in the availability calculations in the presence of storage and discontinuous fuel supply. It was shown that the radial availability formula can be used as a building block in order to derive the availability formulae for the ring and ladder networks. The power supply availability was calculated for typical values of grid failure and restoration characteristics observed during tropical cyclones. It was seen that the incorporation of storage and a diverse set of sources in the form of a microgrid can greatly improve power supply availability during extreme events like tropical cyclones when the microgrid goes into island mode.

Finally, in chapter 7, three cases studies for ICT site behavior during hurricanes Katrina, Ike and Sandy were presented. It was seen that current backup systems are insufficient in providing sufficient availability performance for the ICT systems which leads to long restoration times and long down times of the ICT facility. The availability models hence developed might help design and plan microgrid with improved availability performance.

FUTURE WORK

The work presented in this dissertation is incipient in nature. Microgrids are growing in number of applications at the present time. With evolving structure and control strategies in the microgrid, the models in this dissertation will have to be adapted to specific applications. The introduction of intelligent controls will also seek to improve microgrid availability therefore developing availability models based on such control strategies is a logical next step for this research. Other possibilities include extending these models to a network of microgrids where in energy sharing is possible, such models will be typical large and computationally intensive and hence developing approximations to evaluating microgrid performance need to be developed.

Bibliography

[ADCIRC 2009] ADCIRC Hurricane Gustav Storm Surge Maximum Water Level figure, Available: http://www.unc.edu.

[Albert et al. 2004] R, Albert, I. Albert, and G. L. Nakarado, "Structural vulnerability of the North American power grid" *Physical Review E*, vol. 69, issue 2, 4 pages, Feb. 2004.

[Arapostathis et al. 2003] A. Arapostathis, A.;R. Kumar, S. Tangirala, "Controlled Markov chains with safety upper bound," *IEEE Transactions on Automatic Control,* vol.48, no.7, pp.1230,1234, July 2003.

[Bahramirad et al. 2012] Bahramirad, S.; Reder, W.; Khodaei, A., "Reliability-Constrained Optimal Sizing of Energy Storage System in a Microgrid," *Smart Grid, IEEE Transactions on* , vol.3, no.4, pp.2056,2062, Dec. 2012

[Basu et al. 2010] Basu, A.K.; Chowdhury, S.; Chowdhury, S. P., "Impact of Strategic Deployment of CHP-Based DERs on Microgrid Reliability," *Power Delivery, IEEE Transactions on* , vol.25, no.3, pp.1697,1705, July 2010

[Billinton and Karki 2001] Billinton, R.; Karki, R., "Maintaining supply reliability of small isolated power systems using renewable energy," *Generation, Transmission and Distribution, IEE Proceedings*- , vol.148, no.6, pp.530,534, Nov 2001

[Bruneau] M.Bruneau *et. al.* "A framework to quantitatively assess and enhance the seismic resilience of communities," *Earthquake Spectra*,vol. 19,pp.733-752.

[Bucciarelli 1984] L. L. Bucciarelli Jr, "Estimating loss-of-power probabilities of stand-alone photovoltaic solar energy systems," *Solar Energy,* vol. 32, pp. 205-209, 1984."

[Capstone] http://www.Capstoneturbine.com/prodsol/products/

[Dames and Moore 1980] Dames and Moore, “Design and construction standards for residential construction in tsunami prone areas in Hawaii,” Federal Emergency Management Agency, Washington, D.C, 1980.

[Dawson et al. 2006] C.N Dawson, J.J. Westerink, J.C. Feyen and D. Pothina, “Continuous, Discontinuous and Coupled Discontinuous-Continuous Galerkin Finite Element Methods for the Shallow Water Equations,” *International Journal for Numerical Methods in Fluids*, vol. 52, issue 1, 10 September 2006, p.63-88.

[Dialynas and Hatziargyriou 2007] Dialynas, E.; Hatziargyriou, N.D., "Impact of Microgrids on Service Quality," *Power Engineering Society General Meeting, 2007. IEEE* , vol., no., pp.1,5, 24-28 June 2007

[Diesel Service Chart] http://www.dieselserviceandsupply.com/temp/Fuel_Consumption_Chart.pdf accessed: 23rd Dec 2013

[DOE] http://www.afdc.energy.gov/fuels/fuel_comparison_chart.pdf accessed: 23rd Dec 2013

[Dueñas-Osorio and Kwasinski 2012] Dueñas-Osorio, L., and A. Kwasinski, (2010). "Quantification of lifeline system interdependencies after the 27 February 2010 Mw 8.8 offshore Maule, Chile earthquake." *Earthquake Spectra 2012*

[Erol-Kantarci et al. 2011] Erol-Kantarci, M.; Kantarci, B.; Mouftah, H.T., "Reliable overlay topology design for the smart microgrid network," *Network, IEEE* , vol.25, no.5, pp.38,43, September-October 2011

[Fahimi et al. 2011] B. Fahimi et. al, “Charge it” *IEEE Power and Energy Magazin*e, vol. 9, no. 4, pp. 54-64, July-Aug. 2011.

[Falahati et al. 2012] Falahati, B.; Yong Fu; Lei Wu, "Reliability Assessment of Smart Grid Considering Direct Cyber-Power Interdependencies," *Smart Grid, IEEE Transactions on* , vol.3, no.3, pp.1515,1524, Sept. 2012

[FEMA 2009] FEMA, "Mitigation Assessment Team Report: Hurricane Ike in Texas and Louisiana Building Performance Observations, recommendations, and Technical Guidance," FEMA P-757 / April 2009.

[Fuel Cell today 2013] http://www.fuelcelltoday.com/media/1889220/13-09-25_the_potential_for_fuel_cell_prime_power_in_japan.pdf

[Gagge 2008] Gagge, J.P., "PEM fuel cells versus diesel generators — which solution to pick?," *Telecommunications Energy Conference, 2008. INTELEC 2008. IEEE 30th International* , vol., no., pp.1,5, 14-18 Sept. 2008

[Galvan et al. 2009] F. Galvan, S. Mandal and M. Thomas,, "Phasor Measurement Units (PMU) instrumental in detecting and managing the electrical island created in the aftermath of Hurricane Gustav," *Power Systems Conference and Exposition*, 2009. PSCE '09. IEEE/PES , pp.1-4, 15-18 March 2009.

[Gavaniduo et al. 1993] Gavanidou, E. S.; Bakirtzis, A.G.; Dokopoulos, P.S., "A probabilistic method for the evaluation of the performance and the reliability of wind-diesel energy systems," *Energy Conversion, IEEE Transactions on* , vol.8, no.2, pp.197,206, Jun 1993

[Girtler 2013] J. Girtler, " Application of the theory of Semi-Markov Processes to determine a limiting distribution of the process of changes of ability and inability states of fuel supply systems in heavy fuel diesel engines" 2013.

[Glahnl et al.] B. Glahn *et. al.* "The Role of the SLOSH Model in National Weather Service Storm Surge Forecasting".

[Graber et al. 2006] H.C. Graber, V.J. Cardone, R.E. Jensen, D.N. Slinn, S.C. Hagen, A.T. Cox, M.D. Powell, and C. Grassl, 2006, “Coastal Forecasts and Storm Surge Predictions for Tropical Cyclones: A Timely Partnership Program,” *Oceanography*, 19 (1), 130-141, March 2006.

[Guerrero 2013] Guerrero, J.M.; Chandorkar, M.; Lee, T.; Loh, P.C., "Advanced Control Architectures for Intelligent Microgrids—Part I: Decentralized and Hierarchical Control," *Industrial Electronics, IEEE Transactions on* , vol.60, no.4, pp.1254,1262, April 2013

[H*wind]H*Wind, Surface Wind Analysis, Hurricane research division, NOAA. Available : http://www.aoml.noaa.gov/hrd/data_sub/wind.html.

[Hadjsaid et al. 2010] Hadjsaid, N.; Le-Thanh, L.; Caire, R.; Raison, B.; Blache, F.; Ståhl, B.; Gustavsson, R., "Integrated ICT framework for distribution network with decentralized energy resources: Prototype, design and development," *Power and Energy Society General Meeting, 2010 IEEE*, vol., no., pp.1,4, 25-29 July 2010

[Han et al .2009] S. Han, S. D. Guikemaan and S. M. Quiring P. W. Daly, “Improving the Predictive Accuracy of Hurricane Power Outage Forecasts Using Generalized Additive Models,” *Risk Analysis*, Vol. 29, No. 10, 2009.

[Hatziargyriou and Zervos 2001] Hatziargyriou, N.; Zervos, A., "Wind power development in Europe," *Proceedings of the IEEE* , vol.89, no.12, pp.1765,1782, Dec 2001

[Hebert 2009] C. Hebert, “A New Method of Classifying the True Destructive Potential of Tropical Cyclones,” presented at the National Hurricane Conference, Austin, April 2009.

[Hirose et al. 2006] J K. Hirose, T. Takeda, and S. Muroyama, “Study on Field Demonstration of Multiple Power Quality Levels System in Sendai,” *in Proc. INTELEC, 2006*, pp. 256-261.

[Huang et al. 2011] Huang Wei; He Zijun; Feng Li; Tian Hongliang; Zhang Li, "Reliability evaluation of Microgrid with PV-WG hybrid system," *Electric Utility Deregulation and Restructuring and Power Technologies (DRPT), 2011 4th International Conference on* , vol., no., pp.1629,1632, 6-9 July 2011.

[IEEE 1366] “IEEE Guide for Electric Power Distribution Reliability Indices,” IEEE Std 1366-2003 (Revision of IEEE Std 1366-2003), 2004.

[IEEE 859] “IEEE Standard Terms for Reporting and Analyzing Outage Occurrences and Outage States of Electrical Transmission Facilities,” IEEE Std 859-1987.

[Kakimoto 2012] Kakimoto, N.; Matsumura, S.; Kobayashi, K.; Shoji, M., "Two-State Markov Model of Solar Radiation and Consideration on Storage Size," *Sustainable Energy, IEEE Transactions on* , vol.5, no.1, pp.171,181, Jan. 2014

[Kantha 2006] L. Kantha 2006, “Time to Replace the Saffir-Simpson Hurricane Scale?” *Eos*, vol. 87, no. 1, pp. 3, 6, January 2006.

[Kashtanov 2010] Kashtanov V.A.: Controlled semi-Markov processes in modeling of the reliability and redundancy maintenance of queueing systems. Applied Statistics and Operation Research, vol. 14, 2010.

[Kennedy 2009] S. Kennedy, “Reliability evaluation of islanded microgrids with stochastic distributed generation,” in *IEEE PES '09*, 2009, pp.1-8.

[Kennedy and Marden 2009] S. Kennedy and M. Marden, “Reliability of islanded microgrids with stochastic generation and prioritized load,” in IEEE Powertech, Bucharest, Jun. 2009

[Khodayar et al. 2012] Khodayar, M.E.; Barati, M.; Shahidehpour, M., "Integration of High Reliability Distribution System in Microgrid Operation," *Smart Grid, IEEE Transactions on* , vol.3, no.4, pp.1997,2006, Dec. 2012

[Kolluri et al. 2009]S. Kolluri,S. Mandal,F. Galvan and M. Thomas, "Island formation in entergy power grid during Hurricane Gustav," Power & Energy Society General Meeting, 2009. PES '09. IEEE, pp.1-5, 26-30 July 2009.

[Krishnamurthy and Kwasinski 2013]V. Krishnamurthy, A Kwasinski, "Characterization of power system outages caused by hurricanes through localized intensity indices," *Power and Energy Society General Meeting (PES), 2013 IEEE* July 2013.

[Krishnamurthy et al. 2008]Krishnamurthy, S.; Jahns, T.M.; Lasseter, R.H., "The operation of diesel gensets in a CERTS microgrid," *Power and Energy Society General Meeting - Conversion and Delivery of Electrical Energy in the 21st Century, 2008 IEEE* , vol., no., pp.1,8, 20-24 July 2008

[Kulkarni 2010]V. G. Kulkarni, Modeling and Analysis of Stochastic Systems, 2nd ed. Boca Raton, FL: CRC, 2010.

[Kwasinski 2008]Kwasinski, A., "Analysis of Electric Power Architectures to Improve Availability and Efficiency of Air Conditioning Systems", *INTELEC 2008*, vol. 10, no. 2, pp. 1-8, San Diego, CA, USA, September 14-18, 2008

[Kwasinski 2008a] http://users.ece.utexas.edu/~kwasinski/ike.html accessed June 1st 2014

[Kwasinski 2009]Kwasinski, A., "Identification of Feasible Topologies for Multiple-Input DC–DC Converters," *IEEE Transactions on Power Electronics*, vol.24, no.3, pp.856,861, March 2009

[Kwasinski 2010]Kwasinski, A., "Technology Planning for Electric Power Supply in Critical Events Considering a Bulk Grid, Backup Power Plants, and Micro-Grids," *Systems Journal, IEEE* , vol.4, no.2, pp.167,178, June 2010

[Kwasinski 2011a]A. Kwasinski, "Local energy storage as a decoupling mechanism for interdependent infrastructures," in Proc. 2011 IEEE Int. Systems Conf.,2011, pp. 435–441

[Kwasinski 2011b] Kwasinski, A., "Effects of notable natural disasters from 2005 to 2011 on telecommunications infrastructure: Lessons from on-site damage assessments," *Telecommunications Energy Conference (INTELEC), 2011 IEEE 33rd International* , vol., no., pp.1,9, 9-13 Oct. 2011

[Kwasinski 2011c] A. Kwasinski, "Quantitative Evaluation of DC Microgrids Availability: Effects of System Architecture and Converter Topology Design Choices," IEEE Transactions on Power Electronics, vol. 26, no. 3, pp. 835-851, March 2011

[Kwasinski 2011d] Kwasinski, A., "Advanced power electronics enabled distribution architectures: Design, operation, and control," *Power Electronics and ECCE Asia (ICPE & ECCE), 2011 IEEE 8th International Conference on* , vol., no., pp.1484,1491, May 30 2011-June 3 2011

[Kwasinski 2012a]http://users.ece.utexas.edu/~kwasinski/sandy.html accessed June 1st 2014

[Kwasinski 2013] A. Kwasinski, "Lessons from Field Damage Assessments about Communication Networks Power Supply and Infrastructure Performance during Natural Disasters with a focus on Hurricane Sandy, FCC workshop on network resiliency 2013.

[Kwasinski and Krien 2007]A. Kwasinski and P. T. Krein, "Telecom Power Planning for Natural and Man-Made Disasters," in *Proc. INTELEC 2007*, 2007, pp. 216-222.

[Kwasinski et al. 2009]A. Kwasinski, W. W. Weaver, P. L. Chapman, and P.T. Krein, "Telecommunications Power Plant Damage Assessment for Hurricane Katrina" Site Survey and Follow-Up Result," *IEEE Systems Journal*, vol.3, issue 3, pp. 277-287, Sept. 2009.

[Kwasinski et al. 2012]Kwasinski, A.; Krishnamurthy, V.; Junseok Song; Sharma, R., "Availability Evaluation of Micro-Grids for Resistant Power Supply During Natural Disasters," *IEEE Transactions on Smart Grid,* vol.3, no.4, pp.2007,2018, Dec. 2012

[Kwasinski 2012]Kwasinski A., Hurricane Sandy Effects on Communication Systems (A preliminary Report) http://users.ece.utexas.edu/~kwasinski/preliminary_20telecom 20report 20v3 20comp.pdf

[Lalitha et al. 2013]Lalitha, Anusha; Mondal, Santanu; V, Satya Kumar; Sharma, Vinod, "Power-optimal scheduling for a Green Base station with delay constraints," *National Conference on Communications (NCC), 2013* , vol., no., pp.1,5, 15-17 Feb. 2013

[Li et al. 2010]H. Li, L. A. Treinish and J. R. M.Hosking,, "A statistical model for risk management of electric outage forecasts," *IBM Journal of Research and Development*, vol.54, no.3, pp.8:1-8:11, May-June 2010.

[Li et al. 2010]Z. Li, Y. Yuan, F. Li, "Evaluating the reliability of islanded microgrid in an emergency mode," in *45th International, Universities Power Engineering Conference (UPEC)*, 2010, pp.1-5

[Liu and Singh 2009]Y. Liu and C. Singh, "Evaluation of Hurricane Impact on Failure Rate of Transmission Lines Using Fuzzy Expert System," *Intelligent System Applications to Power Systems*, 2009. ISAP '09., pp.1-6, 8-12 Nov. 2009.

[Liu and Singh 2011]Yong Liu and Singh, C., “A Methodology for Evaluation of Hurricane Impact on Composite Power System Reliability,” *IEEE Transactions on Power Systems,* vol.26, no.1, pp.145-152, Feb. 2011.

[Liu et al .2007]H. Liu, R. A.Davidson and T. V. Apanasovish, "Spatial generalized linear mixed models of electric power outages due to hurricanes and ice storms,” *Science Direct,*Vol. 22, NO.4,November 2007.

[Liu et al .2009a]H. Liu *et. al.*, “Statistical Forcasting of Electric Power Restoration Times in Hurricanes and Ice Storms,” *IEEE Transactions on Power Systems*. Vol. 22, No. 4, November 2007.

[Lorincz et al. 2012]Lorincz J, Garma T and Petrovic G " Measurements and Modelling of Base Station Power Consumption under Real Traffic Loads, ”*Sensors 2012*, 12, 4281-4310

[Maish 1999]A. Maish, "Defining Requirements for Improved Photovoltaic System Reliability," *Progress in Photovoltaics: Research and Applications*, vol.7, pp. 165-173, 1999

[Marshall and Olkin 2007]A.W. Marshall, I. Olkin, “Life Distributions: Structure of Nonparametric, Semi parametric and Parametric Families”, Springer Series in Statistics.

[Migawa 2013]K. Migawa, “Semi-Markov model of the availability of the means of municipal transport system”2009.

[Military Reliability Handbook] Reliability Prediction of Electronic Equipment, U. S. Department of Defense, Pentagon, Washington, DC, MIL-HDBK-217, Feb. 1995.

[Mitra et al. 2012]Mitra, J.; Vallem, M.R., "Determination of Storage Required to Meet Reliability Guarantees on Island-Capable Microgrids With Intermittent Sources," *IEEE Transactions on Power Systems*, vol.27, no.4, pp.2360,2367, Nov. 2012

[Moon et al. 2006]J. Moon, J. Kim, H. Lee, Y. Sang-Seung, Y. Yoon and K. Song, "Time-varying failure rate extraction in electric power distribution equipment," *Probabilistic Methods Applied to Power Systems*, 2006. PMAPS 2006, pp.1-6, 11-15 June 2006.

[NHEC 2012]http://www.nhec.com/rates_electricchoice_loadprofiles.php

[NHEC 2012a] http://www.nhec.com/pdf/September%202011%20through%20August%202012%20Load%20Profiles%20all%20classes.xlsx [Chapter4referencesend]

[NOAA 1999]NOAA, "Hurricane Basics," May 1999.

[NOAA Surge]Storm Surge, National Hurricane Center, Available: http://www.nhc.noaa.gov.

[NTT Docomo 2012]Measures for Recovery from the Great East Japan Earthquake Using NTT Docomo 2012 R&D Tech", DoCoMo Technical Journal Vol 13. No. 4

[NTT 2013] https://www.NTT Docomo 2012.co.jp/english/info/media_center/pr/2013/0322_01.html

[NTT 2013a]https://www.NTT Docomo 2012.co.jp/english/info/media_center/pr/2013/pdf/20130322_attachment02.pdf

[Ospina et al. 2014] A.V. Ospina et al., "Resilient pathways:the adaptation of the ICT sector to climate change", ITU Report 2014

[Powell et al. 1998]M. D. Powell, S. H. Houston, L. R. Amat, and N Morisseau-Leroy, 1998: "The HRD real-time hurricane wind analysis system," *J. Wind Engineer. and Indust. Aerodyn.* 77&78, 53-64.

[Powell et al.]M. D. Powell and T. A. Reinhold, "New Scales for the Destructive Potential of Tropical Cyclones."

[Ragone] Ragone, D., "Review of Battery Systems for Electrically Powered Vehicles," SAE Technical Paper 680453, 1968, doi:10.4271/680453.

[Reed et al. 2009] D. A. Reed *et. al.* , "Methodology for Assessing the Resilience of Networked Infrastructure," *IEEE System Journal*, Vol. 3, No. 2, June 2009.

[Retterath et al. 2004]B. Retterath, S.S. Venkata and A.A. Chowdhury, "Impact of time varying failure rates on distribution reliability," *Probabilistic Methods Applied to Power Systems*, 2004, pp. 953- 958, 12-16 Sept. 2004.

[Saffir-Simpson]The experimental Saffir-Simpson scale, NOAA, Available: http://www.nhc.noaa.gov/sshws.shtml.

[Sandia 2013] https://share.sandia.gov/news/resources/releases/2006/microgrid.htm

[Solar tech Data Sheet]http://www.solardesigntool.com/components/module-panel-solar/1-SolTech/842/1-STH-250/specification-data-sheet.html

[Song et al. 2010]Junseok Song; Toliyat, A.; Turtle, D.; Kwasinski, A., "A rapid charging station with an ultracapacitor energy storage system for plug-in electrical vehicles," *2010 International Conference on Electrical Machines and Systems (ICEMS),* , vol., no., pp.2003,2007, 10-13 Oct. 2010.

[Song et al. 2013] J. Song, V. Krishnamurthy, A. Kwasinski, and R. Sharma, "Development of a Markov-chain-based energy storage model for power supply availability assessment of photovoltaic generation plants," IEEE Trans. Sustain. Energy, vol. 4, no. 2, pp. 491–500, Apr. 2013.

[Spink and Saathoff 2013]Spink, Scott; Saathoff, Sandra, "Superstorm Sandy: Fuel Cell Design for Disaster Recovery vs. Backup Power," *Telecommunications Energy Conference 'Smart Power and Efficiency' (INTELEC), Proceedings of 2013 35th International* , vol., no., pp.1,6, 13-17 Oct. 2013

[Tammam et al. 2012]Tammam, B.; Adrian, I.; Rafic, Y.; Jean, P., "A new multi-hybrid power system for grid-disconnected areas Wind — Diesel — Compressed Air Energy Storage," *Renewable Energies for Developing Countries (REDEC), 2012 International Conference on* , vol., no., pp.1,8, 28-29 Nov. 2012

[Tang 2008]A. Tang, "Telecommunications Performance – May 2008, Wenchuan, Sichuan Earthquake," in *Proc. TCLEE 2009: Lifeline Earthquake Engineering in a Multihazard Environment*," pp. 1407-1415

[Tankut]A. Tugrul Tankut, "Earthquakes and Tsunamis: Civil Engineering Disaster Mitigation Activities Implementing Millenium Development Goals."[Tanrioven 2005] M. Tanrioven 2005, "Reliability and cost benefits of adding alternate power sources to an independent micro-grid community," *Journal of Power Sources*, vol. 150, pp. 136-149, 2005.

[TCLEE 2012]TCLEE Report of the 11 March 2011 Mw 9.0 Tohoku, Japan Earthquake and Tsunami

[Theristis and Papazoglou 2014] Theristis, M.; Papazoglou, I.A., "Markovian Reliability Analysis of Standalone Photovoltaic Systems Incorporating Repairs," *Photovoltaics, IEEE Journal of* , vol.4, no.1, pp.414,422, Jan. 2014

[US Census 2008]U.S Census Bureau, http://www.census.gov/popest/housing/HU-EST2008-4.html.

[Varaiya et al. 2011]Varaiya, P.P.; Wu, F.F.; Bialek, J.W., "Smart Operation of Smart Grid: Risk-Limiting Dispatch," *Proceedings of the IEEE* , vol.99, no.1, pp.40,57, Jan. 2011

[Wang et al. 2005]H. Wang *et. al.*, "Hurricane Charley Characteristics and Storm Tide Evaluation," April 2005.

[Wiegler et al. 2005]L. Wiegler, “The challenge for those in power electricity supply restoration],” *IEE Review* , vol.51, no.11, pp. 24- 25, Nov. 2005.

[Winkler et al. 2010]J. Winkler ,D. O. Leonardo, R. Stein and D. Subramanian, “Performance assessment of topologically diverse power systems subjected to hurricane events,” *Reliability Engineering and System Safety,* 95 (2010), 323–336.

[Wunderground 2012] http://www.wunderground.com/blog/JeffMasters/comment.html?entrynum=2302

[Xioahong et al. 2010]Xiaohong Guan; Zhanbo Xu; Qing-Shan Jia, "Energy-Efficient Buildings Facilitated by Microgrid," *Smart Grid, IEEE Transactions on* , vol.1, no.3, pp.243,252, Dec. 2010.

[Ying-Yi and Ruo-Chen 2012] Ying-Yi Hong; Ruo-Chen Lian, "Optimal Sizing of Hybrid Wind/PV/Diesel Generation in a Stand-Alone Power System Using Markov-Based Genetic Algorithm," *Power Delivery, IEEE Transactions on* , vol.27, no.2, pp.640,647, April 2012

[Yokoyama et al. 2008] R. Yokoyama, T. Niimura, and N. Saito, “Modeling and evaluation of supply reliability of microgrids including PV and wind power,” in *Proc. Power and Energy Society General Meeting*, 2008, pp. 1-5.

[Yong-Hua 2009] Yong-Hua Li, "Optimal Allocation of Fuzzy Multi-state Reliability in Diesel Engine," *Information and Computing Science, 2009. ICIC '09. Second International Conference on* , vol.1, no., pp.195,199, 21-22 May 2009.

[Zhao et al. 2012]Bo Zhao; Xuesong Zhang; Jian Chen, "Integrated Microgrid Laboratory System," *Power Systems, IEEE Transactions on* , vol.27, no.4, pp.2175,2185, Nov. 2012.

[Zhao et al. 2013]Bo Zhao; Xuesong Zhang; Jian Chen; Caisheng Wang; Li Guo, "Operation Optimization of Standalone Microgrids Considering Lifetime Characteristics

of Battery Energy Storage System," *Sustainable Energy, IEEE Transactions on* , vol.4, no.4, pp.934,943, Oct. 2013

[Zhou 2006]Y. Zhou, A. Pahwa and S Yang, "Modeling Weather-Related Failures of Overhead Distribution Lines," *IEEE Transactions on Power Systems*, vol.21, no.4, pp.1683-1690, Nov. 2006.

[Zhu et al. 2007]D. Zhu *et. al.* , "Storm modeling for prediction of power distribution system outages," Electric Power Systems Research, Vol. 77,No. 8, 2007, p.973-979.

Vita

Vaidyanathan Krishnamurthy is from India. He received bachelor's in electrical and electronics engineering from RV College of Engineering in 2006. He worked as a software engineer from 2006 to 2008. He obtained a masters in electrical in computer Engineering from the University of Texas at Austin in 2010. He has been in the PhD program at since 2010.

Permanent address vaidyanathan@utexas.edu:

This dissertation was typed by the author.